Study of the high temperature translaminar fracture in aeronautical woven-ply thermoplastic laminated composites : experimental characterization and numerical simulation

Juan Daniel Pujols Gonzalez

Normandie Université

THESE

Pour obtenir le diplôme de doctorat

Spécialité Mécanique des matériaux

Préparée au sein de l'Institut National des Sciences Appliquées de Rouen

Study of the high temperature translaminar fracture in aeronautical woven-ply thermoplastic laminated composites: experimental characterization and numerical simulation

Présentée par

Juan Daniel PUJOLS GONZÁLEZ

Thèse soutenue publiquement le 15 décembre 2020
devant le jury composé de

M. Zoheir ABOURA	Professeur des Universités, Université de Technologie de Compiègne	Président
M. Christian HOCHARD	Professeur des Universités, Université d'Aix-Marseille	Rapporteur
M. Eric MARTIN	Professeur des Universités, Bordeaux INP	Rapporteur
Mme Xiaojing GONG	Professeur des Universités, Université Toulouse III	Examinatrice
M. Benoit VIEILLE	Professeur des Universités, INSA de Rouen	Directeur de thèse
M. Christophe BOUVET	Professeur ISAE-SUPAERO, Institut Supérieur de l'Aéronautique et de l'Espace	Co-directeur de thèse

Thèse dirigée par Benoit VIEILLE (GPM – INSA Rouen) et Christophe BOUVET (ISAE-SUPAERO)

INSA INSTITUT NATIONAL DES SCIENCES APPLIQUÉES ROUEN

ED PSIME

GPM Groupe de Physique des Matériaux

Acknowledgements

The work developed during these three years in my thesis, has been without a doubt, the most difficult and enriching project that I have been able to carry out in my short existence. This thesis represents not only my effort but also the support, energy and motivation of my supervisors, colleagues, family and friends. Now it is time to take advantage of these few lines to acknowledge and thank all those people who made the completion of this thesis possible.

My first thoughts go to my thesis supervisors. All my recognition, thanks and great appreciation to my thesis supervisor at INSA-Rouen, Benoit VIEILLE, who I can say is a remarkable person both on a scientific and professional level and on a human level, for having welcomed me in the laboratory and for having supervised me from the master's internship to the writing and defense of this thesis. Benoit, your good sense of humour and availability made this path more pleasant, thank you very much for having accompanied me until the end to overcome all the obstacles, giving me your countless advices... that harmonic noise of the fibers breaking in unison will always resonate in my life when I remember the great experience and honor that has been worked by your side. In the same way, I want to address all my thanks to my thesis supervisor at ISAE-SUPAERO, Christophe BOUVET, with whom I had the luck and privilege of working in the numerical simulation part, for having introduced me to this field of numerical modelling in a very pedagogical way and for having been always present despite the distance throughout my training. Thanks again to my thesis supervisors for having allowed me to carry out this thesis on composite materials, I hope that I have shown myself worthy of their trust with the results obtained.

I would like to thank all the members of the jury for having accepted to evaluate this work: Christian HOCHARD and Eric MARTIN who took on the hard task of reading and reporting my manuscript, their comments and constructive advice embodied in their respective reports allowed me to broaden a little more the horizon of the thesis on the day of the defense; Zoheir ABOURA who did me the honor of being the president of this jury; Xiaojing GONG for his willingness and for having accepted to be the examiner of this thesis. Thanks to all of you for your comments and valuable advice, the questions and exchanges on the day of the defense were undoubtedly a great contribution to the future improvement of the work presented here.

The financial support provided for this research by the Ministry of Higher Education, Science and Technology (MESCYT) of the Dominican Republic is greatly appreciated.

I would like to thank two members of the neighboring LMN laboratory with whom I had the opportunity to work on a parallel project to my thesis, Thomas BRETEAU and Christophe GAUTRELET, for their help in the conception and assembly of the Charpy pendulum. I would like to thank the technical staff: Romain FLEURY (ERMECA Team) and David (INSA-Rouen), for helping me in the fabrication of the various experimental assemblies. I would also like to thank Elisabeth LESAGE, secretary of the GPM laboratory, for her availability and her great kindness.

I also take this opportunity to thank all the members of the GPM laboratory for their welcome during my thesis years. I especially want to thank my colleagues of the ERMECA team for their help, support and kindness. I would also like to thank them for the confidence they have shown in me by allowing me to get involved in the collective life of the team. The human relationships I have enjoyed with them have created true bonds of friendship that in my eyes are priceless. May you all be assured of my deepest gratitude and esteem. A special thought for my different office colleagues, members of the Team Composite!, with whom I had the opportunity to share and discuss different topics linked to composite materials, and to share good moments outside INSA-Rouen: Yann, David, Estève, Asih and the last one to arrive David Philippe. Also a thought for all the past and present PhD students I had the opportunity to meet, Luc, Baptiste, Oscar, Mathieu and Alireza, as well as the postdoctoral researcher, Hossein, Josiane, Morgane, Yosra and Adem, and the permanent team members, Taleb, Clément, Fabrice, Mouldi and Alain, who always showed their availability and good sense of humour. Not to mention all the interns who I had the great experience and opportunity to supervise.

I cannot finish these few lines without addressing and thanking my family, my grandmothers, my aunts, my uncles, my cousins, for the love and support they have given me, thank you for supporting me in everything and encouraging me throughout this experience.

To conclude, I want to express my deepest gratitude, reconnecting and loving to my parents and my brothers, without you I could not have been writing these lines today, I love you very much, thank you for the love, motivation and sacrifices you have provided me throughout my life in good times and bad. To my father, Anibal, for always being by my side in spite of the distance, for worrying and encouraging me almost daily with our usual calls. To my brother, Ramon, thank you for your concern in all economic and personal senses, you have been the person who has lifted me up when I have felt tired and down, you have given me strength of will and inspired me to keep going along this road I have traveled, thank you for your wise advice. Leaving home was difficult for me, I hope you are proud of me.

To my mother, Dania, and my big brother, Gregorio, although they are not physically with me today, I always carry them in my heart.

Synthèse en français

Les matériaux composites sont reconnus pour leurs propriétés mécaniques spécifiques élevées (ramenées à leur masse volumique). Le principe d'un matériau composite est de combiner les avantages de matériaux différents, le plus souvent des fibres résistantes et fragiles, avec une matrice moins résistante et plus ductile. L'utilisation des matériaux composites dans les différents domaines industriels a été intensifiée au cours des dernières décennies. L'industrie aéronautique ne fait pas exception, car les avions commerciaux actuels sont composés jusqu'à 50% en masse de matériaux composites. Les composites à matrice thermodurcissables (TD) ont été largement utilisés pour des applications aéronautiques. Les industriels se posent désormais la question : quels matériaux composites pour les avions de demain ?

Outre les questions environnementales, le développement de nouveaux procédés de fabrication, la réduction des coûts, les possibilités de recyclage et les exigences de certification, on observe un intérêt croissant pour les polymères thermoplastiques (TP) haute performance. En effet, ces polymères offrent un certain nombre d'avantages par rapport aux résines TD classiques (telles que les époxy) : un haut niveau de résistance chimique, une excellente tolérance aux dommages et une bonne résistance à l'impact, et ils peuvent être utilisés sur une large gamme de température. Enfin, il existe de nombreuses raisons techniques pour lesquelles les composites TP haute performance sont pertinents pour des pièces d'aérostructures : excellent ténacité, très bonne tenue au feu. En outre, ils sont associés à des procédés de fabrication à faible coût comme le thermoformage, l'emboutissage, le soudage ou la co-consolidation, et enfin ils possèdent un bon potentiel en termes de recyclage.

La généralisation des composites à matrice organique (CMO) dans de nombreux secteurs industriels s'est confrontée à la compréhension et à la quantification des mécanismes de rupture au sein de matériaux dont le comportement est fortement hétérogène et anisotrope. Les structures composites principalement utilisées dans le secteur industriel sont obtenues par empilement de plusieurs plis et sont communément appelées composites stratifiés. L'assemblage « sur-mesure » des plis permet d'optimiser le comportement mécanique (rigidité, résistance) des composites stratifiés. Ainsi les composites stratifiés sont des matériaux multi-échelles (Figure 1). Trois échelles différentes sont généralement identifiées : l'échelle microscopique (≈ 10 µm) est l'échelle des constituants (fibre et matrice) et de l'interface fibre/matrice – l'échelle mésoscopique (≈ 100 µm) dans laquelle l'architecture du renforcement est décrite par des fils de fibres homogènes entrelacés et incorporés dans la matrice (pli élémentaire) – l'échelle macroscopique (≈ 1 mm) est l'échelle de la structure (empilement de plis élémentaires constituant le stratifié).

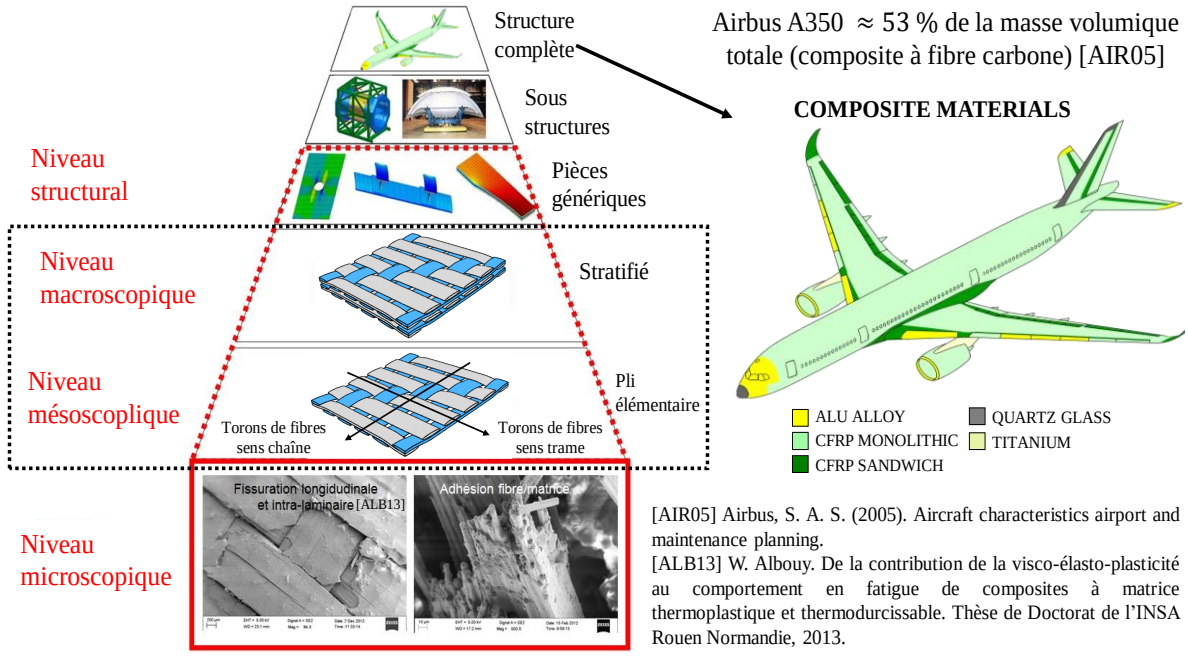

Figure 1. Différents niveaux d'analyses sur une structure composite

Le caractère multi-échelle des composites stratifiés rend complexe l'analyse et la prévision de leur comportement lorsqu'ils sont soumis à différents types de chargement thermo-mécanique. Les mécanismes de rupture multiples se traduisent par des discontinuités locales au sein du matériau appelées fissures. L'initiation de la rupture peut être considérée comme la création de microfissures à l'échelle microscopique (celle des constituants), à partir d'un défaut et la propagation de la rupture est le résultat de la création de nouvelles surfaces (par coalescence des microfissures) à l'échelle mésoscopique. L'initiation de la rupture se produit généralement bien avant qu'un changement de comportement macroscopique ne soit observé. En fonction de la nature des matériaux constitutifs, et de la séquence d'empilement, les composites stratifiés sont généralement caractérisés par trois modes principaux de rupture (Figure 2) : rupture interlaminaire (souvent appelée délamination), rupture intralaminaire (notée comme fissuration matricielle) et rupture translaminaire. En effet, les mécanismes de rupture qui peuvent apparaître dans un composite stratifié, impliquent différents modes de dégradation à différentes échelles, qui sont influencés par la stratification et les propriétés mécaniques des constituants. C'est pourquoi il est important de comprendre leur comportement à toutes les échelles d'observation pour éviter la ruine de la structure.

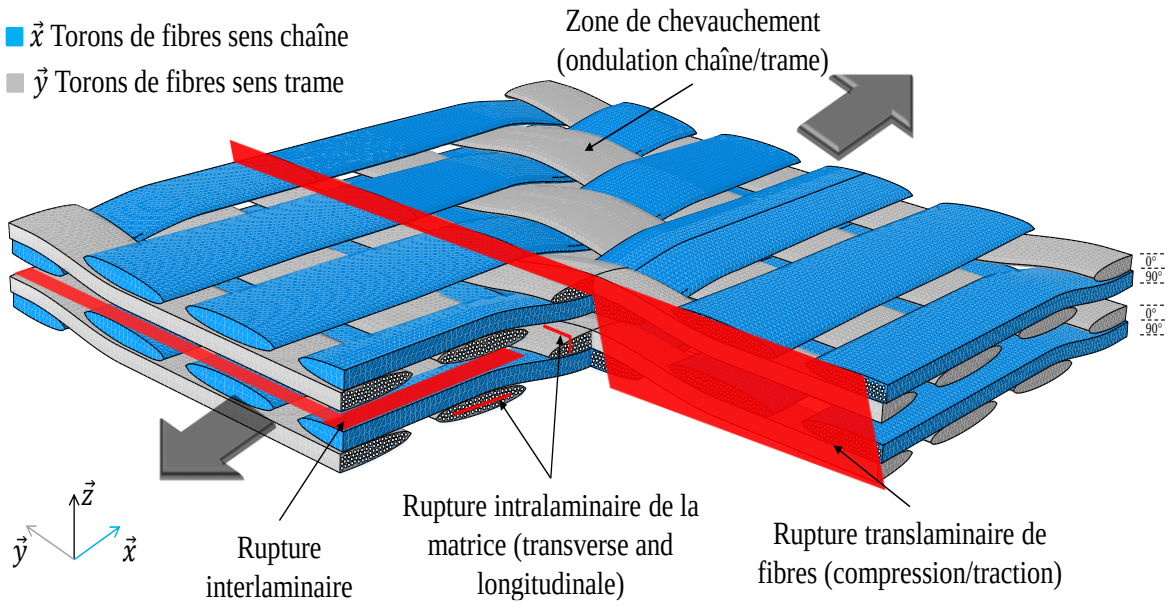

Figure 2. Vue d'ensemble des modes de rupture dans un composite stratifié renforcé par un renfort tissé satin de 5

Le mode de rupture le plus critique, et en général le dernier à se développer, est la rupture translaminaire, c'est-à-dire une rupture traversant totalement la plaque composite (contrairement à des dommages tels que des délaminages ou la fissuration matricielle qui vont endommager localement le stratifié). Dans les composites stratifiés soumis à des chargements en traction et en compression, les renforts fibreux supportent l'essentiel du chargement mécanique. La rupture translaminaire d'un stratifié se manifeste à l'échelle mésoscopique par la rupture des fibres en traction et par la rupture des fibres en compression liée à la formation de bandes de flambement (kink-band) plastiques. Paradoxalement la rupture translaminaire et la rupture de fibres associée, ont été moins étudiées dans la littérature que les modes de rupture interlaminaire (délaminage ou fissuration matricielle). Ce mode de rupture est souvent négligé dans le dimensionnement des structures composites, bien qu'il joue un rôle important dans la défaillance des composites entaillés.

Afin de fiabiliser les matériaux composites et d'éviter une ruine catastrophique, les critères de rupture sont appliqués pour déterminer si la structure résistera aux sollicitations externes auxquelles elle sera soumise. Dans la démarche classique de conception, la première approche consiste à examiner si la résistance de la structure est supérieure à la contrainte appliquée prévue. Mais cette approche s'avère généralement insuffisante car elle ne tient pas compte de certains dommages préexistants au sein des structures (par exemple des microfissures), ou de endommagements résultants d'événements accidentels (tels que des impacts). En outre, les structures composites présentent très souvent de petites fissures, par exemple dans des zones de singularité telles que les trous de rivets ou dans des zones de variation de section. La deuxième approche basée sur la tolérance aux dommages consiste à prévenir les défaillances structurelles en présence d'un défaut jusqu'à ce que la réparation puisse être réalisée.

Lorsqu'une structure contient un défaut, ou des dommages préexistants, il est nécessaire de pouvoir prévoir les conditions dans lesquelles une fissure commencera à se propager et conduira ensuite à la ruine de la structure. C'est l'objectif de la mécanique de la rupture qui fournit des informations sur l'énergie mécanique dissipée par les mécanismes de rupture au voisinage de la pointe de la fissure (associée au facteur d'intensité de contrainte critique). La connaissance de grandeurs telles que le taux de restitution d'énergie, il est possible de savoir si la fissure se propage ou non, et de quantifier l'énergie dissipée lors de la rupture.

Dans les matériaux composites présentant un comportement élastique-fragile, l'utilisation des normes dérivées des matériaux métalliques est largement répandue car elles s'appliquent relativement bien et donnent des résultats fiables dans la mesure où la plupart des concepts de la mécanique de la rupture élastique linéaire sont valables (Figure 3). La plupart des études traitant de la rupture translaminaire en mode I (ouverture) des stratifiés multidirectionnels est basée sur la quantification de la ténacité des stratifiés unidirectionnels, en revanche très peu d'études sont dédiées aux stratifiés à renforts tissés. Des études expérimentales ont montré que les structures composites tissées présentent une résistance interlaminaire et une tolérance aux dommages plus élevées que les composites unidirectionnels, motivant ainsi l'intérêt pour ce type de matériau.

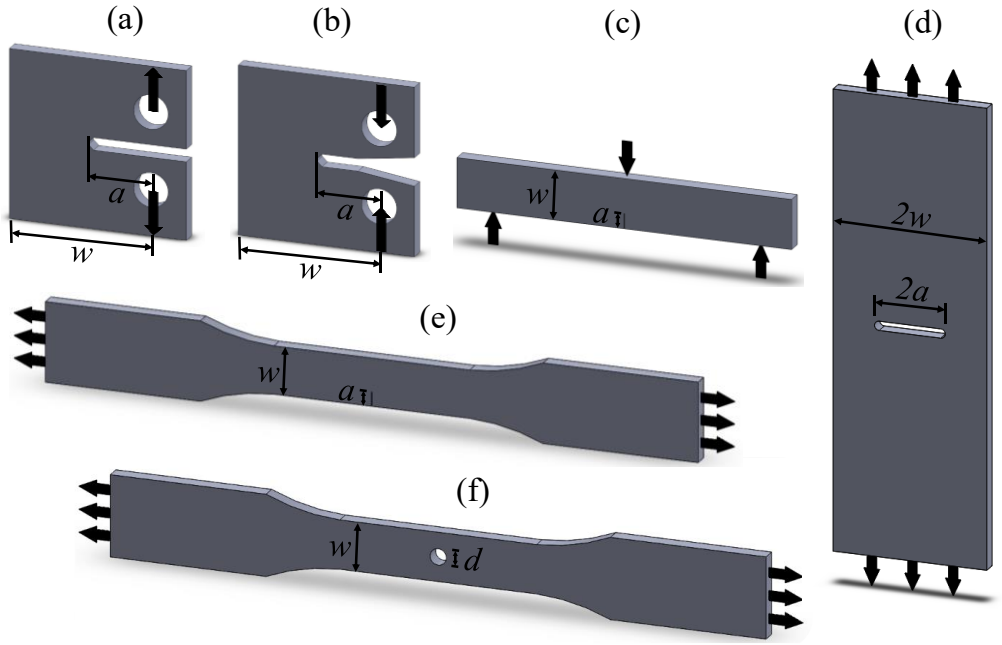

Figure 3. Configuration des éprouvettes utilisée pour étudier la rupture translaminaire dans les composites à matrice organique (CMO) : (a) Traction Compacte - (b) Compression Compacte - (c) Flexion Simple Entaille– (d) Traction avec entaille centrale (également utilisée en compression) - (e) Traction Simple Entaille – (h) Traction trouée non habitée (également utilisée en compression)

Lorsque la matrice polymère est ductile (le cas dans les composites à matrice thermoplastique PEEK), sa contribution à la réponse mécanique et au comportement à la rupture est accrue dans des conditions de température supérieure à sa température de transition vitreuse (T_g). Ainsi, les stratifiés à base de TP se caractérisent par une excellente ténacité intrinsèque (l'un de leurs

principaux avantages par rapport aux composites thermodurcissables). Celle-ci est associée à des mécanismes d'endommagement spécifiques qui sont des processus dissipatifs d'énergie conditionnant leur ténacité extrinsèque. Les ténacités intrinsèque et extrinsèque contribuent alors globalement à l'augmentation de l'énergie de rupture des composites TP.

La plupart des références de la littérature se concentre sur la rupture translaminaire des composites stratifiés associant renfort unidirectionnel et matrice polymère thermodurcissable. Aussi l'originalité de cette thèse réside dans l'étude de la rupture translaminaire au sein des composites à matrice thermoplastique PEEK renforcée un tissu de fibres de carbone. En outre, la rupture translaminaire dépend des conditions de chargement mécanique qui impliquent des mécanismes et une chronologie d'endommagement différents. Le comportement mécanique des CMO TP étant caractérisé par une forte dépendance aux conditions de température, ces travaux visent également à appréhender la contribution de la ductilité (phénomène thermiquement activé) aux mécanismes de rupture translaminaire à $T>T_g$.

Ce travail se décline selon deux axes (expérimental et numérique d'études du comportement à la rupture des composites à matrice thermoplastique PEEK renforcée par des fibres de carbone tissées (Figure 4). Dans la partie expérimentale, l'objectif est d'investiguer la rupture translaminaire à haute température ($T>T_g$) en fonction des conditions de chargement mécanique. Dans la partie numérique, un modèle implémenté dans le code Eléments Finis Abaqus/Explicit a été adapté afin de prédire le comportement en rupture translaminaire.

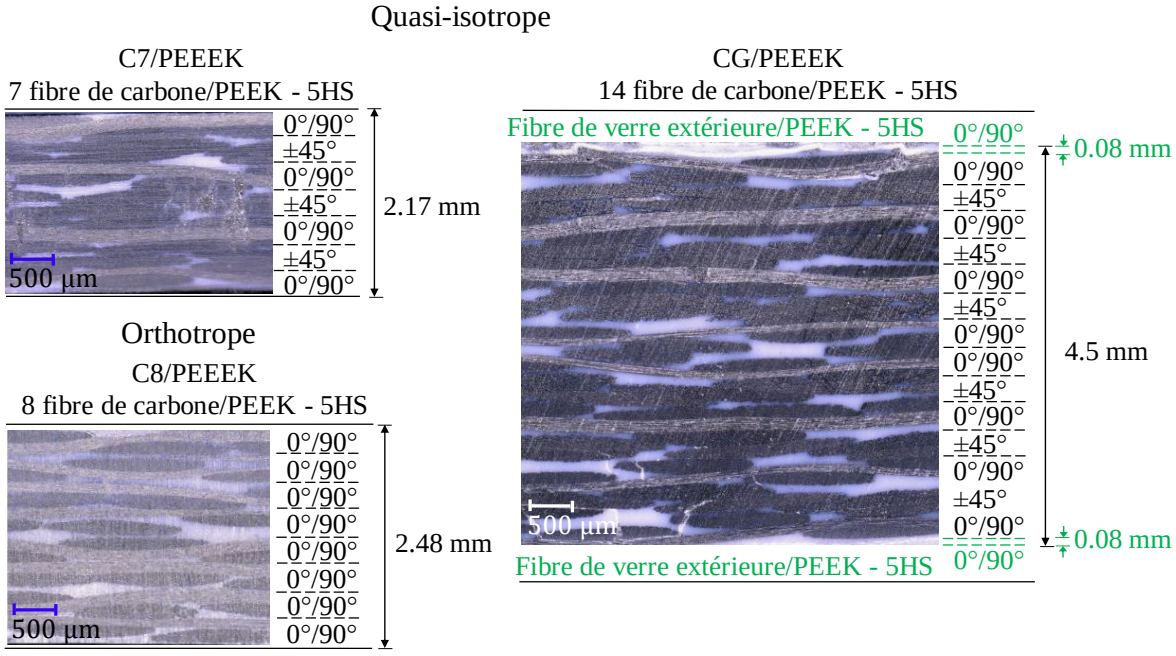

Figure 4. Séquence d'empilement et épaisseur des composites stratifiés tissés étudiés

Du point de vue expérimental, le but était de caractériser la rupture translaminaire de trois types de stratifiés thermoplastiques (Figure 4). En utilisant des éprouvettes de type Compact Tension (CT) et Compact Compression (CC) pour induire la rupture translaminaire en traction et en compression (Figure 5), ces stratifiés ont été testés à température ambiante (TA) et à 150°C (lorsque la ténacité et la ductilité de la matrice PEEK est exacerbée). Ces essais ont permis de

quantifier la ténacité à rupture translaminaire et d'obtenir les courbes G-R représentant l'évolution du taux de restitution d'énergie en fonction de la croissance de la fissure transverse. Ces essais reposent sur une mesure in situ de la propagation de la fissure, basée sur une technique de corrélation d'images numériques (CIN) adaptée à une caractérisation à haute température (dans une enceinte thermique) et un algorithme de binarisation. Il est ainsi possible d'évaluer l'influence de la séquence d'empilement et de la température sur le comportement en rupture de fibres en mode I en traction et en compression ; cela passe notamment par la mesure du taux de restitution d'énergie critique à l'initiation et l'énergie de rupture lors de la propagation.

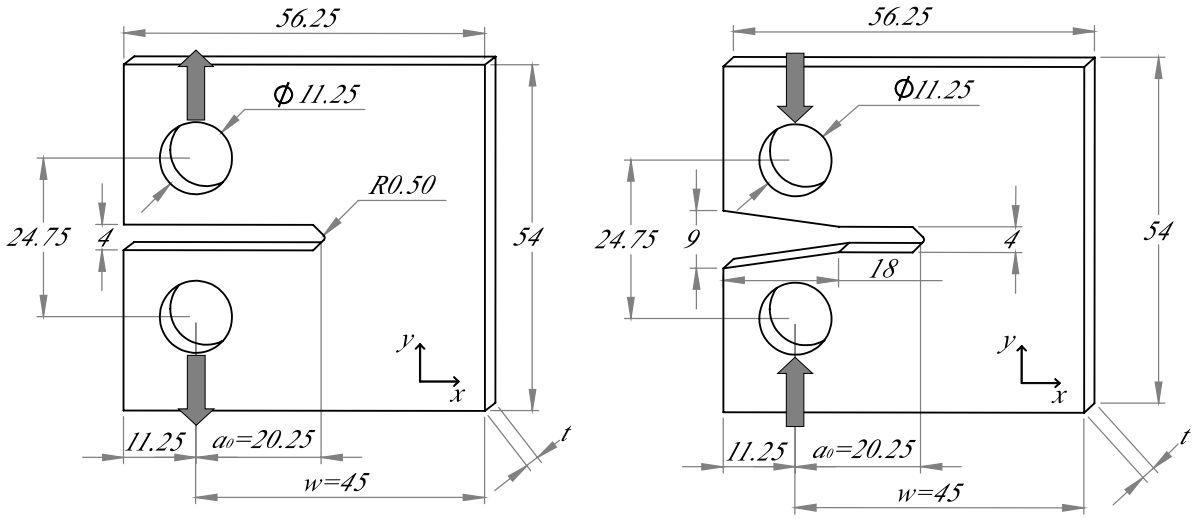

(a) Compact Tension - CT (b) Compact Compression - CC

Figure 5. Dimensions des éprouvettes (en mm) pour des essais de rupture de fibres : (a) traction - (b) compression

Une analyse post-mortem des zones endommagées a permis de mieux appréhender les mécanismes responsables de la tolérance aux dommages de composites à matrice TP et de comprendre l'influence de la température sur les mécanismes de déformation qui jouent un rôle dans la rupture translaminaire. Les essais de traction ont montré que dans un stratifié orthotrope, la zone de plasticité est très étendue en point de fissure en raison de son faible module de cisaillement (ténacité intrinsèque). La plasticité locale provoque également une ténacité importante liée à un écrasement localisé (matage) dans la zone d'application de la force (ténacité extrinsèque). Dans les stratifiés quasi-isotropes, l'épaisseur contribue à augmenter l'effort à l'initiation de la rupture et ralentit la propagation de la fissure. La rupture en compression par flambement plastique sur le bord opposé à l'entaille est facilitée par la ductilité accrue de la matrice PEEK à $T>T_g$. Les essais de compression révèlent une rupture en compression des fibres à 0° et la formation de bandes de flambement plastique. Comme dans le cas de la traction, le faible module de cisaillement induit une zone de plasticité importante, une ténacité extrinsèque importante et rend difficile l'évaluation du taux de restitution d'énergie critique dans les stratifiés orthotropes. A haute température ($T>T_g$), la rupture ductile associée à un écrasement localisé des plis est favorisée par la déformation plastique de la matrice PEEK.

L'évaluation du taux de restitution d'énergie critique à partir de la norme ASTM-399 s'est montrée pertinente pour les stratifiés tissés quasi-isotropes donnant des valeurs similaires comparativement à la méthode de la compliance (Figure 6). Pour les stratifiés fortement orthotropes, le calcul du taux de restitution d'énergie critique à partir d'un comportement global (la courbe force-déplacement) est liée à la dissipation d'énergie au niveau des points d'application des efforts associée à des mécanismes de plasticité plus importants en pointe de fissure. En traction, les courbes G-R tendent à converger vers une asymptote avec une valeur quasi constante (Figure 6), alors qu'en compression les courbes G-R ont une tendance à l'augmentation due à l'écrasement localisé qui se traduit par une contrainte de talonnage constante (Figure 7). Enfin, à $T>T_g$, il y a une augmentation modérée de la ténacité à rupture translaminaire en traction. L'épaisseur augmente la zone de coupure de fibres provoquant une augmentation de la ténacité à rupture translaminaire en traction. En traction, le taux de restitution d'énergie critique des stratifiés quasi-isotropes augmente avec l'épaisseur d'environ (19 à 50 kJ/m^2). En compression, l'épaisseur ne semble pas influencer la taille de la bande de flambement (qui est associée au diamètre de la fibre et au comportement mécanique en cisaillement de la matrice). La ténacité à rupture translaminaire en compression diminue fortement avec la température, car le ramollissement de la matrice dans les zones de chevauchement facilite le mouvement hors-plan des torons de fibres. En compression, le taux de restitution d'énergie critique est d'environ 30 à 40 kJ/m^2, avec une diminution spectaculaire avec la température. Pour les stratifiés orthotropes, le calcul du taux de restitution d'énergie critique devra être confirmé par un calcul local de type intégral J ou par thermographie infrarouge en raison du comportement à la rupture ductile.

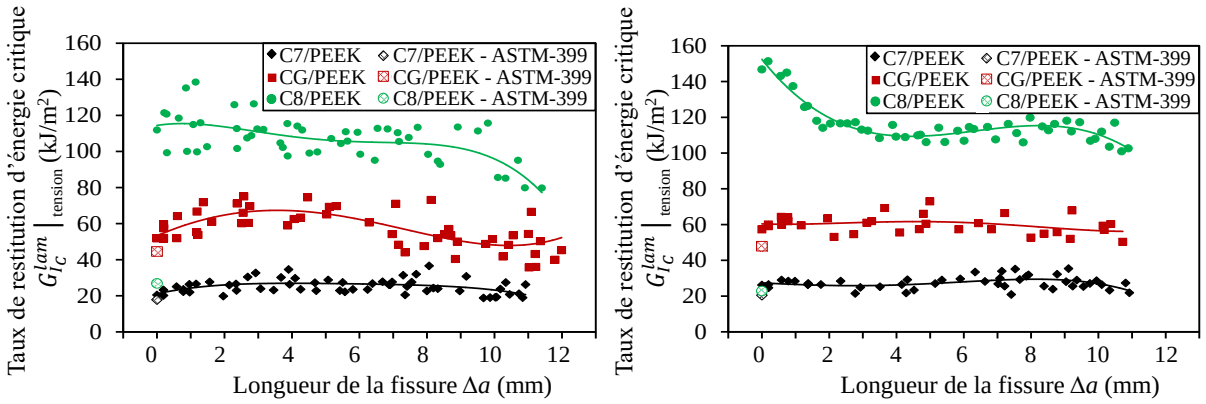

(a) Compact Tension à température ambiante

(b) Compact Tension à 150°C

Figure 6. Courbes G-R obtenues avec la méthode de la complaisance à partir des essais CT: (a) TA - (b) 150°C

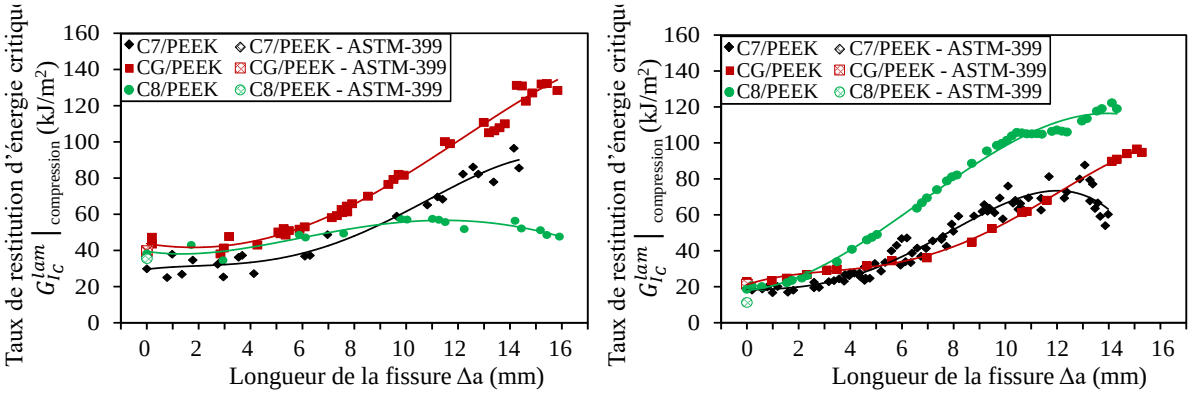

(a) Compact Compression at room temperature (b) Compact Compression at 150°C

Figure 7. Courbes G-R obtenues avec la méthode de la complaisance à partir des essais CC: (a) TA - (b) 150°C

Afin de mieux comprendre l'influence des effets de contraintes et de la température sur le taux de restitution d'énergie critique de composites hybrides quasi-isotropes à matrice PEEK renforcée par des tissu carbone/verre (CG/PEEK), deux géométries d'éprouvettes ont été testées avec des longueurs d'entaille initiale différentes. D'une part, des essais ont été réalisés à température ambiante (TA) et à 150°C ($T>T_g$) avec le but d'examiner l'influence de la température sur l'énergie de rupture. D'autre part, des essais ont été effectués sur des éprouvettes Single-Edge-Notch Tensile (SENT) et Single-Edge-Notch Bending (SENB) avec différents rapports a/w pour étudier l'influence de l'effet de contrainte sur la mesure du taux de restitution d'énergie critique (Figure 8). Les courbes G-R sont dérivées de la perte de complaisance et de l'évaluation de la croissance de la fissure transverse en accord avec la norme ASTM E1820.

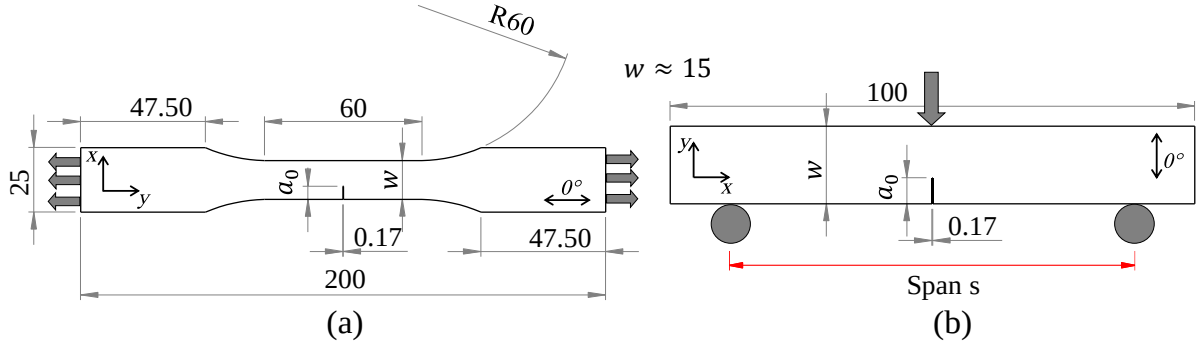

Figure 8. Géométrie des éprouvettes simplement entaillées (en mm) : (a) Traction (SENT) - (b) Flexion trois points (SENB)

La réponse mécanique macroscopique et le comportement à rupture du stratifié quasi-isotrope montrent que la fissure translaminaire est dominée par la rupture des fibres de carbone à 0°. La fissure transverse est auto-similaire (elle reste dans le plan de l'entaille initiale) dans les éprouvettes SENT et SENB. La ruine des éprouvettes résultant principalement de la rupture des fibres de carbone en traction (SENT) et en traction/compression (SENB), il s'avère que la température a très peu d'influence sur la ténacité à rupture translaminaire en mode I $K_{Ic}|_{tension}$ alors que la ductilité de la matrice PEEK est exacerbée à $T>T_g$. Il apparaît également que l'effet

de contrainte a très peu d'influence sur $K_{I_C}\,|_{\text{tension}}$ car les éprouvettes SENT et SENB ont pratiquement la même valeur moyenne (environ 45 MPa.$\sqrt{\text{m}}$ - Figure 9).

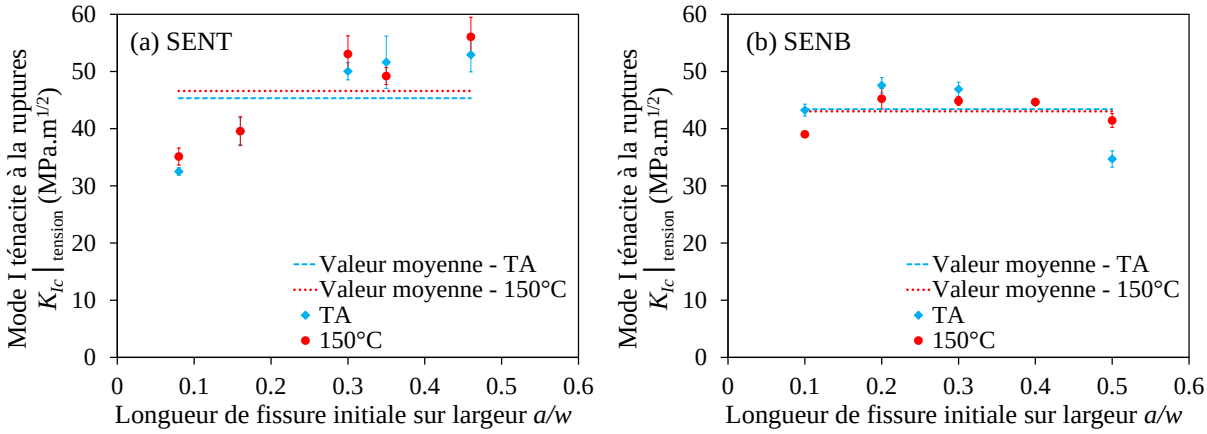

Figure 9. Influence de la température et de l'effet de contrainte sur la ténacité à rupture translaminaire en mode I des stratifiés QI CV/PEEK : (a) SENT - (b) SENB

Des courbes G-R « équivalentes » ont été obtenues à partir d'éprouvettes SENB pour différents rapports a/w (de 0.2 à 0.5). Ces courbes sont caractérisées par un plateau qui correspond au taux de restitution d'énergie critique en mode I lors de la propagation (Figure 10). L'augmentation tardive de la ténacité à rupture translaminaire résulte à la fois de la ténacité intrinsèque et extrinsèque qui sont spécifiquement améliorées à T>T_g. L'énergie de rupture est associée à la rupture fragile des fibres de carbone conduisant à un pontage progressif des fibres de verre (contribuant à la ténacité extrinsèque du matériau), alors que la matrice PEEK hautement ductile confère au matériau composite sa ténacité intrinsèque en raison d'une déformation plastique locale au pointe de fissure et autour des extrémités des fibres cassées (mécanismes dissipatifs d'énergie).

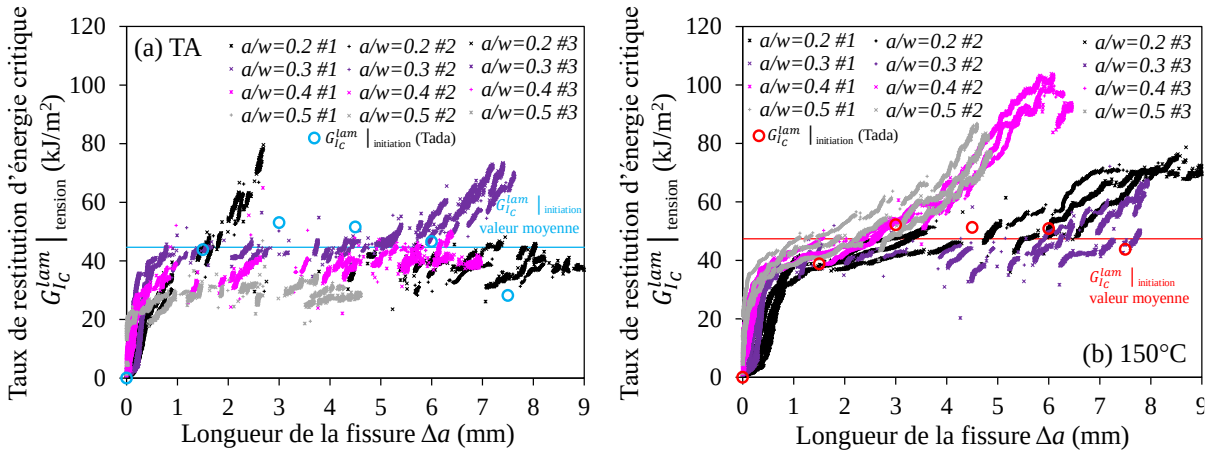

Figure 10. Évolution du taux de restitution de l'énergie critique avec la croissance de la fissure dans les éprouvettes SENB avec différents rapports a/w: (a) TA – (b) 150°C

Concernant le volet numérique de la thèse, le but était de développer des outils numériques capables de rendre compte du comportement à rupture des composites stratifiés à plis tissés. Il est donc possible de tester les paramètres liés à la rupture (par exemple le taux de restitution critique, la contrainte d'écrasement, la déformation à la rupture en traction et en compression) et de simuler les phénomènes qui induisent une plasticité élevée pour obtenir les valeurs valides pour fiabiliser la conception de structures composites. Un modèle numérique a été développé sur le code Eléments Finis Abaqus/Explicit dans le but de mieux comprendre l'influence de la séquence d'empilement et de l'épaisseur du stratifié sur le comportement à rupture. Ce modèle est basé sur des données expérimentales issues d'essais CT et CC permettant d'induire la rupture translaminaire en traction et en compression. Il prend en compte trois phénomènes physiques responsables de la dissipation de l'énergie mécanique: la rupture de fibre, la plasticité de cisaillement de la matrice PEEK dans le plan et la plasticité lors de l'écrasement en compression. Trois séquences d'empilement (un stratifié orthotrope et deux stratifiés quasi-isotropes, Figure 4) ont été considérées pour les deux conditions de chargement (CT et CC - Figure 11). Sous sa forme actuelle, seules les simulations à l'ambiante ont été réalisées. L'objectif principal de ce modèle était de développer une simulation numérique capable de reproduire le comportement mécanique macroscopique de stratifiés thermoplastiques à plis tissés avec différentes séquences d'empilement et épaisseurs. L'objectif était double: (1) mettre en évidence la dépendance de la rupture translaminaire à ces paramètres et (2) comprendre comment l'énergie mécanique est dissipée.

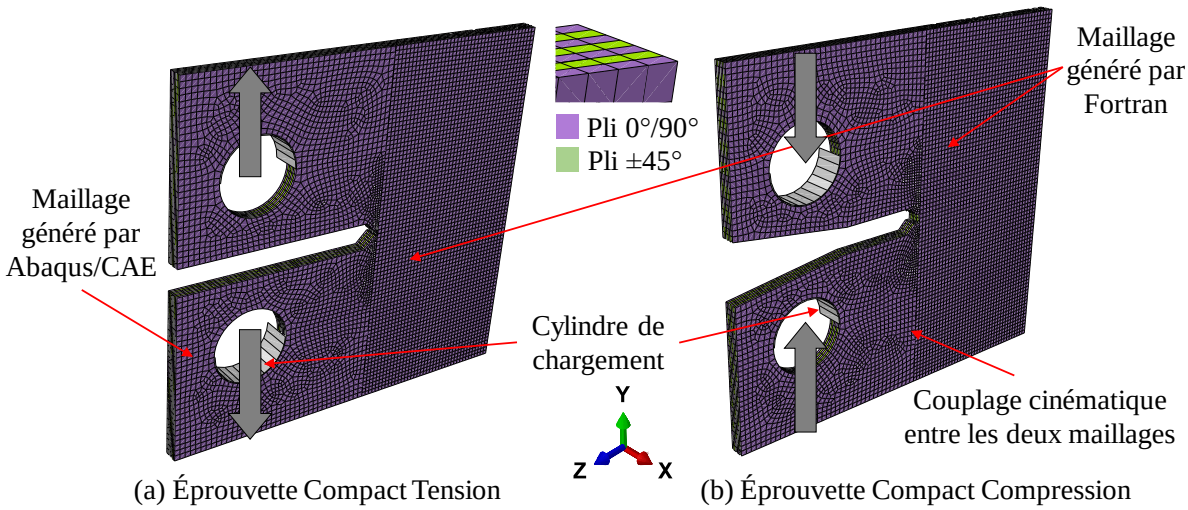

Figure 11. Maillage et conditions aux limites utilisées dans le modèle numérique pour des stratifiés constitués de 7 plis tissés

Ainsi, le modèle numérique développé permet une meilleure compréhension du comportement de rupture translaminaire en traction et particulièrement en compression, plus difficile à analyser en raison de la combinaison de phénomènes physiques complexes et simultanés (flambement, écrasement et rupture de fibres). Il est également très difficile de séparer la plasticité globale, qui induit une dissipation d'énergie globale, appelée ténacité extrinsèque, de l'énergie dissipée par la pointe de fissure, qui est la véritable dissipation d'énergie, appelée ténacité intrinsèque.

Les simulations des essais CT ont montré un bon accord avec les essais expérimentaux pour tous les stratifiés (Figure 12). Lors de la simulation du comportement à la rupture de stratifiés quasi-isotropes, différentes valeurs de ténacité à rupture translaminaire en traction ont été utilisées. La réponse mécanique macroscopique est caractérisée par un comportement quasi-linéaire. Par conséquent, il valide les observations expérimentales suggérant que la ténacité à rupture translaminaire en traction est une valeur dépendante de l'épaisseur. Les simulations réalisées sur des stratifiés orthotropes montrent que le comportement élastique-ductile est associé à une dissipation d'énergie importante résultant de la plasticité de cisaillement dans le plan. Cela suggère qu'une valeur de la ténacité à rupture translaminaire en traction à partir d'un calcul global basé sur les courbes force-déplacement n'est pas satisfaisante.

Après la validation en traction, des essais CC ont été simulés pour vérifier si la fissuration translaminaire en compression peut être décrite par le même modèle (Figure 13). Pour les stratifiés quasi-isotropes, seuls les stratifiés minces (environ 2mm) mettent en évidence un bon accord avec les données expérimentales du point de vue de la réponse mécanique macroscopique. Les stratifiés plus épais (environ 4mm) se traduisent par un plateau conduisant à un effet courbe R en raison d'une variation de volume importante lors de l’écrasement. Le modèle numérique actuel n'est pas en mesure de traduire cet effet. La simulation des stratifiés orthotropes sous chargement en compression ne décrit que partiellement le comportement élastique-ductile. Lorsque la première chute de charge apparaît, un plateau à charge constante est observé jusqu'à ce que la charge recommence à diminuer. Ceci suggère que les déplacements hors-plan ne sont pas convenablement pris en compte par le modèle.

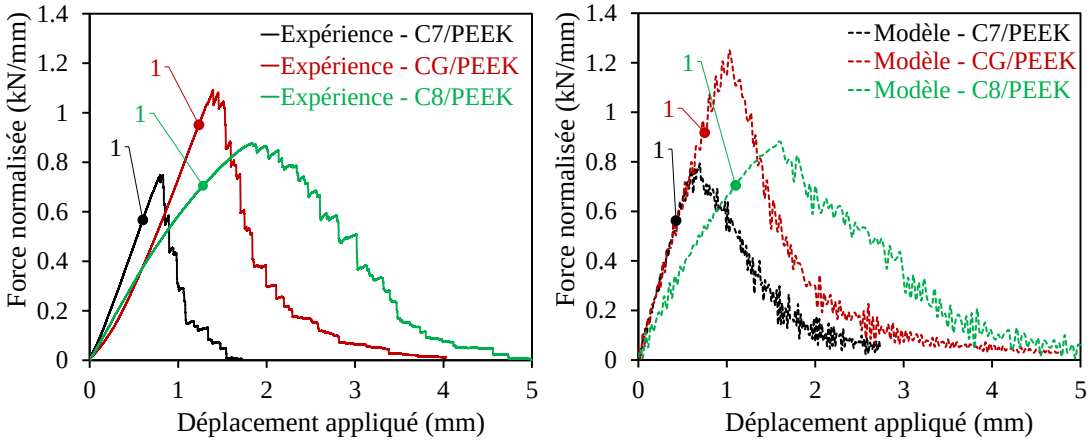

C7/PEEK: [(0/90),(±45),(0/90),(±45),(0/90),(±45),(0/90)] - 2.17 mm d'épaisseur
CG/PEEK: $[(0/90)_G,(0/90),(\pm45),(0/90),(\pm45),(0/90),(\pm45),(0/90)]_S$ - 4.5 mm d'épaisseur
C8/PEEK: $[(0/90)]_8$ - 2.48 mm d'épaisseur

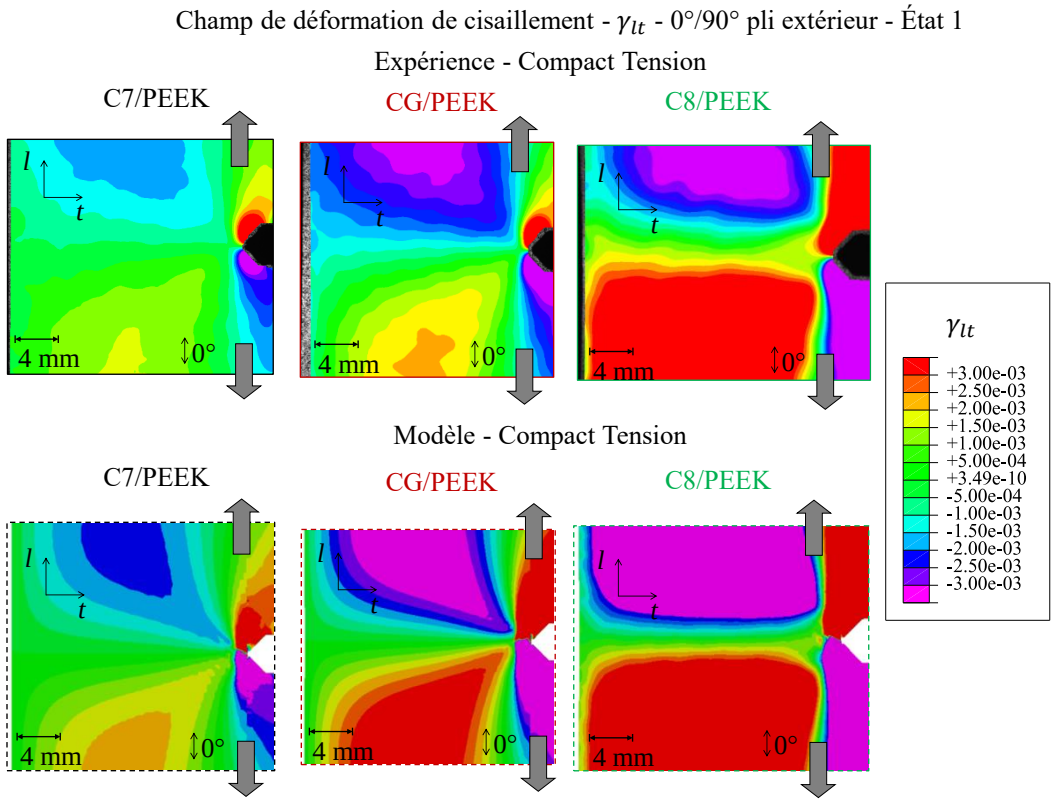

Figure 12. Comparaison expérimentale/numérique des trois stratifiés en traction : courbes de force normalisée par l'épaisseur en fonction du déplacement et champ de déformation de cisaillement dans le plan à la surface du stratifié avant le début de la fissuration translaminaire (état 1)

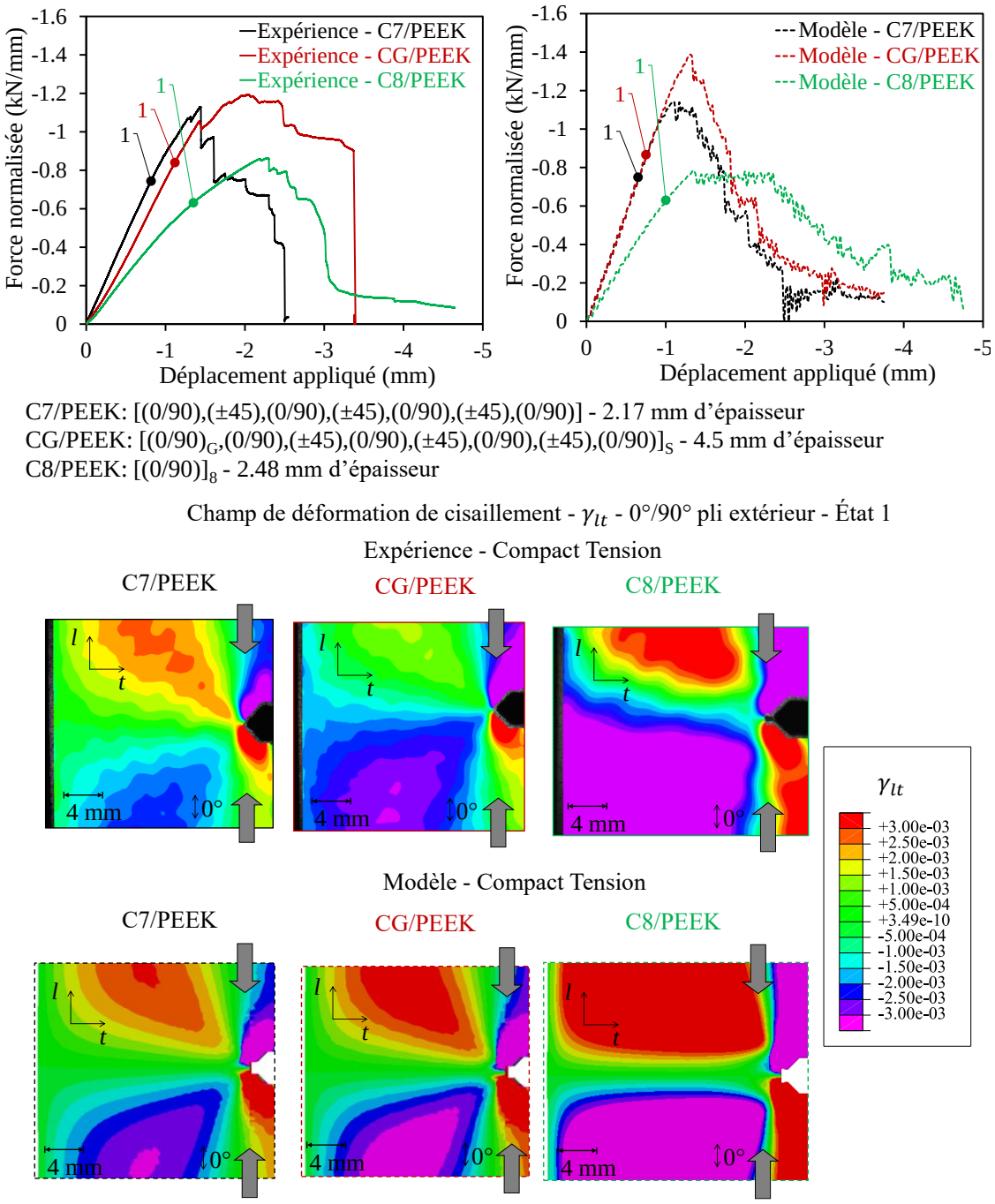

Figure 13. Comparaison expérimentale/numérique des trois stratifiés en compression : courbes de force normalisée par l'épaisseur en fonction du déplacement et champ de déformation de cisaillement dans le plan à la surface du stratifié avant le début de la fissuration translaminaire (état 1)

Enfin, le modèle présenté dans cette thèse se révèle efficace pour étudier la fissuration translaminaire en traction dans les composites stratifiés thermoplastiques à plis tissés, ce modèle présente les caractéristiques suivantes : respect de la direction des fibres dans le drapage du stratifié, un nombre relativement limité des paramètres du matériau et une variable d'endommagement traduisant la propagation de la fissure. Pour améliorer les capacités prédictives du modèle dans le cas de chargements en compression, d'autres phénomènes

physiques tels que l'effet courbe R et le déplacement hors-plan doivent être pris en compte dans la formulation du modèle. Comme cela a été mis en évidence par la partie expérimentale, les essais SENB sont caractérisés par une propagation stable des fissures. De plus, dans ces conditions de chargement, on observe une combinaison d'écrasement local des bords supérieurs dans la zone de contact et de rupture de fibres en compression lors de la propagation. La simulation des essais SENB est représentative d'états de contrainte complexes (traction-compression) au sein des stratifiés. Ainsi, ils semblent pertinents pour valider les capacités prédictives du modèle numérique appliqué à des composites stratifiés à matrice TP renforcée par des tissus de fibres. Les résultats préliminaires ont montré que le modèle numérique est capable de décrire le comportement mécanique macroscopique des essais SENB (Figure 14). Au-delà de la comparaison avec les résultats expérimentaux (en termes de valeurs G_{I_C} et de courbes G-R), ce modèle numérique est complémentaire de la base de données expérimentales et pour la compréhension des mécanismes d'endommagement. En effet, il donne un aperçu du rôle joué par différents mécanismes d'endommagement ainsi que de la contribution de l'orientation des plis dans les processus dissipatifs.

En conclusion, la mécanique de la rupture et la modélisation par éléments finis offrent un cadre très efficace pour mieux comprendre le comportement à rupture translaminaire des composites stratifiés à plis tissés et matrice PEEK ainsi que l'origine de leur tolérance aux dommages. Cependant, les valeurs caractéristiques de la ténacité à rupture et les courbes G-R correspondantes peuvent être difficiles à déterminer et à interpréter. Enfin, ces travaux de thèse mettent en évidence les limites des outils de la mécanique de la rupture appliqués aux structures composites stratifiées.

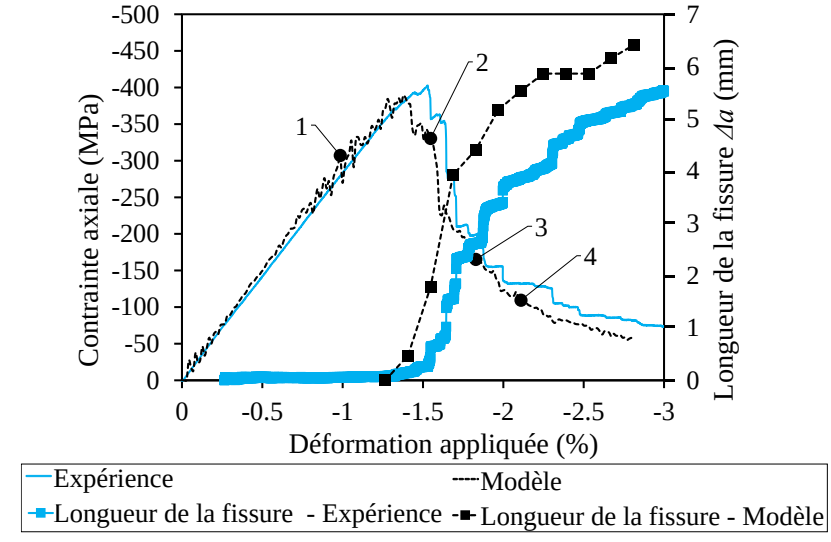

(a)

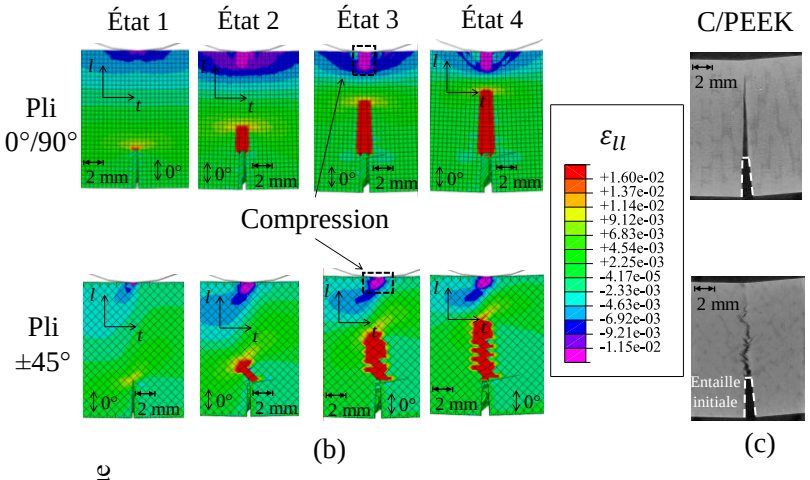

(b) (c)

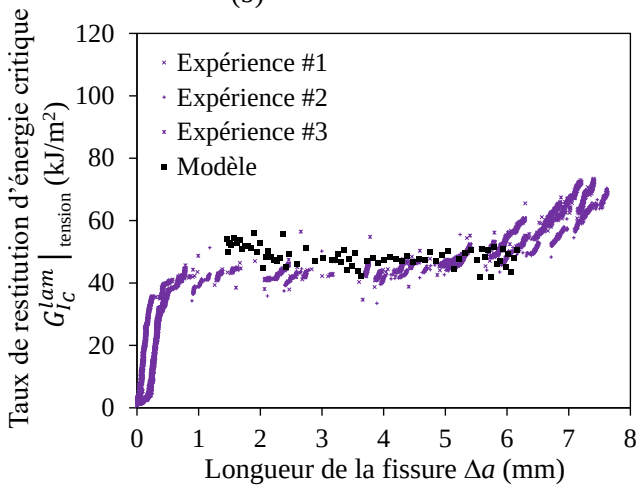

(d)

SENB CG/PEEK – $a/w = 0.3$

$[(0/90)_V,(0/90),(\pm45),(0/90),(\pm45),(0/90),(\pm45),(0/90)]_S$ - 4.5 mm d'épaisseur

Figure 14. Simulation numérique des essais SENB (ratio $a/w = 0.3$) à TA: (a) Comparaison avec les essais expérimentaux - (b) Evolution de la Fracture Process Zone dans les différents plis du stratifié - (c) Observations tomographiques post-mortem des échantillons SENB - (d) Evolution du taux de restitution d'énergie avec la croissance de la fissure

Contents

Notation

Lower case Roman letters

a	crack length
a_0	initial crack length
a/w	initial notch length to specimen width ratio
d	damage variable
f_l	plastic function in the longitudinal direction
f_t	plastic function in the transverse direction
f_{lt}	in-plane shear plastic function
$f(a/w)$	geometric correction function for a specimen of finite width
r_{pl}	plastic rotational factor
s	span between the support points
t	specimen thickness
w	specimen width as defined in relevant figure

Upper case Roman letters

C	compliance
C_i	crack opening compliance
C_I	orthotropic elastic coefficient in plane-stress conditions in mode I
E_x	Young's modulus in the x direction
E_y	Young's modulus in the y directions
E_z	Young's modulus in the out-of-plane direction
F_T	function associated with damaged and undamaged areas
F^u	maximum force borne by the specimen at failure
G_{lt}, G_{lz}, G_{tz}	shear modulus of the material
G_{xy}	shear modulus of the laminate
$G_I^{l,C}$	Strain energy release rate in compression in the longitudinal direction
$G_I^{t,C}$	Strain energy release rate in compression in the transverse direction
$G_I^{l,T}$	Strain energy release rate in tension in the longitudinal direction
$G_I^{t,T}$	Strain energy release rate in tension in the transverse direction
$G_{I_c}^d$	fracture toughness in mode I of the resin

$G_{I_C}^{f,C}$	critical strain energy release rate in compression
$G_{I_C}^{f,T}$	critical strain energy release rate in tension
$G_{I_C}^{lam}$	mode I critical strain energy release rate of the laminate
$G_{I_C}^{lam} \mid_{\text{compression}}$	mode I critical strain energy release rate of the laminate in compression
$G_{I_C}^{lam} \mid_{\text{tension}}$	mode I critical strain energy release rate of the laminate in tension
$G_{II_c}^{d}$	fracture toughness in mode II of the resin
H_{ij}	orthotropic stiffness coefficients
K_T	stress concentration factor
K_{I_C}	mode I critical stress intensity factor
P	load
P_c	critical load ensured at crack initiation
P^u	ultimate load
S	specimen cross section
V	volume of the element

Lower case Greek letters

γ_{lt}^{p}	plastic plane shear strain
δ	displacement
ε_0^C	failure strain in compression
ε_0^T	failure strain in tension
ε_1^C	strain in fiber direction at final failure in compression
ε_1^T	strain in fiber direction at final failure in tension
$\varepsilon_{bending}$	bending strain
ε_{ij}	components of strain tensor
ε_l^p	plastic strain in longitudinal direction
ε_t^p	plastic strain in transverse direction
η	strain hardening exponent
λ	strength index or strength coefficient
$\nu_{lt}, \nu_{lz}, \nu_{tz}$	Poisson's ratios of the material
ν_m	crack opening displacement at notched edge
ν_{xy}	Poisson's ratio of the laminate
ρ	radius of the notch at the crack tip
σ	remote applied stress

$\sigma_{bending}$	bending stress
σ_C	critical remote applied stress ensured at crack initiation
σ_{ij}	components of stress tensor
σ^{crush}	crushing stress
σ^u	ultimate strength
σ_t^d	ultimate strength of the resin in transverse
σ_{lt}^d	ultimate strength of the resin in shear direction
τ_{lt}	in-plane shear stress
τ_{lt}^0	in-plane shear yield stress

Upper case Greek letters

Δa	change in crack length
ΔF	difference in the applied tensile loads
Δ_{pl}	plastic component of load point displacement
$\Delta\varepsilon_x$	difference in the longitudinal strains obtained from a blade-extensometer

Chapter I: General introduction

I.1 Scientific and problematic issues

To illustrate the general problematic of these PhD works, we can do a quick exercise, which consists in listing some illustrative images by typing the following keywords in an internet search engine: damage - rupture - crack - composites - aeronautics. Most of the results refer to damage induced by impacts with birds in flight or obstacles during the aircraft parking-phase.

Curiously, there is very little mention of cracked parts in service under normal conditions of use. This is surprising because it is known that all aircraft present micro-cracks or even manufacturing defects, particularly in areas subject to high mechanical stresses or around holes in riveting or bolting assembly areas. A few examples of aircraft's parts are given in Figure I.1.

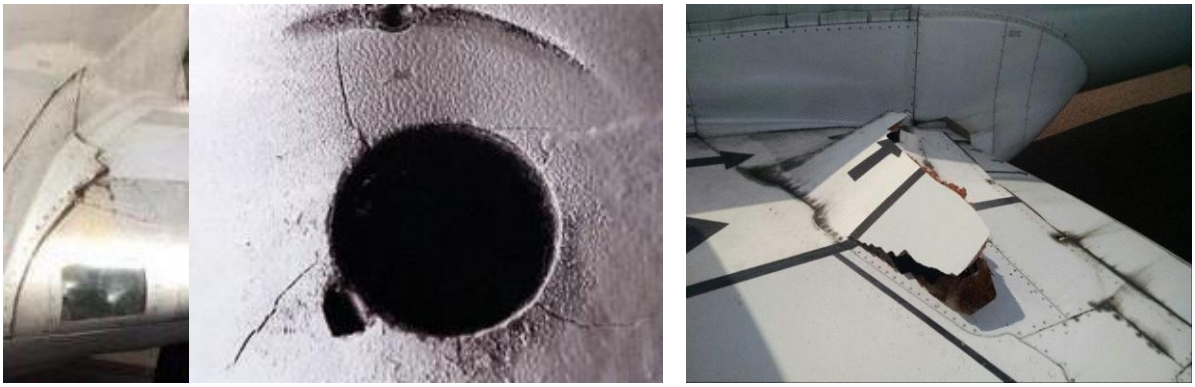

Figure I.1. Illustration of crack initiation and propagation within aircraft's composite parts in service conditions (Photo credit: DGAC).

It is also not possible to dissociate the damage mechanisms within aircraft's parts from their constitutive materials. Reinforced composite materials have been widely used in many industrial fields for more than 40 years. Most applications combine a polymer matrix with fibrous reinforcements. The design of polymer matrix composites is now well mastered, and many failure criteria have been implemented in industrial calculation codes. Thermosetting-based (TS) composites have been extensively used for aeronautics applications purposes. Aircraft manufacturers are now asking themselves the question: which composite materials for tomorrow's aircrafts? Along with environmental issues, development of new manufacturing techniques, costs reduction, recycling possibilities and certifications requirements, there has been a growing interest lately to use high performance thermoplastic (TP) matrix in aeronautics. Today, in a global market monopolized by TS matrix composites, TP matrix composites represent only 20% of the total number of composites. However, their development is considered twice as great as that of the TS composites. Most TPs have poor mechanical properties at high temperature and 90% of TP matrix composite applications concern short fiber reinforced thermoplastics (PA, PP, PC, PET, PPO). However, the use of fiber-reinforced thermoplastics is not a novelty since the 70's, GMT (Glass Mat Thermoplastics) have emerged with the development of a new manufacturing technique (stamping) in the automotive industry. In the 80's, high performance TP resins such as the PEEK, PES, PI, PEI and PPS have been

combined with long carbon fibers to cutting-edge applications in aeronautics, aerospace and the military field. Thus, these materials have been widely studied in the 1990s, as evidenced by a rich literature on that subject, with a particular focus on the behavior of carbon fibers reinforced PEEK composites. At the same time, several theses proposed an assessment of the mechanical performances of composites carbon/PEEK for aeronautics [1-4]. In the early 2000s, TP resins returned to a relative anonymity. TP resins are back in the spotlight with the development of the A380, which integrates several parts in TP composites with in particular the wings leading edges. Consisting of an assembly of 8 composite glass/TP parts measuring 26 meters, the use of this type of material allows for a weight gain of 400 kg. The revival of composites is launched so that in 2004, the journal “Industrie et Technologies” titled: "Dare thermoplastic composites!"

In addition to the nature of the constitutive materials, the type of reinforcement (in the form of fillers, long or short fibers), the architecture (unidirectional, woven, mat) and the manufacturing method (allowing to obtain solid or laminated parts) are characteristics that condition the main damage mechanisms within fibrous composites (Figure I.2): matrix cracking (longitudinal and transverse), fiber breakage, fiber/matrix debonding and delamination (interlaminar cracking).

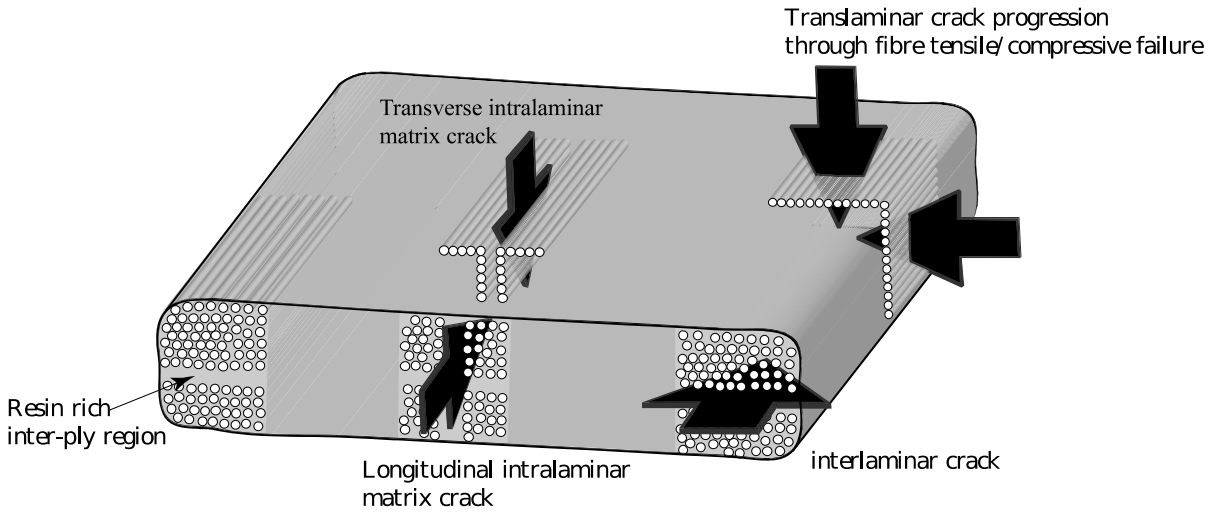

Figure I.2. Primary damage mechanisms observed in unidirectional fiber reinforced polymer matrix composites [5].

These complex damage mechanisms may have different causes (Figure I.3): manufacturing defects, maintenance or service conditions (normal or severe). It is therefore of the utmost importance to determine the criticality of these defects and to know their influence on the short- and long-term behavior of the composite parts in further service conditions.

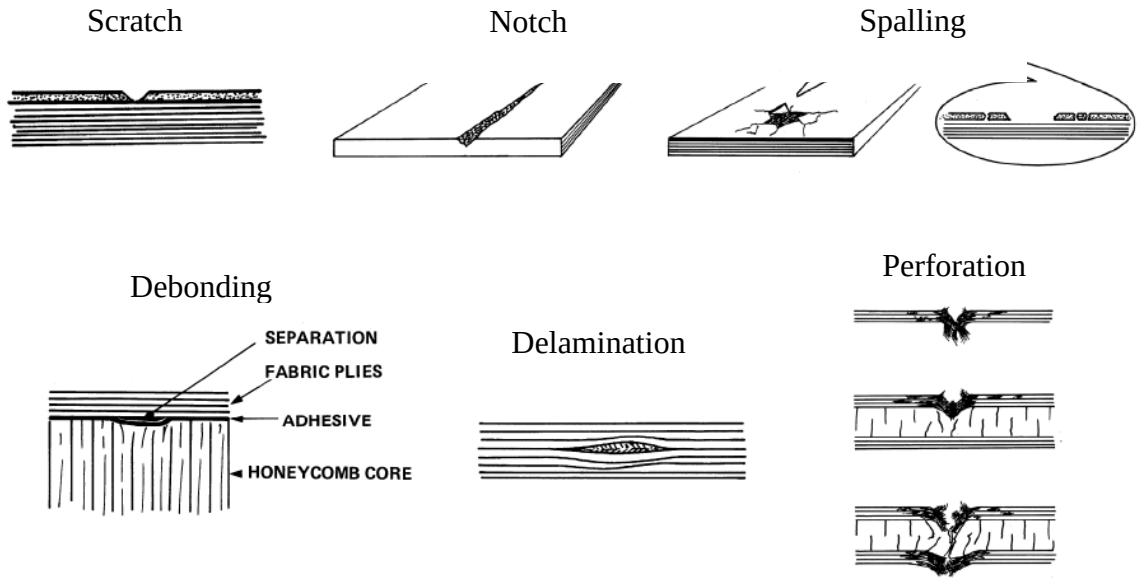

Figure I.3. Different types of defects within composite materials: manufacturing defects, maintenance or service conditions (normal or severe) [6].

In most service conditions, a "binary" elasticity-fracture approach to dimensioning is not sufficient because damage (generally similar to a crack) may appear in a localized and non-critical manner. It is then necessary to know how this damage is initiated and propagated within fiber-reinforced composite materials, in which the growth of the damage will be potentially thwarted by local mechanisms (presence of fibers or matrix near the crack) which depends strongly on the characteristics of the material and especially on the loading conditions. This problem responds to the damage tolerance of composite materials, which should be quantified at different stages of failure (initiation and propagation).

Predicting the initiation and propagation of a type of damage is a major issue in assessing the damage tolerance of composite materials. Linear Elastic Fracture Mechanics (LEFM) is an approach classically adopted based on the concepts developed for homogeneous isotropic materials (typically metals). In composite materials, these three modes of failure (I: opening, II: in-plane shear, III: out-of-plane shear) are found for the different types of damage, so that the standards developed for metallic materials can be adapted and transposed in some cases. This will be further detailed in Chapter II.

When it comes to fracture behavior, the main differences between metals and composites result from the highly heterogeneous and anisotropic nature of composite materials. The fracture behavior (damage scenario and growth) of composite materials will depend on the location of the defect within the composite mesostructure. For example, both crack initiation and propagation will be significantly influenced by the presence of matrix-rich areas by means of local plastic deformation (Figure I.4). This mechanism contributes to the dissipation of mechanical energy brought to the material, what usually results in increasing its toughness.

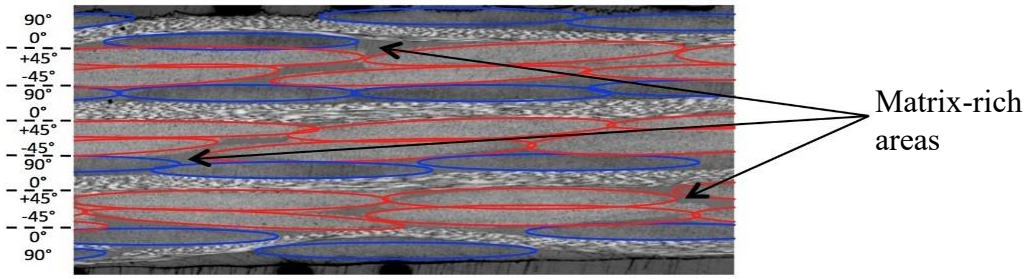

Figure I.4. Through-the-thickness microscopic observation of a quasi-isotropic carbon woven-fibers reinforced PPS laminates showing the presence of matrix-rich areas within the mesostructure [7].

Most of the studies dealing with the fracture mechanics of composite materials focus on multi-layer (or laminated) composites. On the one hand, there are numerous references on the application of fracture mechanics tools to interlaminar cracking, associated with the most critical damage mechanism in laminated composites (the delamination of the laminate plies). This specific issue has been well addressed in the literature and will not be presented here. On the other hand, the number of references dealing with fiber failure is limited. The literature review on that particular subject will be presented in Chapter II. This is the originality of the present work along with the study of woven-fibers reinforced TP-based composites.

I.2 Aim of the thesis and objectives of the study

Among the quantities generally used in engineering to characterize the fracture behavior of materials are classically the critical stress intensity factor K_c (or fracture resistance) and the strain energy release rate (denoted G or J depending on whether the material behavior is elastic or ductile) which represents the mechanical energy required to induce the growth of a crack (or fracture driving energy), according to the approach initially proposed by Irwin in the 1950s.

Contrary to the case of interlaminar fracture (between the plies of a laminate), translaminar fracture is relatively little addressed by fracture mechanics approaches because composites are not dimensioned in this case. Most of the work on the subject are based on the extension of the tools developed for metallic to polymeric materials, as previously mentioned.

The present work focuses on the failure of fibers in composite laminates with a PEEK (Polyether ether ketone) thermoplastic matrix reinforced by long carbon fibers. This failure mechanism is also called translaminar failure. The fracture mode then depends mainly on the stacking (or draping) sequence of the laminate, i.e. the orientation of the fibers in each ply. The spatial distribution of the fibers will then condition the ability of the material to dissipate mechanical energy during the growth of damage within a laminate composite. Thus, the methods to be implemented to evaluate this energy dissipation during rupture will be oriented by the contribution of the different plies to the translaminar fracture (Figure I.5). Three characteristic stacking sequences classically rule the thermo-mechanical response of composite laminates:

- Quasi-isotropic with plies at 0°, 90°, +/-45°: the macroscopic mechanical response is elastic with a quasi-brittle fracture. The approaches developed for metallic materials with isotropic behavior can be applied (LEFM).

- Orthotropic with plies at 0° and 90°: the macroscopic mechanical response is also elastic with a quasi-brittle fracture. In this case, the specific contribution to the fracture of the 0° and 90° plies is investigated but an important shear deformation can appear due to the poor shear resistance of the laminate.

- Oriented plies at +/-45°: the macroscopic mechanical response is elastic-ductile. The approaches developed for metallic materials with ductile behavior can be applied (Elastic Plastic Fracture Mechanics - EPFM).

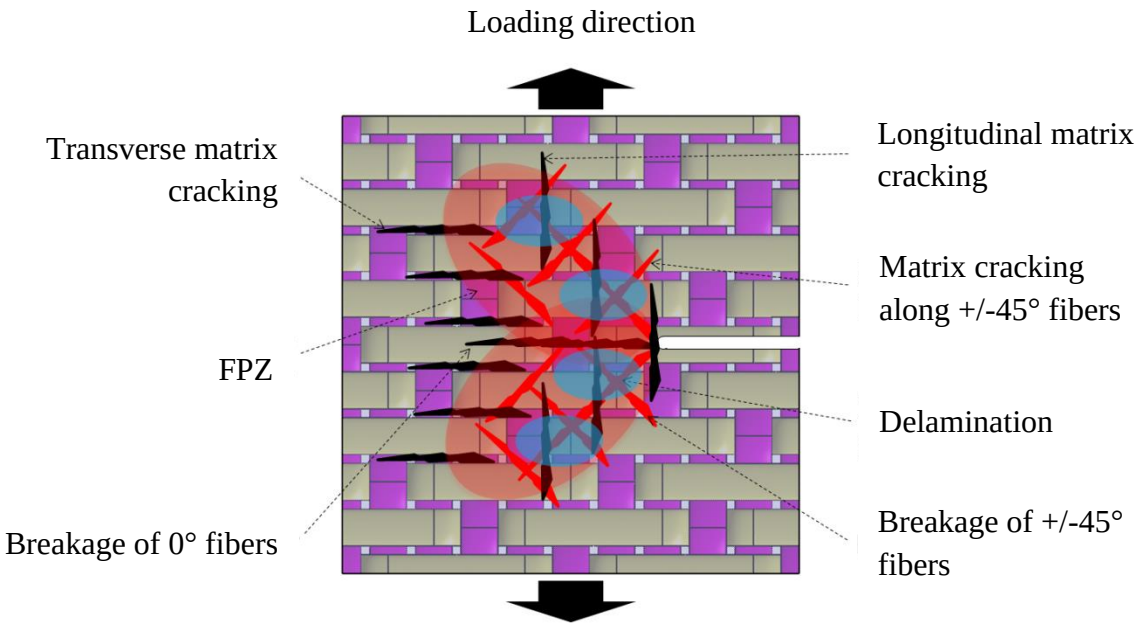

Figure I.5. Area of damage growth (Fracture Process Zone) and main damage mechanisms in woven-ply composite laminates – Single Edge Notch tension case [8].

Depending on the loading conditions (mechanical loading and temperature conditions), the general objective of this PhD is to study the translaminar fracture behaviour at high temperature in PEEK-based woven plies laminates. This will be achieved in different steps:

- (i) to characterize the translaminar fracture behaviour by testing different experimental techniques

- (ii) to quantify the material fracture toughness (associated with a given fracture mode), crack growth, evolution of the strain energy release rate

- (iii) to simulate the translaminar fracture behavior

I.3 Organization of the thesis

This thesis consists of experimental studies completed by numerical simulations. This first chapter allowed introducing the issue of the translaminar failure in composite structures. Afterwards, the aim and study objectives of the thesis were presented. The rest of the thesis consists of five chapters.

In the second, a literature review focuses on translaminar failure will be presented according to the loading conditions (tension and compression) with a particular focus on the parameters (temperature, stress rate, nature of the matrix, reinforcement architecture) influencing the mechanical energy dissipation during translaminar failure.

In the third and fourth chapters, the methods for experimental measurement of translaminar failure will be detailed. In practice, these methods are based on specimens with a specific geometry (depending on the mode of solicitation: tension, compression, bending) and a pre-defect (notch). The interest of a pre-defect machined in the material is to concentrate the stresses in a damage growth zone (Fracture Process Zone - FPZ) which will foster different dissipative damage mechanisms (see Figure I.5). These mechanical energy dissipation modes are mainly related to the matrix fracture mode (brittle or ductile). Thus, the methods developed also depend on the overall mechanical response (elastic-brittle or elastic-ductile) during composite failure. Chapter III and Chapter IV mostly differ by the loading conditions: Compact Tension and Compact Compression (Chapter III) and Single-Edge-Notch Bending (Chapter IV).

Chapter V deals with translaminar cracking and damage propagation modelling in PEEK-based woven-ply laminates. A numerical model will be adapted in order to simulate the translaminar cracking on Compact Tension (CT) and Compact Compression (CC) specimens. The three most common physical phenomena responsible for the dissipation of mechanical energy during the translaminar fracture in these specimens will be simulated: fiber failure, plane shear plasticity and crushing plasticity.

The last chapter will conclude this thesis by recalling the main conclusions and presenting the prospects opened by this work.

Chapter II: Literature review - Positioning of the research work

Nowadays, the composite materials are used in many fields. In particular, they are attractive for applications in aeronautics, automobiles, wind energy and sports articles. The generalization of organic matrix composites in aeronautical structures poses a problem at different levels: design, manufacture, assembly and control of reliability in service. When the structure contains a defect, or some pre-existing damage, it is necessary to understand and quantify the fracture mechanisms.

In the first part of this chapter, a brief reminder on composite materials and the main failure mechanisms taking place in Fiber Reinforced Polymer (FRP) composites will be presented. A few methods to determine the translaminar fracture toughness in composite materials will be introduced. Additionally, a brief overview of the literature dealing with the experimental characterization of translaminar fracture toughness applied to UD FRP composites under tensile and compressive loadings will open the way to the study of translaminar fracture toughness in woven-ply laminated composites.

Chapter II outline

II.1 Composite materials

A composite material is a solid and heterogeneous material consisting of two or more combined constituents that are combined at a macroscopic level and that are not soluble in each other. This association allows the creation of a new material having performance superior to the initial constituents alone, making possible an improvement in many properties: strength, stiffness, fatigue and impact resistance, thermal conductivity, corrosion resistance, etc… Generally, a composite material is a material composed of a resistant material that is called the reinforcement and a binding material that is called the matrix. The reinforcement is a material having high mechanical performance in terms of stiffness, strength and/or hardness, which ensures the mechanical rigidity of the material. The matrix allows the transmission of external mechanical stresses to the fibers and insures the geometry of the assembly as well as the protection against harsh environments.

II.1.1 Reinforcement

The reinforcement is classically dispersed in the composite material in form of particles or fiber. However, the most used commonly reinforcement are presented in form of fibers. Fiber Reinforced Composite (FRC) are either long fibers (continuous) or short fibers (discontinuous) which can be distributed in a random or preferred orientation, thus giving an anisotropic behavior to the material. The reinforcement is also defined according to its nature (natural, mineral, artificial or synthetic) and its architecture.

Long fibers are usually supplied in the form of bundles called strands. A fiber bundle consists of multiple continuous filaments that run along the length of the strand, each filament having a diameter of few tens of micrometers. The spatial arrangement of fibers provides different reinforcement architectures, as shown in Figure II.1:

- Unidirectional reinforcement fabric has the continuous fibers in just one direction.
- The cross-ply non-crimp fabric is a bi-directional assembly where the continuous fibers run typically in two perpendicular directions (0° and 90°) without crossing each other, thus defining the warp and weft directions. The absence of intersection between the cross-ply eliminates the effects of shearing.
- The woven fabric is a bi-directional assembly where the warp and weft strands intersect alternately. The warp strands run along the length of the fabric, in an upward or downward reciprocating motion and the weft strands follow the defined pattern of movement, creating a specific fabric structure. The most used woven fabrics are taffeta, twill and satin.
- Multidirectional fabrics are woven in three dimensions, they are characterized by the number of weaving directions: 3D, 4D, etc. In addition to the warp and weft directions in the plane, there is a fibrous reinforcement through the thickness. The objective of the additional fibrous reinforcement is to improve the characteristics of the composite, for example its impact behavior by increasing its resistance to delamination.

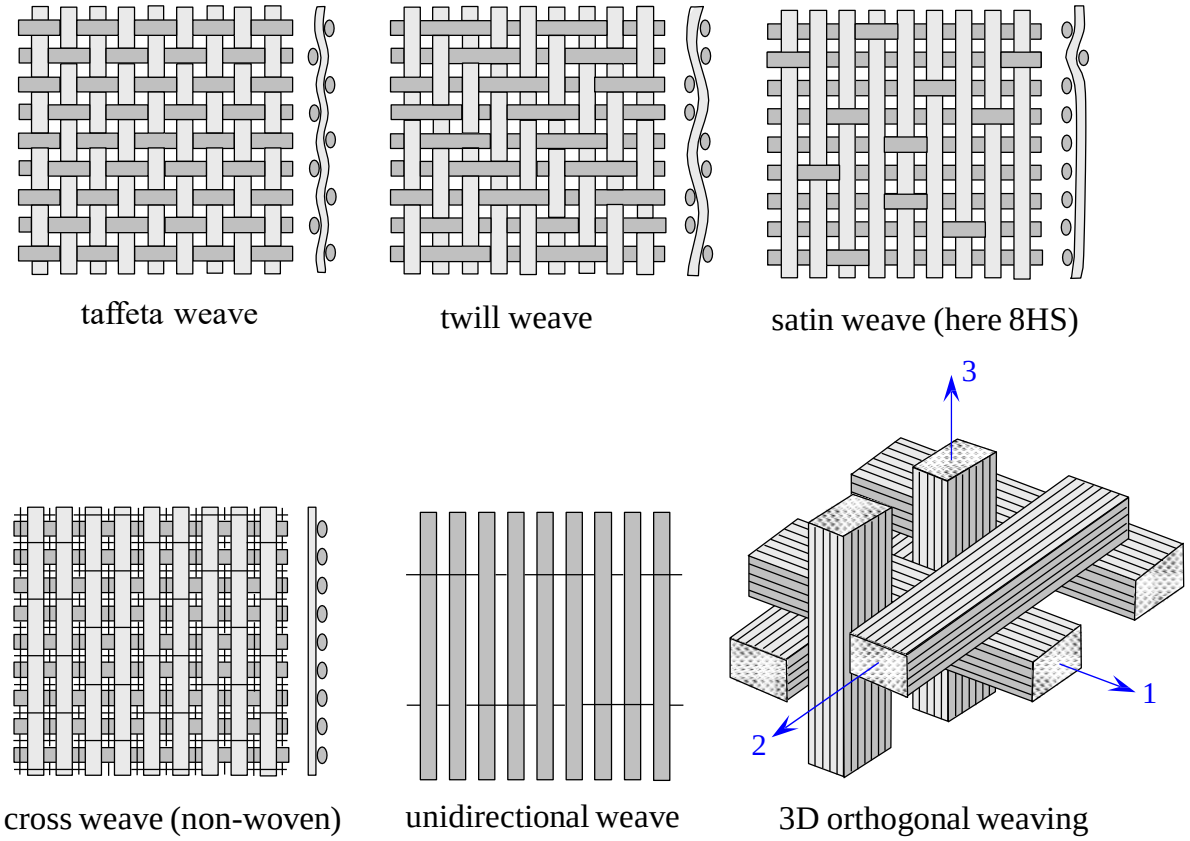

Figure II.1. The main reinforcement architectures used for weaving fabrics in fibrous composites [9].

II.1.2 The matrix

The matrix is a homogeneous material in which the reinforcement is immersed and whose purpose is to ensure the cohesion of the reinforcement. It makes it possible to bond the fibers together and to preserve the geometric arrangement of the reinforcement giving the desired shape geometric to the material. The matrix also protects the fibers from aggressive external environments.

Composite materials are classified according to the nature of their matrix. Three large families are usually distinguished:

- Polymer matrix composites (PMCs) are the most used on an industrial scale, because of their high specific properties (in relation to their density) and their unit costs sufficiently reduced to be able to be produced in large series. However, this type of composite can only be used in the range of temperatures not exceeding 200°C to 300°C. There are two types of resin used in the PMCs which differ in their molecular structure: thermosets and thermoplastics. The thermosetting (TS) resins are characterized by strong bonds which make them infusible and insoluble after polymerization. In the thermoplastic (TP) resin, the molecules are linked by the weak bonds of the Van Der Waals type, which gives to the molecular structure a reversible character.

- Metal matrix composites (MMCs) are used in the range of temperatures up to 1000°C. The metal matrix provides the composite with additional properties such as abrasion resistance, creep resistance, thermal conductivity and dimensional stability. They are high-performance materials, but they are penalized by a high density and finally they are very expensive.

- Ceramic matrix composites (CMCs) can withstand very high temperatures (may exceed 1000°C) exhibiting good chemical stability and excellent thermochemical performance. They are mainly used in the space industry, but the fragility of the ceramic matrix has limited their used in other fields.

II.1.3 Failure mechanisms in Fiber Reinforced Polymer (FRP) composites

Fiber Reinforced Polymers (FRPs), also known as Fiber Reinforced Plastics, are composite materials made of a polymer matrix reinforced with fibers. Glass, carbon and aramid are the most widely used reinforcement fibers. Continuous FRPs are commonly used in the aerospace, automotive, marine, and construction industries where high strength and stiffness to weight ratio are required.

The composite structures mainly used in industry are obtained by stacking several plies and are commonly called laminated composites. The assembly of these plies is oriented in most cases to build a laminated composite optimized in terms of rigidity and mass with respect to their application.

The final structure of the laminated composite turns it into a multi-scale material. Three different scales are identified (Figure II.2):

- The microscopic scale (≈ 10 μm) is the scale of the constituents (fiber and matrix) and the fiber/matrix interface.

- The mesoscopic scale (≈ 100 μm) in which the reinforcement architecture is described by interlaced homogeneous fiber yarns embedded in the matrix (ply or lamina).

- The macroscopic scale (≈ 1 mm) is the scale of the structure (fully laminate).

The multi-scale nature of the laminated composites makes then complex to analyze and to predict their behavior when they are subjected to specific types of load. The failure mechanisms produce a local discontinuity in the laminates called crack. The initiation of failure can be considered as the creation of microcracks at the microscopic scale and the propagation of failure is the result of the creation of new fracture surfaces at the mesoscopic scale from existing microcracks. The initiation of failure usually occurs long before a change in macroscopic behavior is observed. Indeed, the failure mechanisms that can be presented in a laminated composite involve different failure modes at different scales, which are influenced at the same time by the stratification and the mechanical properties of the constituents. This is why it is important to understand their behavior at several scales of observations to avoid the failure of the structure.

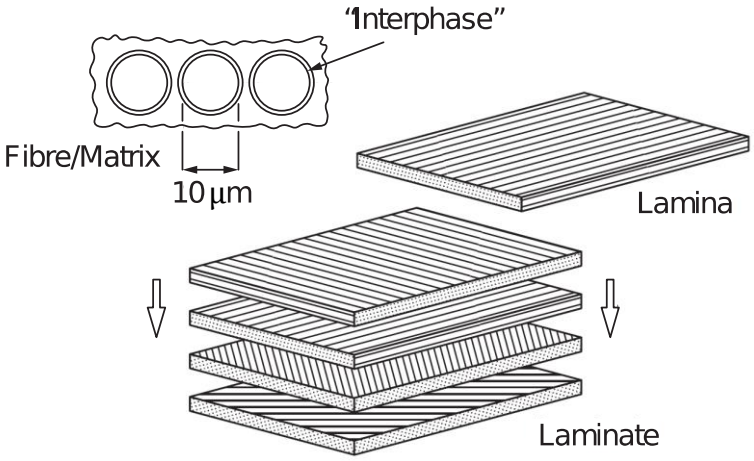

Figure II.2. Structure of a continuous Fiber Reinforced Composite [10].

Due to the laminated nature of these material systems, the failure modes are conventionally studied at the mesoscopic scale. Consequently, the fracture characteristics and crack propagation are divided into three categories according to the orientation of the failure plane with respect to the reinforcement directions (Figure I.2):

- Intralaminar failure: consists in the formation of in-plane cracks within the resin, parallel to the reinforcement direction, sometimes denoted as splitting. In the worst case, these intralaminar cracks can cut through the entire thickness of the laminate.

- Interlaminar failure: consists in the progressive separation of plies within the laminated stack, often denoted as delamination.

- Translaminar failure: associated with the tensile or compressive failure of the reinforcement fibers. The initiation and propagation of translaminar cracks depends on three different failure mechanisms, namely fiber-matrix debonding, the actual fiber failure and fiber pull-out.

The behavior of laminated composites and their failure modes at the ply-level are also influenced by the parameters at the microstructure scale: the nature of the fibers and the resin, the fiber volume fraction, or the fiber-matrix adhesion. In this material, the damage begins at microscopic scale with the fiber-matrix interfacial decohesion and matrix microcracks, then appears at the mesoscopic scale (ply-level) and eventually causes the catastrophic failure of the laminate.

Intralaminar fracture is the result at the microscopic scale of fiber-matrix interfacial decohesion and matrix cracking at the mesoscopic scale that propagates either longitudinally or transversally with respect to fibers, as shown in Figure I.2. Under increased loading, these cracks propagate to the interfaces between plies and cause the initiation of interlaminar failure (Figure II.3).

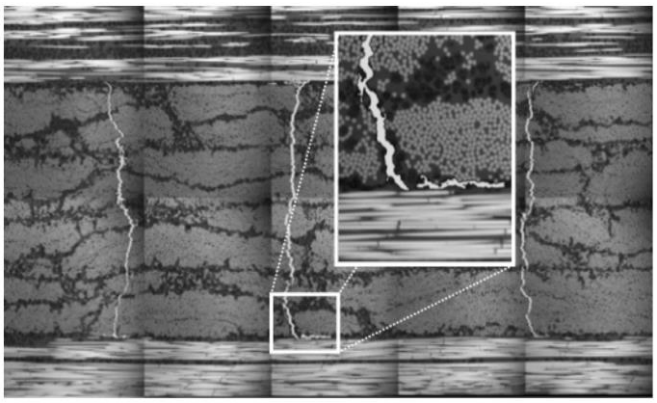

Figure II.3. Local delamination crack observed at the tip of the transverse matrix crack in a cross-ply laminate (detail of the crack deviation in the inset) [11].

Figure II.3 show a micrographic section of a cross-ply laminate, local delamination cracks are observed at the tips of transverse matrix cracks in the laminate. Even if in-ply matrix damage (intralaminar damage) is not a catastrophic failure mode for laminated composite structures contrary to delamination that can be catastrophic, the coupling between intralaminar and interlaminar damage are then in competition and evolve until the crack density in the plies comes to a saturation point.

The most critical failure mode, and usually the last one to develop, is the translaminar failure (Figure I.2 and Figure II.4), that is, the rupture of fiber bundles at the mesoscopic scale. This usually results in completely cutting the laminated composite (unlike damage such as delamination or matrix cracking which will damage locally the laminate). Paradoxically, the translaminar failure and associated fiber breakage have been studied less than delamination or matrix cracking in the literature and is often neglected in design, although they may still play a significant role in the failure of notched composite structural elements.

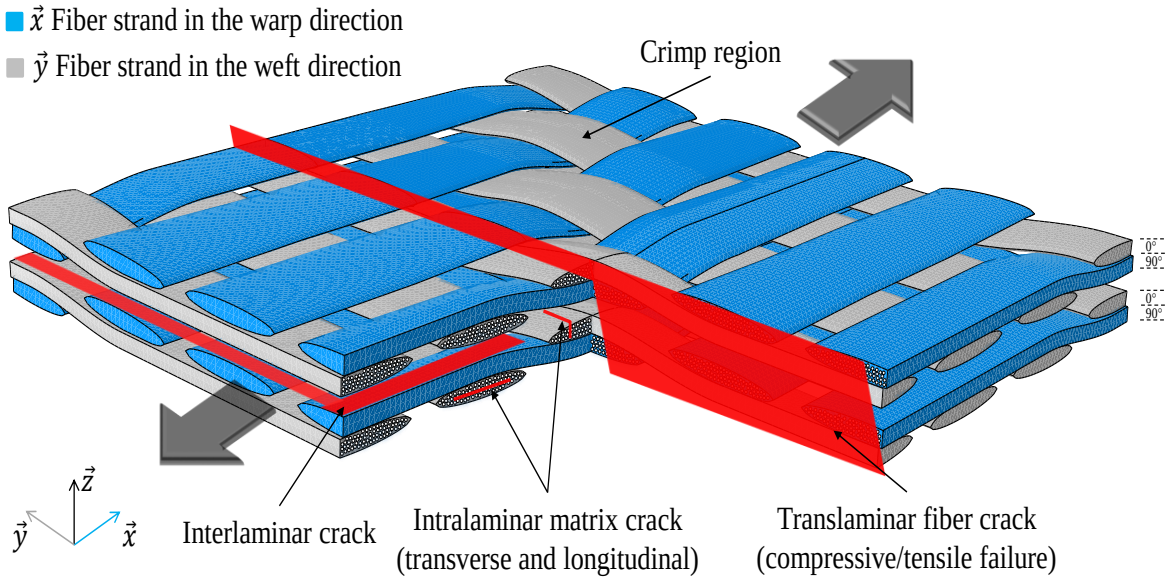

Figure II.4. Overview of ply-level failure modes on a weave pattern.

II.2 Methods to determine the translaminar fracture toughness in composite materials

In order to have a safe structural design and to avoid catastrophic failure in composite structures, the fracture criteria must be applied to determine whether the structure will withstand the external solicitations to which it will be subjected. The first approach in the design process of a mechanical structure consists in comparing the strength of the structure to the expected applied stress. However, this approach may be insufficient because it usually does not take into account some pre-existing damage present in the structure, for example small undetectable cracks, or large cracks due to accidental events (Figure I.3). In addition, composite structures very often exhibit small cracks, for example in particular areas such as rivet holes or in areas of section variation. The second approach based on the damage tolerance is to prevent the structural failures in the presence of a flaw until it is repaired.

When a structure contains a flaw, or some pre-existing damage, it is necessary to be able to predict the conditions under which a crack will begin to propagate and subsequently leads to failure of the structure before being detected. Thus the study of cracks, their propagation, or their non-propagation, is the subject of fracture mechanics. Fracture mechanics provides information on the available energy at the locale state close to the crack tip (called critical stress intensity factor), in order to conclude whether the crack will propagate or not, and how much energy will be dissipated during the fracture process from a value called critical strain energy release rate.

The following part is addressed to study the experimental approaches used to characterize the translaminar fracture in FRP composites based on some theoretical elements of Linear Elastic Fracture Mechanics (LEFM). Paradoxically, the translaminar failure and associated fiber breakage have been studied less than delamination or matrix cracking in the literature and is often neglected in design, although they may still play a significant role in the failure of notched composite structural elements.

II.2.1 The linear Elastic Fracture Mechanics

Fracture mechanics consists of the characterization of the crack-tip stress field in terms of the stress-intensity factor K_i (with $i=I, II$ or III according to the mode of loading) and the energy release rate (noted G or J depending on the behavior of the material, elastic or ductile), according to the approach proposed by Irwin and Rice [12-13] which are based on the fundamental principles of Linear Elastic Fracture Mechanics (LEFM). These concepts of the fracture mechanics developed for homogeneous isotropic materials (typically metals) can be also applied to FRP composites [5, 14].

The propagation crack in a continuous medium is represented by an irreversible separation into two new surfaces, called edge cracks or crack lips, introducing a discontinuity in the displacement field. The fracture modes are separated according to the relative displacements of the crack lips according to the three directions of space. Figure II.5 shows the three fundamental fracture modes for a stationary crack to propagate from an applied load.

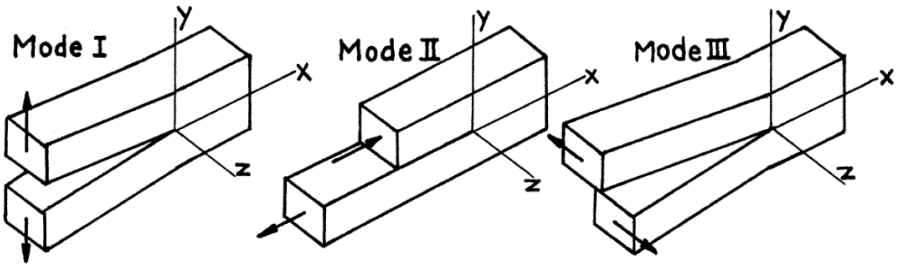

Opening mode In-Plane shear mode Out-of-Plane shear mode

Figure II.5. Three modes of crack surface displacements [15].

II.2.2 Fracture mechanics-based computation methods

Most of the studies dealing with mode I (opening mode) translaminar failure of FRP composites are based on the quantification of the fracture toughness of multidirectional laminates made from elementary unidirectional (UD) plies [5, 14, 16-18], while very few studies are dealing with 2D woven fabrics [19]. The measurement of fracture toughness depends on the stacking sequence of the laminates and the validity of these measurements will be determined by the failure mechanisms, which can combine and interact within each ply. It is then necessary to use a specific specimen geometry to induce stable crack growth by fiber breakage in tension or in compression in order to quantify the translaminar fracture toughness. The specimen geometry and the fracture mechanics methods applied to composite materials are very often based on the standards used for metallic materials. Classically, specimens with initial notches or holes, which induce a local stress concentration and thus favor damage localization so that the fracture toughness is quantified in different loading conditions [5, 14-15, 20].

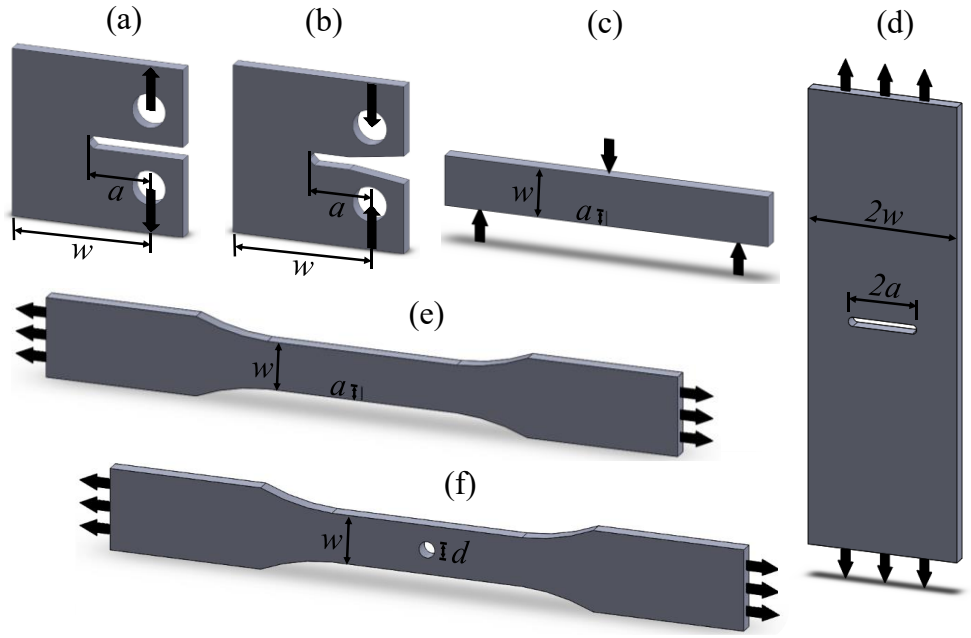

Figure II.6. Specimen configuration used for translaminar fracture measurement: (a) Compact Tension - (b) Compact Compression - (c) Single Edge Notched Bending– (d) Centre Notched Tension (has also been used for compressive tests) - (e) Single Edge Notched Tension – (h) Open Hole Tension (has also been used for compressive tests).

Figure II.6 illustrates specimens with different geometries that are conventionally used to quantify the translaminar fracture toughness of FRP composites. Compact Tension (CT), Compact Compression (CC) and Single Edge Notched Bending (SENB) specimens allows inducing a progressive and stable crack growth. This notion of crack stability is essential to plot the evolution of the critical strain energy release rate as a function of the macroscopic crack length, in the form of R-curves. The Eccentrically loaded Single-Edge-notch Tensile (ESET) specimen is not shown in Figure II.6, but is the only specimen configuration that has become standardized for translaminar testing. In Figure II.6, w represents the distance from the load line to the right edge of the specimen. The ratio a/w of the initial notch length (a) to the distance (w) is a parameter allowing to modulate the stress intensity factor at the crack tip.

II.2.3 Data reduction schemes

For composites characterized by an elastic-brittle behavior, the methods derived from metallic materials apply relatively well and give reliable results insofar as most concepts of Linear Elastic Fracture Mechanics (LEFM) are valid [5, 14, 16, 21]. The evaluation of the fracture toughness in FRP composites is based on different calculation methods (area method, compliance calibration) as well as standards [ASTM-E399, ASTM-E1820] specific to isotropic metallic materials which have been adapted more recently [ASTM-E1922] to composite materials:

- E399-12, Standard Test Method for Linear-elastic Plane-strain Fracture Toughness K_{Ic} of Metallic Materials (2012)
- ASTM, E1820–05, Standard test method for measurement of fracture toughness. (2005)
- ASTM E1922 − 15, Standard Test Method for Translaminar Fracture Toughness of Laminated and Pultruded Polymer Matrix Composite Materials (2015).

These fracture toughness measurement methods are generally based on the overall mechanical response of the laminates (force-displacement curves) resulting from tests on specimens with different geometries (Figure II.6). Specific techniques such as Digital Image Correlation are classically used to determine the Crack Tip Opening Displacement (CTOD) or the Crack Mouth Opening Displacement (CMOD). These quantities offer alternatives to traditional methods based on force-displacement data. The interest of measuring displacements as close as possible to the crack tip is to avoid additional displacements associated with the boundary conditions or deformations.

In addition, a variety of methods are used to compute the strain energy release rate based on finite element analysis. Among the most widely used method for analyzing the fracture behavior of composites are the methods called "Virtual Crack Closure Technique" (VCCT) and "Virtual Crack Extension" (VCE) [22].

The compliance calibration method, ASTM-E399 and ASTM-E1820 standards will be detailed in the experimental part of this thesis (Chapter III and Chapter IV).

II.2.4 Translaminar tensile fracture toughness

Translaminar tensile fracture toughness in multidirectional FRP laminates is often characterized using CT testing and the R-curve are drawn using various data reduction methods (Figure II.7). Most of the studies on the translaminar tensile fracture toughness have been carried out using carbon fiber reinforced epoxy laminates with a 0/90 cross-ply lay-up [14, 16-18], as shown in Figure II.7. With such lay-up, the CT tests show force-displacement curves that are almost linear elastic with a stable crack growth. It means that fundamental principles of Linear Elastic Fracture Mechanics (LEFM) are definitely applicable. The R-curves tend towards an asymptote, physically meaning that damage is localized at the crack tip and that the FPZ is reached from the beginning and does not evolve much (Figure II.7). X-ray imaging monitoring during tests was used by Teixeira et al. [18] to clearly show a very localized damage area ahead of the crack tip.

(a) ASTM E399 - Pinho et al. [14]
FRP laminate: C/Epoxy T300/913 – $[90/0]_{8S}$

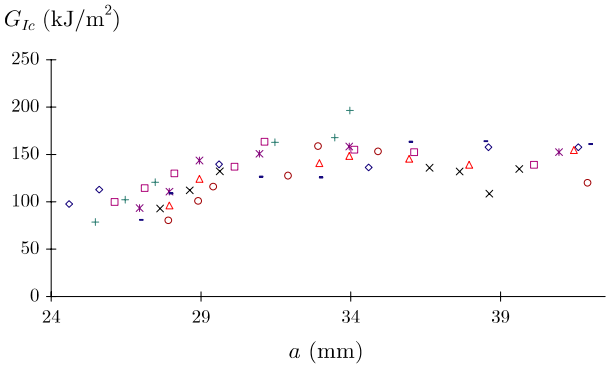

(b) Compliance calibration - Laffan et al. [16]
FRP laminate: C/Epoxy T300/920 - $[(90/0)_8/90]_S$

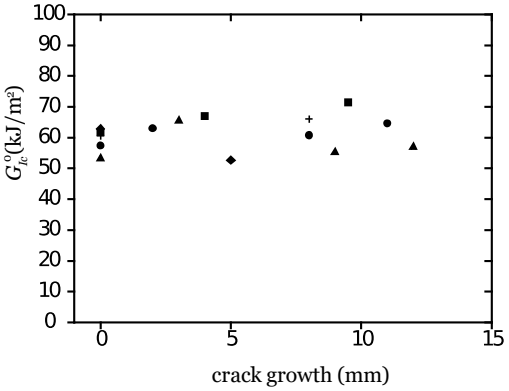

(c) J-integral from DIC - Catalonatti et al. [17]
FRP laminate: C/Epoxy IM7-8552 - $[90/0]_{8S}$

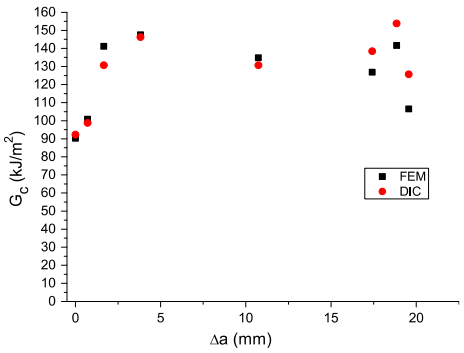

(d) Modified compliance calibration - Teixeira et al. [18]
FRP laminate: C/Epoxy T800s/M21

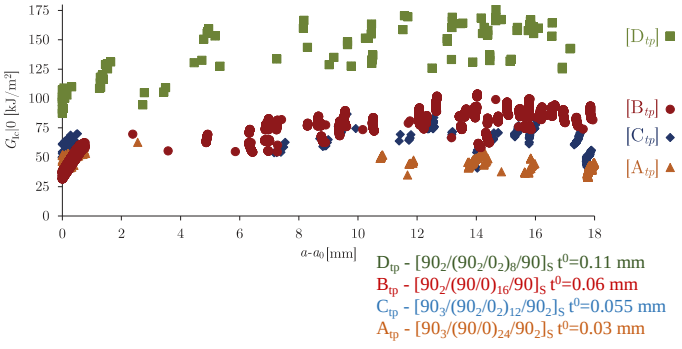

Figure II.7. R-curves obtained with the different data reduction methods from CT testing found in the literature: (a) ASTM E399 [14] – (b) Compliance calibration [16] – (c) J-integral from DIC [17] – (d) Modified compliance calibration [18]

Teixeira et al. [23] have measured the translaminar fracture toughness (during both initiation and propagation) of individual plies to calculate the translaminar fracture toughness of three multidirectional laminates. Following the original idea proposed by a few authors to measure the fracture toughness of laminates plies in order to relate it to the toughness of laminates

considering the rule of mixtures [14, 24], they have used the analytical models to calculate the translaminar fracture toughness of cross-ply laminates from the 0° ply fracture toughness [25, 26]. These models assume that fracture of the laminate is associated with fiber fracture in the load bearing plies (typically the plies aligned with the loading direction). In addition, these authors assumed the additivity of the energy dissipated by each ply in the total energy dissipated by failure in the laminates when using the rule of mixtures. It also means that the failure processes in each ply do not affect the failure processes in another. In quasi-isotropic laminates, they show that the effect of blocking two 0° plies together results in tripling the translaminar fracture toughness value whereas blocking 45° plies affected slightly the latter [23, 27].

In cross-ply laminates, Teixeira et al. [18] have studied the influence of thickness dependence on the translaminar fracture behavior of laminates consisting of thin-ply C/Epoxy prepregs [28]. They concluded that translaminar toughness is not an absolute, but rather on in-situ property, and it depends strongly on the 0° ply-block thickness, even in situations where delamination and diffuse damage are inhibited. Based on four different 0° ply-block thicknesses (ranging from 0.03 mm to 0.12 mm). They observed that translaminar fracture toughness values are doubled (from 46 to 104 kJ/m² at initiation), and are tripled (from 49 to 160 kJ/m^2 at propagation) (Figure II.7(d)).

The same trend was observed by Cugnoni et al. [29] in hybrid C/epoxy thin-ply composites. In quasi-isotropic and cross-ply laminates, it is observed that the translaminar toughness decreases nearly proportionally with ply thickness both at initiation and during propagation. Such changes were ascribed to a linear decrease in the length of the fiber pull-out. These laminates made of two types of carbon fibers (HM/HS fibers) are designed to generate sub-critical fiber fragmentation to promote fiber pull-out. The translaminar R-curves of quasi-isotropic (QI) and cross-ply (CP) laminates are also compared. As expected, the QI laminates exhibit a consistently lower translaminar strength compared to CP because of their lower fraction of 0° plies.

II.2.5 Translaminar compressive fracture toughness

Through compressive failure comes along with different issues, CC tests are often used to characterize the critical strain energy release rate in compression. Jackson and Ratcliffe [30] considered specimens with a CT geometry to conduct compressive tests. Pinho et al. [14] have investigated the compressive fiber failure mode mostly in UD-ply laminates. CC tests have been carried out on carbon epoxy T300/913 UD-ply laminates with a $[0/90]_{8S}$ stacking sequence. From force-displacement curves (Figure II.8(a)) and kink-band growth are drawn the R-curves (Figure II.8(c)). An increasing trend is observed on all R-curves, such an artificial trend in R-curves is explained by the contact forces taking place in the kink-bands during the closing of edge cracks. These forces imply additional energy dissipation and also induce other damage modes (Figure II.8(b)). Post-mortem C-scan images clearly show that damage is localized far from the crack plane. In other words, CC tests are not fully suitable for drawing R-curves. Only initiation values seem to be the most relevant measurement of the critical energy release rate associated with the kink-band formation in compression.

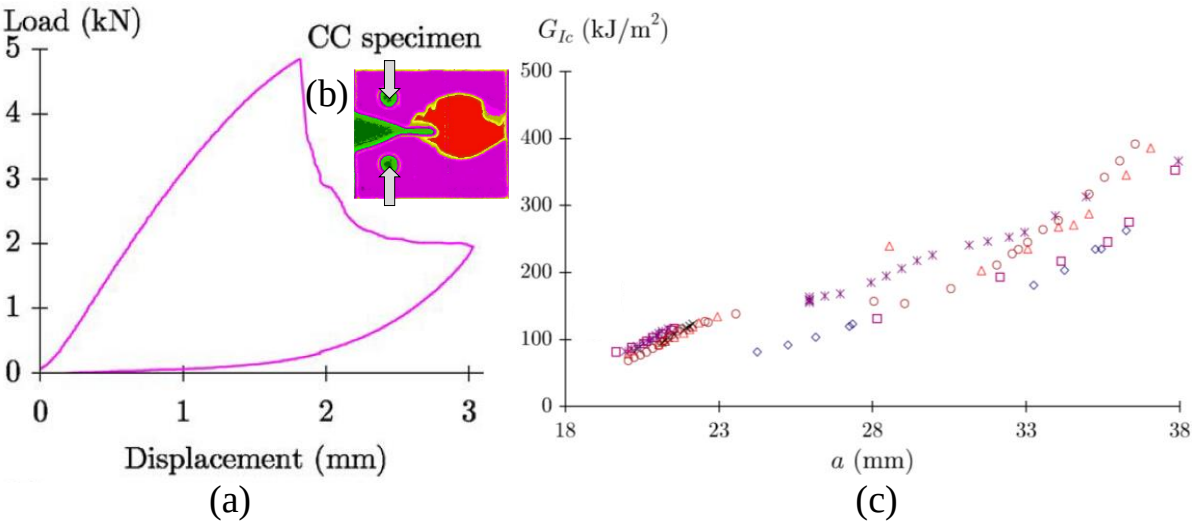

Figure II.8. CC test on T300/913 carbon/epoxy UD-laminates with a $[0/90]_{8S}$ lay-up [14]: (a) Force-displacement curve – (b) Post-mortem damage observation by C-scan imaging – (c) R-curve obtained using ASTM 399 standard

II.3 Conclusion

The purpose of this chapter was to provide a brief presentation of the fracture mechanics concepts applied to translaminar fracture in composite materials. This phenomenon is particularly important in the context of certification/design of damage tolerant composite structures.

This brief overview shows that the fracture mechanics concepts, developed for homogeneous and isotropic materials, applied to composite laminates should be used with caution. FRP composite structures are heterogeneous and anisotropic making complex their fracture behaviors at different scales (microscopic, ply-level, laminates). The literature review reveals that it is very difficult to propagate a translaminar crack without inducing many secondary damages, depending on the reinforcement architecture (UD-ply or woven-ply). The measurement of the characteristic quantities associated with the crack propagation of an elementary mode (K_{I_C}, G_{I_C}, ...) is then more or less complex depending on the loading mode (traction, compression) and the stacking sequence of the laminates.

Several experimental techniques have been developed in the literature to characterize the parameters associated with the translaminar cracking. Most of them are based on analytical developments (compliance calibration method, area method,..), established within the framework of Linear Elastic Fracture Mechanics. These methods do not require the knowledge of material parameters, but remain so-called "global" methods, from which it is not possible to dissociate the energy dissipated by each damage mechanism. Numerical methods are also used as alternative methods, but they require to determine the constitutive laws of the material and to identify their materials parameters.

The present work gives an insight into the study of translaminar fracture toughness and corresponding damage mechanisms in woven-ply thermoplastic laminates. It is based on

experimental characterization (Compact Tension, Compact Compression and Single-Edge Notched Bending) of translaminar fracture as well as the use of a numerical model adapted to woven-ply laminates. The experimental methods are presented in Chapter III and Chapter IV. In Chapter III, the critical strain energy release rate is estimated from Compact Tension and Compact Compression tests, using force-displacement curves and Digital Correlation Image technique to monitor the crack propagation. In Chapter IV, the influence of both temperature and constraint effect have been investigated using Single-Edge Notched Bending tests. Finally, the numerical model presented in Chapter V was aimed at better understanding the contribution of the woven-ply laminates (associated with different fiber bundle orientations) on the energy dissipated during translaminar fracture, depending on the loading conditions.

Chapter III: High temperature translaminar fracture of woven-ply thermoplastic laminates in tension and in compression

Several information emerged from the bibliographical review (Chapter II) have allowed to verify the application of the Linear Elastic Fracture Mechanics (LEFM) to mode I translaminar failure on Fiber Reinforced Polymer (FRP) composites, although most of these works dealing with unidirectional-ply laminates. In this context, this chapter is focuses on the experimental characterization of the translaminar fracture of high-performance thermoplastic composites.

In the first part of this chapter, a brief background about the experimental estimation of translaminar fracture toughness on FRP composites is presented. Then, the main objectives of this chapter are detailed. In the second part, the materials, experimental set-up and data reduction methods are specified. In the third part, the main result of this study are presented and discussed. First, the influence of the temperature and the stacking sequence on the damage mechanisms is studied. Thereafter, the G-R curves of all laminated composites are computed. In the last part of this chapter, the main conclusions are detailed.

The work presented within this chapter has been submitted to Engineering Fracture Mechanics as a paper entitled “High temperature translaminar fracture in tension and in compression of woven-ply thermoplastic laminates”, it is currently under review.

Chapter III outline

III.1 Introduction

The widespread use of organic matrix composites in many industrial sectors has been confronted with the need to understand and quantify the fracture mechanisms within materials whose behaviour is highly heterogeneous and anisotropic. In addition, they can be subjected to different mechanical loads, but also to different environmental conditions (temperature, humidity, etc.) when it comes to aeronautical applications.

Among the main damage modes observed in composite laminates, the breaking of fibers in tension or compression is less studied, compared to delamination. These different damage mechanisms result in the development of a "Fracture Process Zone" (FPZ) in regions where the material is damaged by high stress concentrations, i.e. near holes, notches, or manufacturing defects [31-32]. Depending on the nature of the constituent materials, and the stacking sequence, laminated composites are generally characterized by three primary failure modes (Figure I.2 and Figure II.4): interlaminar, intralaminar and translaminar failure. These modes can be observed at different scales (Figure II.2): microscopic scale (fiber/resin interaction), mesoscopic scale (laminate ply) and macroscopic scale (laminate). Translaminar fracture occurs at the mesoscopic scale, with the breakage of fiber bundles. There are two modes of translaminar failure in fiber-reinforced laminates: fiber breakage in tension and in compression [14, 33]. In the case of compressive loadings, fiber failure is mainly due to the formation of fiber buckling bands (also known as kink-bands).

Fracture toughness plays a fundamental role in the damage tolerance of a composite structure. It depends on the stacking sequence of the laminate [16, 18, 34, 35], the loading conditions and the architecture of the reinforcement. Most of the studies dealing with translaminar mode I (opening) failure of multidirectional laminates are based on the quantification of the fracture toughness of unidirectional-ply laminates [14, 16-18, 24, 34, 36-39], while very few studies are dealing with woven-ply laminates [19, 33, 40-42].

III.1.1 Experimental estimation of translaminar fracture toughness

The ASTM-E1922 standard provides recommendations on specimen geometry for estimating the translaminar fracture toughness of composite materials ("Eccentrically loaded Single-Edge-notch Tensile"), the use of standards derived from metallic materials is widely used for composite materials [5, 39]. Damage growth is characterized by the resistance curve (R-curve), which represents the evolution of the critical strain energy release rate as a function of the macroscopic crack length. It is therefore necessary to induce stable crack growth by means of a specific specimen geometry: "Compact Tension/Compression" (CT/CC) [14, 16-18, 24, 33, 34, 35, 39-42], three-/four-point bending [36-37, 42] and "Eccentrically loaded Single-Edge-notch Tensile" (ESET) [19, 43-44].

CT specimens were mainly used to estimate the translaminar fracture toughness, since in this type of geometry damage around the crack tip causes fiber breakage as the primary failure mechanism. Similarly, the measurement of compressive fracture toughness related to the formation of kink-bands in compression has been reported in many publications using CC specimens, but the values thus obtained are only valid at the initiation of the fracture and not

during propagation, because of the energy dissipated by the delamination that comes along with the propagation of the kink-bands [14, 17].

Many studies have focused on the development of the best technique for quantifying translaminar fracture toughness [17, 24] in terms of reproducibility and simplicity of results. Laffan et al. [24] concluded that the method of compliance calibration based on effective crack length is the most appropriate method, because it does not require optical measurement of crack growth during the test. The parameters used in this method to determine the length of the crack are a function of a stiffness model (force-displacement) and do not depend on the size of the specimen, they are related to the elastic compliance measured from the force-displacement curve. In another study presented by Catalonatti et al [17], a digital image correlation technique based on the computation of the J-integral around the crack tip was shown to be suitable for capturing the critical energy release rate associated with the breakage of longitudinal fibers.

Some studies have also pointed out that fracture toughness is not an absolute value. Indeed, translaminar fracture toughness depends on the thickness of the plies. Teixeira et al. [34] showed that the increase in fracture toughness is related to the large amount of fiber bundles pull-out at 0° [16, 18], the blocking effect provided for the two 0° plies together triples the value of the translaminar fracture toughness while the blocking resulting from the 45° plies has little effect on the translaminar fracture toughness.

III.1.2 Translaminar fracture in woven-ply thermoplastic laminates

Over the past 50 years, several studies have been conducted to understand and quantify translaminar fracture toughness in organic matrix composites. Most of them have been dedicated to unidirectional (UD) thermosetting laminates, using two main types of laminates: carbon/epoxy [14, 16-18, 24, 33, 34, 36-37, 39] and glass/epoxy [36, 39]. Translaminar fracture in woven-ply laminates has been little studied compared to UD-laminates. Woven-ply laminates allow the processing of parts with complex geometries and have good damage tolerance. As with unidirectional-ply laminates, the various techniques for quantifying fracture toughness have proven to be well applicable to woven-ply laminates. The characterization of translaminar fracture in woven-ply laminates focuses mainly on the thermosetting materials carbon/epoxy [33] and glass/epoxy [19, 33, 39-40]. Many studies have concluded that in glass/epoxy woven-ply laminates, matrix microcracking is the predominant damage phenomenon at the crack tip [[19, 39-40]. Even if this phenomenon is present, the quantification of fracture toughness remains reliable in the case of near-brittle fracture.

The behaviour of Polymer Matrix Composites (PMC) is also characterized by temperature dependence [45-49]. Numerous studies have been carried out on the influence of high temperatures on interlaminar fracture in unidirectional [45] and woven-ply thermoplastic (TP) laminates [46], but little work has been done on translaminar fracture of woven-ply thermoset laminates [19, 33, 41] and almost no work has been done on woven ply TP laminates. It should be noted that TP matrix composites are known for their excellent damage tolerance [10]. In the next chapter (Chapter IV) [50], the translaminar fracture behavior of a hybrid woven laminate of reinforced carbon and glass fibers combined with a PEEK matrix will be studied. By means of tests carried out on notched specimens in tensile and three-point bending at room temperature

and $T>T_g$, it will be shown that temperature has little influence on the translaminar fracture toughness in mode I. In addition, it may promote the intrinsic toughness at the crack tip and the extrinsic toughness at the mechanical loading zones [51], which results in a slight increase of the R-curve.

Table III.1 summarizes a few translaminar tensile and compressive fracture toughness values available in the literature for unidirectional and woven-ply reinforced polymer matrix laminates.

III.1.3 Objectives of this chapter

The work presented in this chapter focuses on the experimental characterization of the translaminar fracture of three types of carbon fiber-reinforced thermoplastic laminates. Using CT and CC specimens to induce translaminar fracture in tension and compression, these laminates were tested at room temperature (RT) and at 150°C when matrix toughness is exacerbated. The objective of this chapter is to analyze the influence of stacking sequence and temperature on the tensile and compressive fracture behavior of fibers in mode I. This involves measuring the critical energy release rate at initiation and the fracture energy during propagation. Thus, the observation and a post-mortem analysis of damaged areas make it possible to quantify the damage tolerance of TP matrix composites and to understand the influence of temperature on the deformation mechanisms of the TP matrix and ultimately on translaminar fracture.

Laminate type	Study (year)	Specimen configuration	Polymeric resin Fiber reinforcement	Methods of data reduction	Fracture toughness G_{I_C} (kJ/m^2)	
					Initiation	Propagation
Unidirectional laminated composite	Tension					
	Slepetz et Carlson [56] (1975)	CT	Epoxy Carbon T300/5208	Compliance calibration	21.2	-
	Mahmoud [53] (2003)	SENT	Polyester E-glass	ASTM E399	4.95	-
	Pinho et al. [14] (2006)	CT	Epoxy Carbon T300/913	VCCT and rule of mixtures	91.6	133.0
	Laffan et al. [45] (2010)	CT	Epoxy Carbon T300/920	Modified compliance calibration	57.0	69.0
	Catalonatti et al. [29] (2010)	CT	Epoxy Carbon IM7-8552	Digital Image Correlation	98.7	133.7
	Teixeira et al. [30][a] (2016)	CT	Epoxy Carbon T800s/M21	Modified compliance calibration	46.0 – 104.0	49.0 – 160.0
	Compression					
	Pinho et al. [14] (2006)	CC	Epoxy Carbon T300/913	VCCT and rule of mixtures	79.9	-
	Catalonatti et al. [29] (2010)	CC	Epoxy Carbon IM7-8552	Digital Image Correlation	47.5	-
	Laffan et al. [54] (2012)	4PB	Epoxy Carbon IM7/8552	VCCT	25.9	-
Woven-ply laminated composite	Tension					
	Rokbi et al. [58][b] (2011)	CT	Epoxy E-Glass	Compliance calibration	31.9 - 37.4	42.0 – 51.0
	Lisle et al. [31][c] (2017)	ESET	Epoxy E-Glass	Infrared thermography	15.8 - 21.6	61.5 – 62.5
	Ortega et al. [51] (2017)	CT	Epoxy Hybrid : Carbon G0926 / Glass S2	Cohesive law and rule of mixtures	97.0	-
	Vieille at al. [67][d] (2018)	SENB	PEEK Hybrid : Carbon HTA40 / E-Glass	ASTM E1820	44.0 - 47.0	-
	Compression					
	Ortega et al. [51] (2017)	CC	Epoxy Hybrid : Carbon G0926 / Glass S2	Cohesive law and rule of mixtures	-	-

[a] Four different 0° ply-block thicknesses ranging from 0.03 mm to 0.12 mm
[b] Two different fiber directions (warp and weft)
[c] Two different lay-up sequences ($[0°]_2$ and $[\pm 45°]_2$)
[d] Two different temperatures, **results presented in the next chapter (Chapter IV)**

Table III.1. Summary of experimental data obtained from characterization of the tensile and compressive translaminar failure mode.

III.2 Materials and manufacture

III.2.1 Materials

The laminates used in this study are obtained by thermo-compression. They consist of a PolyEther Ether Ketone (PEEK) thermoplastic matrix reinforced with a continuous carbon fiber fabric (Tenax®-E HTA40 3K), structured in a 5-harness satin weave. The average ply thickness of the laminates is 0.31 mm.

Three types of woven laminates are tested (Figure III.1). Two laminates with the same ply ratio at 0°/90° and ±45°, but with different thicknesses qualified as quasi-isotropic [49]:

- [(0/90),(±45),(0/90),(±45),(0/90) ,(±45),(0/90)]] (2.17 mm thick, noted as C7/PEEK)
- $[(0/90)_G,(0/90),(\pm45),(0/90),(\pm45),(0/90),(\pm45),(0/90)]_S$ having two outer plies of glass fabric (5-harness satin weave) and PEEK matrix (4.5 mm thick, noted as CG/PEEK), the 0.08 mm thick $(0/90)_G$ surface glass fabric is used as corrosion protection and electrical protection with the aim of reducing the galvanic torque and thus avoiding galvanic corrosion of aluminum and steel with carbon.
- An eight-ply orthotropic laminate $[(0/90)]_8$ (2.48 mm thick, noted as C8/PEEK).

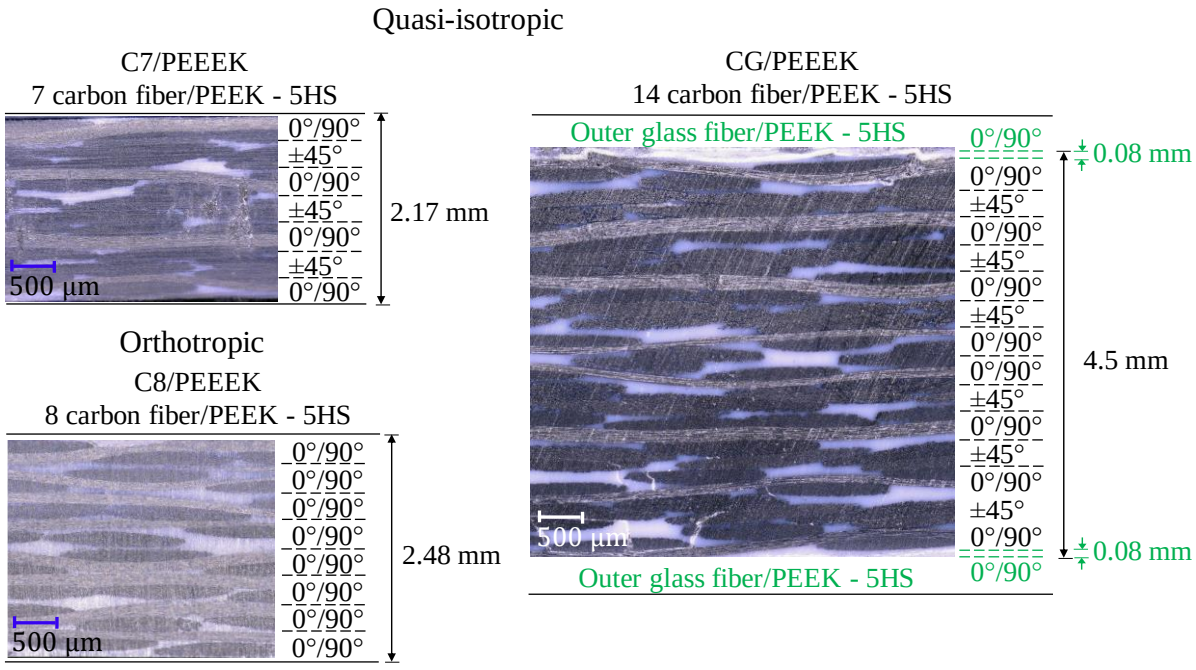

Figure III.1. Lay-up and thickness of the woven-ply laminated composites studied.

The main mechanical properties of the elementary ply are specified in Table III.2.

	Carbon/PEEK		**Glass/PEEK**	
Nominal ply thickness (mm)	0.31		0.08	
T_g (°C)	143		143	
	TA	150°C	TA	150°C
Longitudinal modulus E_x (GPa)	60	55.04	22	
Transverse modulus E_y (GPa)	60	55.04	20	
Shear modulus G_{xy} (GPa)	4.83	4.43	6.55	
Poisson's coefficient ν_{xy}	0.04	0.037	0.04	

Table III.2. A few properties of the elementary ply of woven carbon and glass fibers reinforced PEEK at RT and 150°C.

III.2.2 Specimen geometries

The dimensions of the CT and CC specimens were chosen in accordance with ASTM test standard E399-12 [52] (Figure III.2). The notched area of the CC specimens (Figure III.2(b)) has been enlarged to avoid contact of the notch faces during compression. Jackson and Ratcliffe [30] described CC specimens as being similar to CT specimens, but used in compression. They found that the stress intensity factor is not affected significantly by the morphology of the opening. Many other authors have used CC specimens to characterize the critical strain energy release rate in compression on Fiber Reinforced Polymer (FRP) composites [14, 17, 33], as shown in Table III.1.

The specimens are cut from a 600 × 600 mm^2 plate using a water jet machine. The fixing holes of the loading device are machined by means of carbide drills. The ratio between the length of the initial notch and the width of the specimen used is approximately a/w = 0.45 for both types of specimens, where a is the crack length and w is the distance from the load line to the right edge of the specimen.

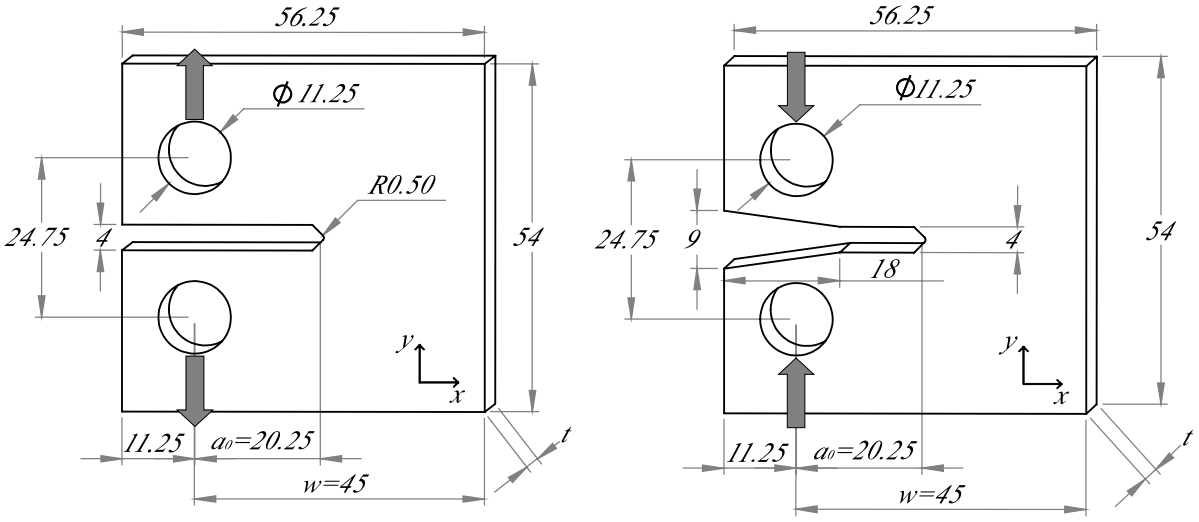

(a) Compact Tension - CT (b) Compact Compression - CC

Figure III.2. Test specimen dimensions (in mm) for: (a) tension and (b) compression translaminar fiber-breaking fracture toughness tests.

III.3 Experimental set-up and methods

III.3.1 Thermo-mechanical testing

All the tests were conducted with a uniaxial servo-hydraulic tensile machine MTS-810 equipped with a 100 kN capacity force cell and a thermal chamber (Figure III.3). The specimens are held in position by a standardized device in accordance with ASTM-399, which is maintained by the hydraulic grips of the machine and transmits the mechanical load via pins inserted in the holes of the specimens (Figure III.3(a)). Six specimens were tested in each configuration (CT and CC) in displacement-controlled mode (1 mm/min) at two temperatures: room temperature (RT) and 150°C.

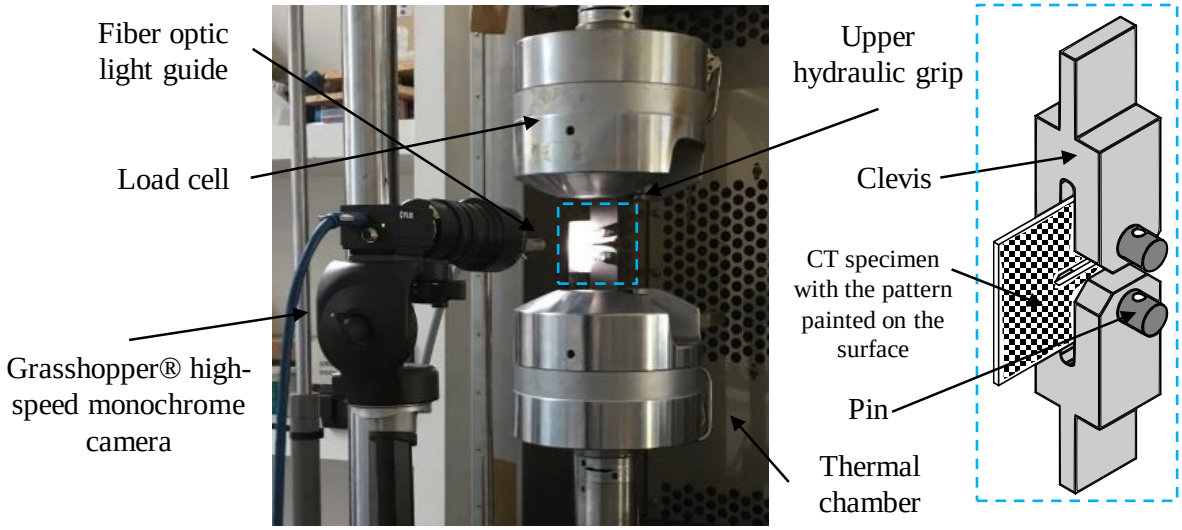

(a) CT test in the MTS 810 servo-hydraulic machine

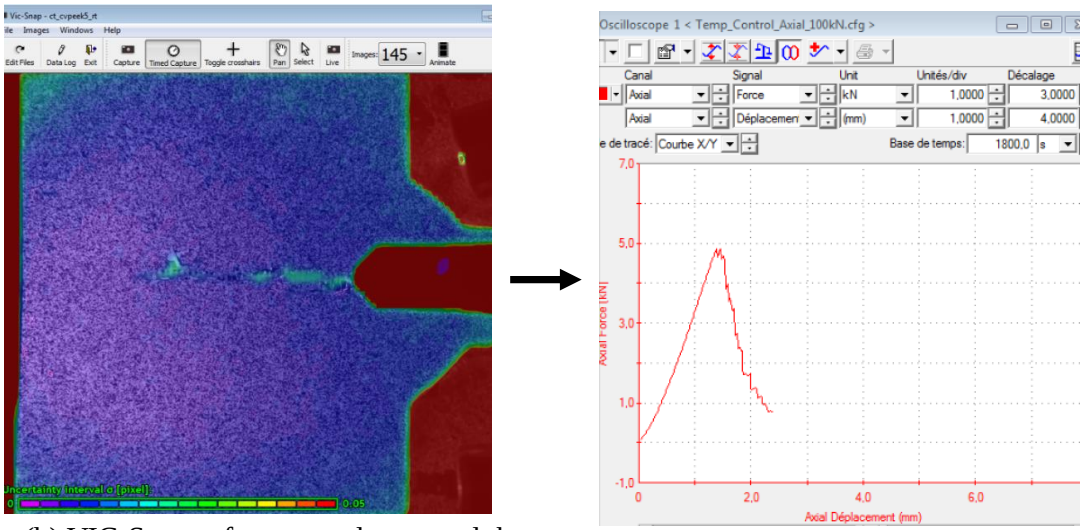

(b) VIC-Snap software used to record the digital image during thermomechanical loading

(c) Force-displacement curve

Figure III.3. MTS 810 servo-hydraulic testing machine during a CT test at RT.

The test temperature at 150°C was chosen because a combination of mechanical and thermal stresses can appear in the surroundings of the aircraft engine, in which the heating of the aircraft

engine can generate continuous service temperatures at beyond (≈180°C) around the nacelle [53], which is higher than the glass transition temperature of the C/PEEK laminates $T_{g|C/PEEK} = 143°C$ here studied.

III.3.2 Fractographic analysis

Damage mechanisms are discussed by means of fractographic analysis. Microscopic observations of the fracture surface were carried with an optical microscope VHX-5000 series provides by Keyence.

III.3.3 Crack propagation measurement by means of a Digital Image Correlation (DIC) technique

DIC pattern is painted on the specimen surface with a non-periodic texture and without preferred orientation (Figure III.3(a)). The use of DIC technique at high temperature requires the use of a high intensity source combined with a fiber optic light guide is used to illuminate the patterns on the surface of the specimen placed into the thermal chamber (Figure III.3(a)). A Grasshopper® high-speed monochrome camera allows digital images to be recorded at full resolution (1920×1200 pixels), and at a rate of one frames-per-second during thermomechanical loading (Figure III.3(b)). The VIC-2D digital image correlation software provides the confidence interval field associated with the convolution factor (sigma indicator) of each pattern in the region of interest [54]. As was defined by Sutton et al. [55], the VIC-2D system utilizes an optimized correlation method to provide full-field two-dimensional displacement and strain. The method compare the digital images for various small regions (known as subsets) throughout the images before and after deformation using fundamental continuum mechanics concepts, locating the positions of each of these subsets after deformation through digital image analysis. When a material discontinuity appears in the pattern, the homogeneous linear mapping in this region does not present deformed surface and the small subset position is not computed.

Using an algorithm implemented in the Scilab code [56], the crack tip is located via the discontinuity of the strain field resulting from the crack propagation (Catalanotti et al. [17] used a similar technique based on the displacement discontinuity within the pattern). A binarization of the full-field strain obtained by the VIC-2D software is applied. The identification of the damaged and undamaged areas in the region of interest is associated with a F_T function (Figure III.4), which takes values of:

$$\forall\ \varepsilon_{xy}(x,y) \neq 0 \Rightarrow F_T(x,y) = 0 \quad \text{(III.1a)}$$

$$\forall\ \varepsilon_{xy}(x,y) = 0 \Rightarrow F_T(x,y) = 1 \quad \text{(III.1b)}$$

$$F_T(x,y) = -1 \quad \text{(III.1c)}$$

- $F_T = 0$ corresponds to the region for the undamaged area.
- $F_T = 1$ is the damaged area where a material discontinuity is present next to the initial crack tip and not information is computed using DIC.
- $F_T = -1$ is the damaged area where material discontinuity appears due to a secondary crack and not information is computed using DIC.

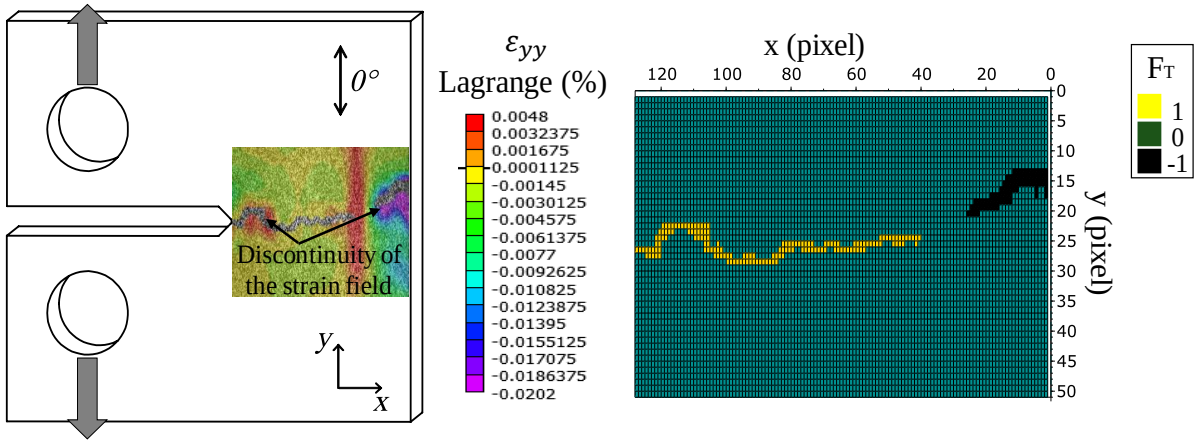

Figure III.4. F_T function used to follow the crack propagation implemented on a CT specimen.

The crack length is then determined from the crack tip position in each pattern, independently of the orientation of crack within the pattern. The spatial resolution of the crack length is defined by the size of the subsets used in the DIC method.

III.3.4 Data reduction methods

III.3.4.1 ASTM-399 test standard

According to ASTM-399 test standard [52], initially developed and validated for metallic isotropic materials, the critical stress intensity factor (fracture toughness) in mode I (opening) K_{Ic} in the case of a CT specimen (Figure III.2) is given by:

$$K_{Ic} = \frac{P_c}{t\sqrt{w}} f(a/w) \qquad \text{(III.2)}$$

with:

$$f(a/w) = \frac{2 + a/w}{(1 - a/w)^{3/2}} [0.886 + 4.64(a/w) - 13.32(a/w)^2 + 14.72(a/w)^3 - 5.6(a/w)^4] \qquad \text{(III.3)}$$

where P_c is the critical load ensured at crack initiation, t is the thickness of the specimen, w is the distance from the load line to the right edge of the specimen (Figure III.2), a is the crack length, whose initial value is a_0 and $f(a/w)$ is a geometric correction function for a specimen of finite width [15, 32]. Equation III.2 is only defined for isotropic materials though the studied laminates are not completely isotropic. To a first approximation and for comparison purposes, the function $f(a/w)$ proposed for isotropic materials has been used to compute the values from the method proposed in ASTM-399 test standard. It is acceptable for C7/PEEK and CG/PEEK laminates. For the C8/PEEK orthotropic materials, the solution proposed by Ortega et al. [57] for a CT specimen should be considered in order to obtain the linear elastic fracture toughness, the stress intensity factor and the compliance at the load line. The solution applies for any orthotropic material whose principal directions are defined by the crack direction, assuming that the crack grows along the symmetry plane of the specimen.

The critical strain energy release rate of the laminate G_{Ic}^{lam} is then calculated from K_{Ic} [15, 21]:

$$G_{Ic}^{lam} = C_I K_{Ic}^2 \tag{III.4}$$

where C_I is the orthotropic elastic coefficient in plane-stress conditions defined by [15, 21]:

$$C_I = \sqrt{\frac{1}{2E_x E_y}} \sqrt{\sqrt{\frac{E_x}{E_y}} - \nu_{xy} + \frac{E_x}{2G_{xy}}} \tag{III.5}$$

where E_x, E_y, G_{xy} and ν_{xy} are respectively the Young's modulus in x and y directions (Figure III.2), the shear modulus and the Poisson's ratio of the laminate. The properties used for the computation of the orthotropic elastic coefficient of the equivalent laminate are given in Table III.3, they are obtained from the properties of the elementary ply (Table III.2) using the laminate theory [9, 31]. The influence of temperature has been taken into account on the properties of the laminates from the standardized tensile tests carried out on different laminates.

	C7/PEEK quasi-isotropic [(0/90),(±45),(0/90),(±45),(0/90),(±45),(0/90)]				**CG/PEEK quasi-isotropic** [(0/90)$_G$,(0/90),(±45),(0/90),(±45),(0/90),(±45),(0/90)]$_S$				**C8/PEEK orthotropic** [(0/90)]$_8$			
	E_x (GPa)	E_y (GPa)	G_{xy} (GPa)	ν_{xy}	E_x (GPa)	E_y (GPa)	G_{xy} (GPa)	ν_{xy}	E_x (GPa)	E_y (GPa)	G_{xy} (GPa)	ν_{xy}
TA	46.57	46.57	15.12	0.25	45.73	45.66	14.82	0.25	60	60	4.83	0.04
150°C	42.73	42.73	13.91	0.25	42.03	41.96	13.65	0.25	55.04	55.04	4.43	0.04

Table III.3. Elastic properties of the equivalent orthotropic laminate.

III.3.4.2 Compliance method

The compliance method is commonly used to calculate the evolution of the strain energy release rate from the force-displacement curve at the initiation and propagation of the crack, making it possible to determine the evolution of compliance $C = \delta/P$ (Figure III.5(a)), where δ is the displacement and P the force:

$$G_{Ic}^{lam} = \frac{P_c^2}{2t}\left(\frac{dC}{da}\right) \tag{III.6}$$

Classically a cubic function of the compliance versus the crack length has been fitted on the whole test for each experiment (Figure III.5(b)) [24], then an analytical derivation has been done to evaluate the fracture toughness.

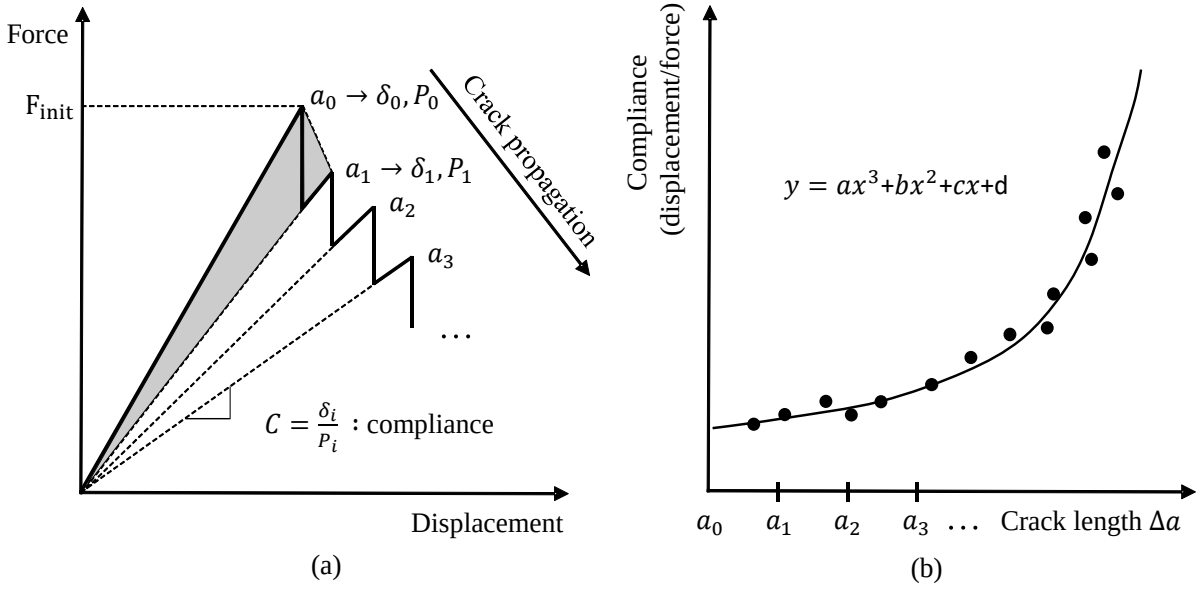

Figure III.5. Force-displacement curve representative of a stable crack growth (a) and evolution of the compliance as a function of crack length (b).

III.4 Thermo-mechanical behavior on woven-ply thermoplastic laminated composites

The purpose of this section is to investigate the thermo-mechanical and fracture behavior of the three composite laminates presented in section III.2.1, which are based on thermoplastic matrix PolyEther Ether Ketone (PEEK) reinforced by a 5-harness satin weave carbon fibers fabric, by means of Compact Tension (CT) and Compact Compression (CC) tests. An orthotropic laminate and two quasi-isotropic laminates (Figure III.1), have been tested at room temperature (RT) and at 150°C (i.e. for a temperature slightly higher than the glass transition temperature, T_g), with the purpose of evaluation the influence of the stacking sequence and the temperature on the damage mechanisms. By means of the 2D Digital Image Correlation and the implementation of an algorithm implemented in the Scilab code, the crack propagation was measured during loading.

In order to compare the thermo-mechanical responses of the studied laminates (whose thicknesses are different), therefore the force is normalized by the thickness of the laminate. Only representative experimental test is presented for each temperature, composite laminates and loading condition. In Annex A, several curves are presented.

III.4.1 Tensile tests

The propagation of the macroscopic crack is identified from the jumps observed on the force-displacement curves. The method defined in section III.3.3 then makes it possible to monitor the evolution of the crack length via the gradual decrease in load during propagation (Figure III.6).

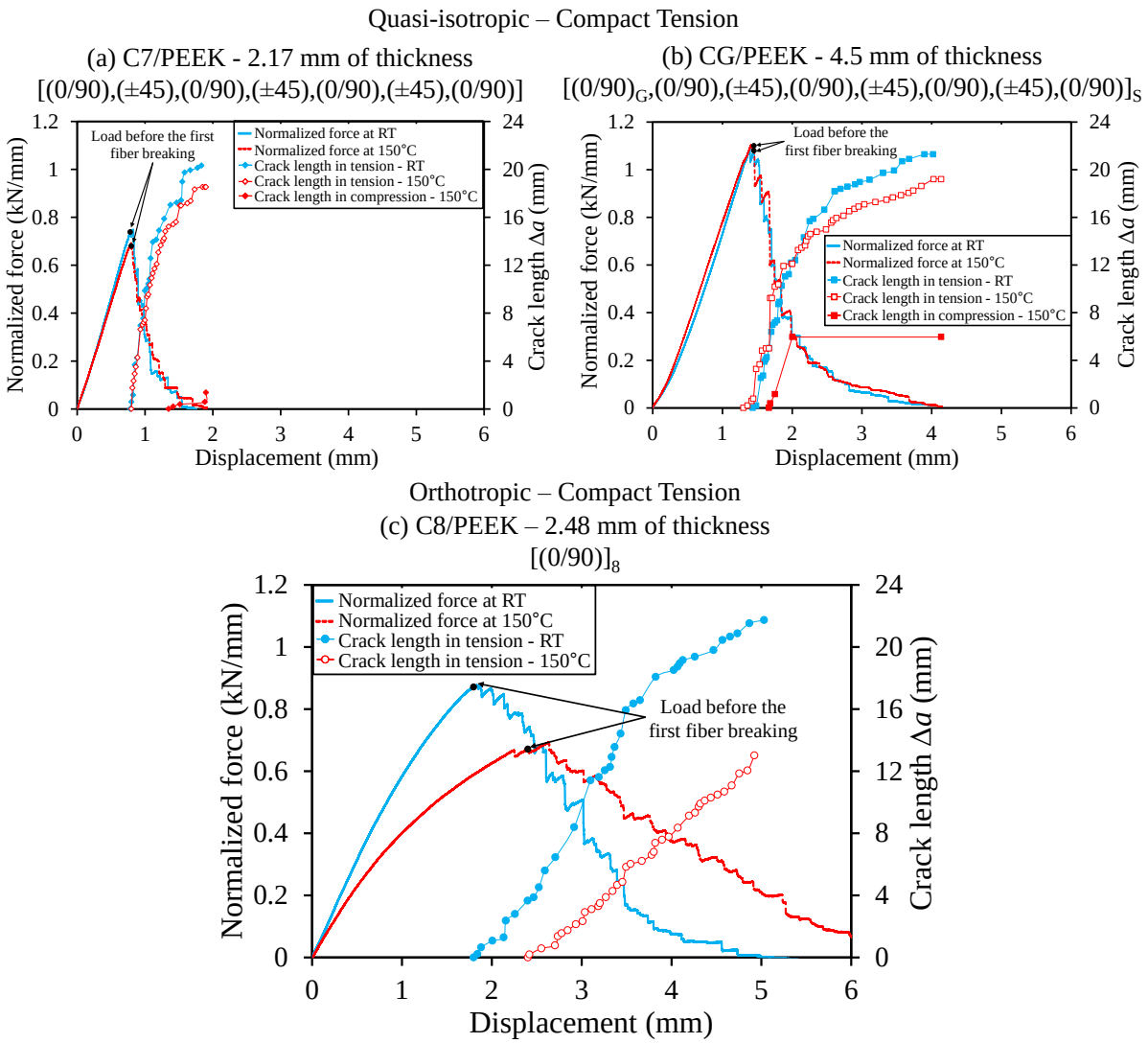

Figure III.6. Macroscopic mechanical responses and evolution of the crack length (based on the DIC analyze) of the different laminates in the case of CT specimens at RT and at 150°C.

From the curves in Figure III.6, it can be observed that quasi-isotropic laminates show similar macroscopic responses with a quasi-linear force-displacement curve before crack propagation, but with a higher initiation load at fracture for the CG/PEEK material. The significant non-linearity observed on the C8/PEEK curve is due to its low shear modulus and to a zone of high plasticity induced by significant damage at the initial crack tip (intrinsic toughness) (Figure III.7) as well as to localized crushing in the zones where the mechanical load imposed by the axes of the intermediate tool (extrinsic toughness) [51, 58-59]. It appears that the shear deformation field of the orthotropic lay-up (Figure III.7) extends beyond the crack tip, causing a more pronounced plastic behavior. In addition, the larger plasticity zone at the loading axes may justify a slower crack propagation in comparison to quasi-isotropic laminates due to a higher dissipated mechanical load.

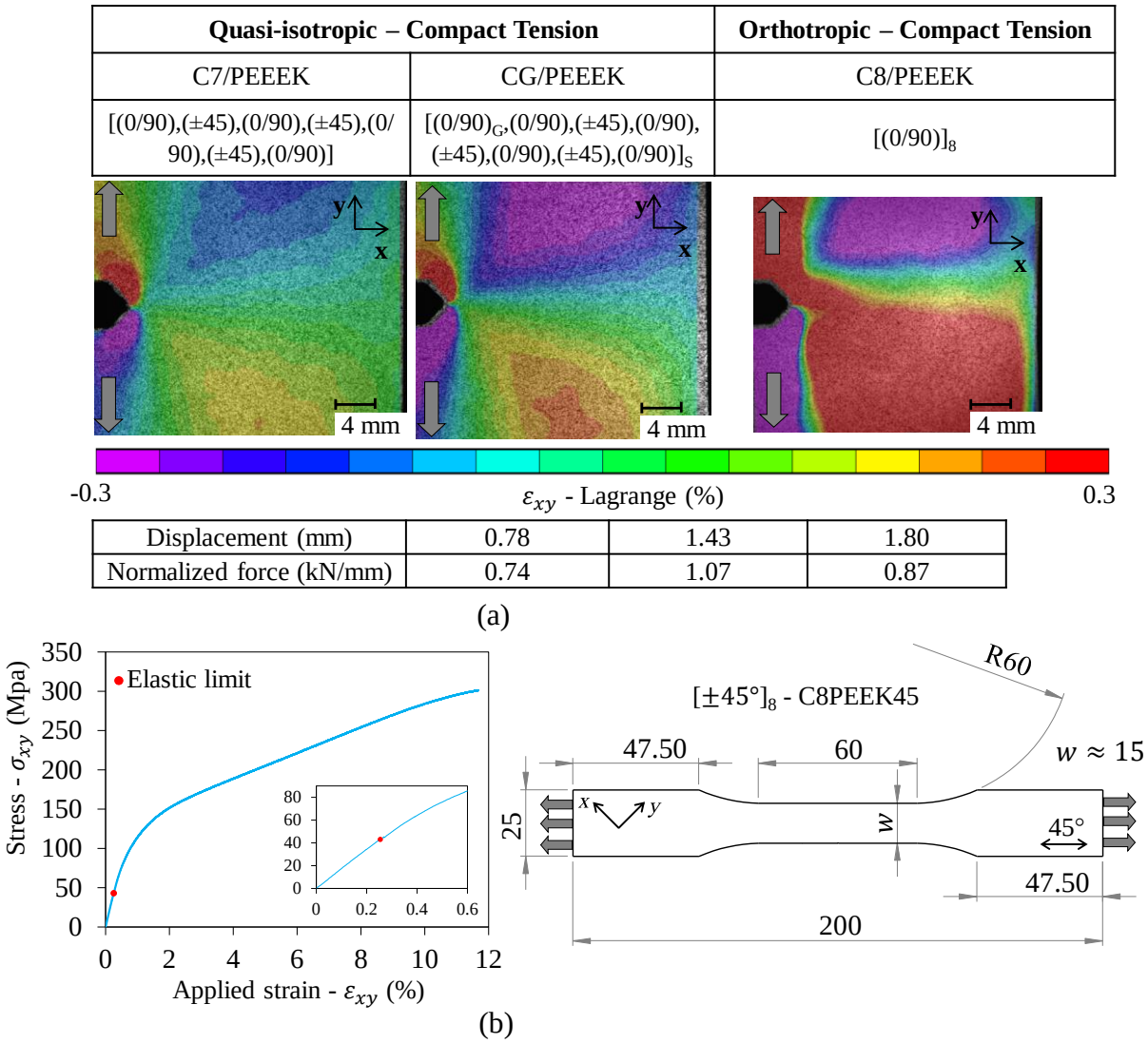

Figure III.7. (a) Shear deformation field before the first fiber breaking of the different laminates in the case of CT specimens at RT obtained by DIC – (b) Curve Stress-Strain of angle-ply laminate C8/PEEK that shows the start of the plasticity behavior at about 0.3% strain (corresponding to red color in the shear field).

Overall, the influence of temperature is not significant, despite the increase in the ductility of the resin at 150°C. The influence of temperature can also be analyzed by examining the post-mortem damage. Macroscopic observations of the damaged area suggest that the ruin of the quasi-isotropic laminates occurs by translaminar failure of the fibers in tension at TA (Figure III.8(a-b)). At 150°C, the onset of compressive failure in the area opposite the initial notch was observed for the CG/PEEK laminate (Figure III.6(b) and Figure III.8(c)). This compressive fracture is associated with buckling on a macroscopic scale, which can be explained by the significant increase in ductility of the PEEK matrix at $T>T_g$ by degrading its shear strength in particular.

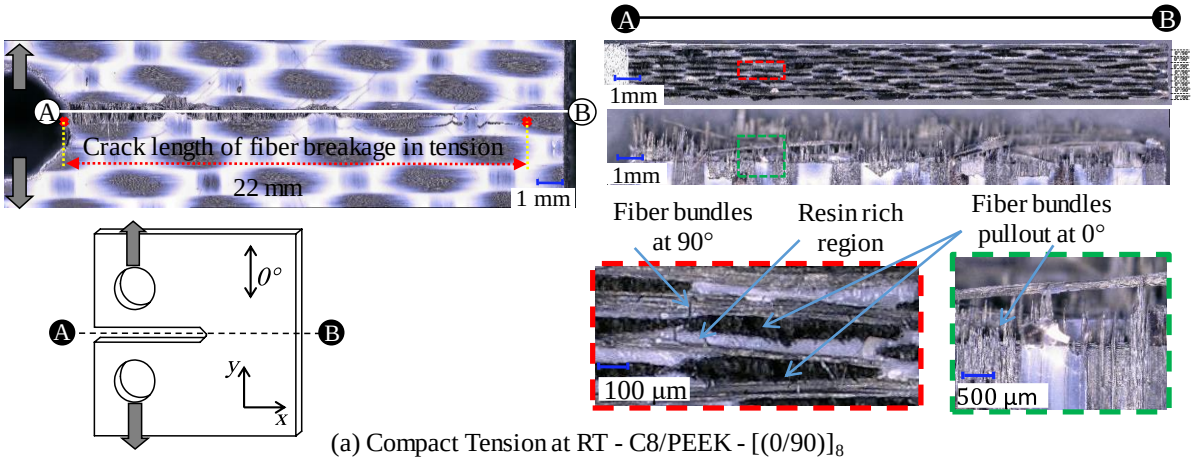

(a) Compact Tension at RT - C8/PEEK - $[(0/90)]_8$

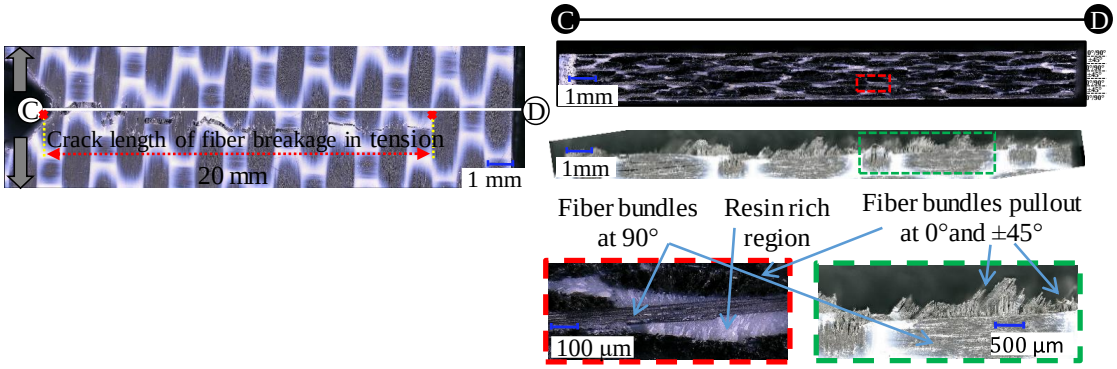

(b) Compact Tension at RT - C7/PEEK - [(0/90),(±45),(0/90),(±45),(0/90),(±45),(0/90)]

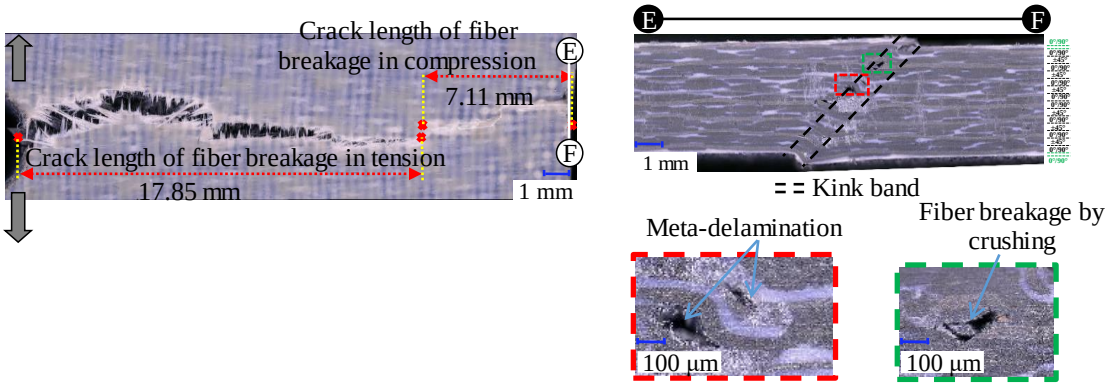

(c) Compact Tension at 150°C - CG/PEEK - $[(0/90)_G,(0/90),(\pm45),(0/90),(\pm45),(0/90),(\pm45),(0/90)]_S$

Figure III.8. Microscopic observations after failure of CT specimens: (a) C8/PEEK at RT, failure dominated by fiber pull-out at 0° - (b) C7/PEEK at RT, failure dominated by fiber pull out at 0° and ±45° (c) CG/PEEK at 150°C, failure dominated by fiber pull-out at 0° and ±45° and fiber kinking failure at the end.

The C8/PEEK orthotropic laminates exhibit an elastic-ductile behavior (Figure III.6(c)). The influence of temperature remains moderate (about 20% on the fracture load of the first fiber bundle), but results in a very pronounced out-of-plane displacement requiring the use of an anti-buckling device. The orthotropic stacking sequence fosters a very gradual propagation of the crack, with jumps of less than 1 mm (Figure III.6(c)).

III.4.2 Compressive tests

In CC specimens, crack growth is mainly related to micro-buckling of the plies at 0°, which results in fiber breakage in compression and the formation of a kink-band. Using the same protocol as for the CT specimens, the crack tip in the area damaged by compression fiber breakage could be located by image analysis. It can be seen that the crack growth is gradual (Figure III.9), but the correspondence between the increases in crack length and the jumps observed on the force-displacement curve is not obvious. In addition, it is observed that the first fiber failure does not correspond to the maximum force, but that the load continues to increase for some time after this first failure. This is because the fiber breakage in compression is less abrupt than in tension, and that after the failure in compression a crushing stress continues to be transmitted.

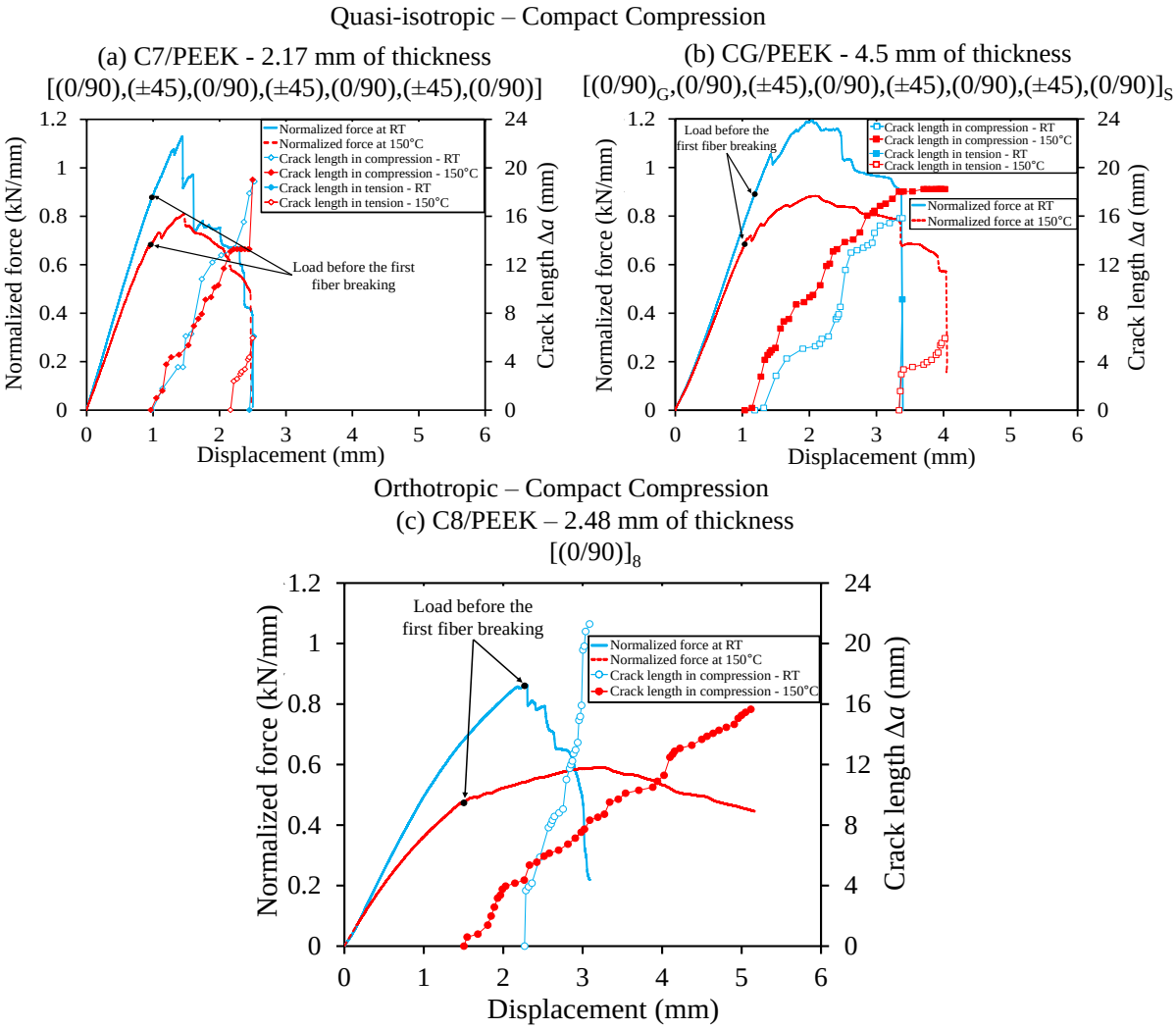

Figure III.9. Macroscopic mechanical responses and evolution of the crack length (based on the DIC analyze) of the different laminates in the case of CC specimens at RT and 150°C.

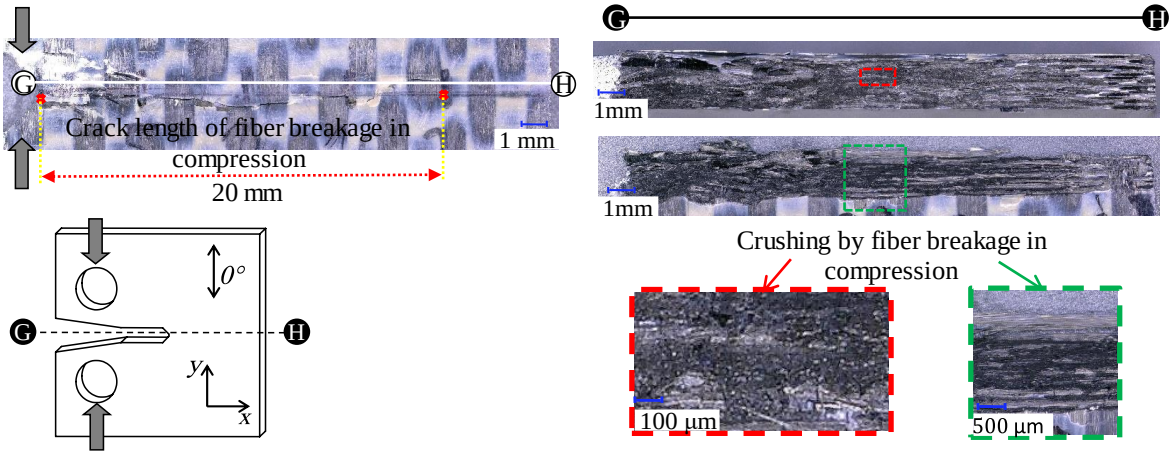

(a) Compact Compression at RT - C8/PEEK - $[(0/90)]_8$

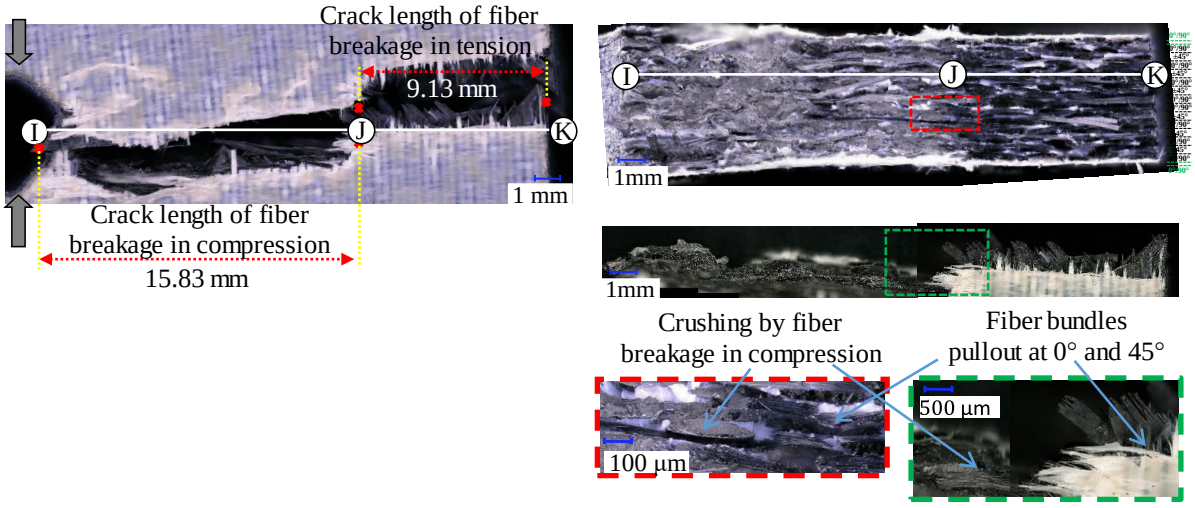

(b) Compact Compression at RT - CG/PEEK – $[(0/90)_G,(0/90),(\pm45),(0/90),(\pm45),(0/90),(\pm45),(0/90)]_S$

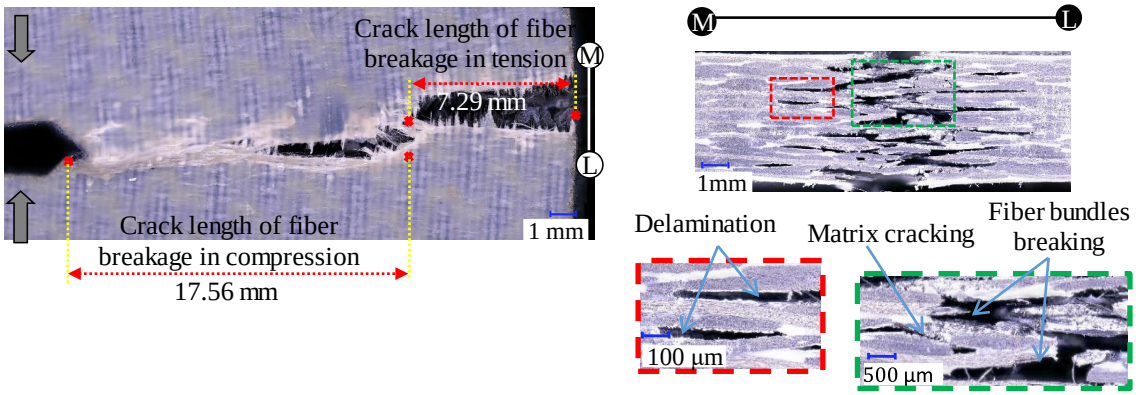

(c) Compact Tension at 150°C - CG/PEEK - $[(0/90)_G,(0/90),(\pm45),(0/90),(\pm45),(0/90),(\pm45),(0/90)]_S$

Figure III.10. Microscopic observations after failure of CC specimens: (a) C8/PEEK at RT, failure dominated by fiber breakage in compression - (b) CG/PEEK at RT, failure dominated by fiber breakage in compression with a final quasi-brittle fracture (c) CG/PEEK at 150°C, failure dominated by fiber breakage in compression and fiber breakage in tension at the end.

From the curves in Figure III.9, it can be noted that quasi-isotropic laminates are characterized by similar macroscopic responses, the force-displacement curve is quasi-linear until the start of propagation, but unlike the case of the CT tests, the load continues to increase after the start of propagation up to about 5 mm crack length. It appears that the failure of the first fiber bundle occurs almost at the same time in the force-displacement curve for quasi-isotropic laminates. The glass plies, as well as the greater thickness of the CG/PEEK, therefore do not seem to significantly influence the resistance to fracture initiation, but delay the growth of the crack.

In compression, the influence of temperature is very pronounced with a decrease of about 35% in fracture initiation resistance for quasi-isotropic laminates. At room temperature, the specimens are characterized by a final quasi-brittle fracture which results in a two-part separation of the specimens along the axis of the initial crack (Figure III.10(b)); this self-similar translaminar fracture [31] occurs when the crack length reaches a critical value due to the stress concentration accumulated on the free-edge of the specimen during the test. The onset of a tensile fiber breakage at the free-edge of the specimen is observed at 150°C for quasi-isotropic laminates (Figure III.9(a-b) and Figure III.10(c)). At 150°C, the more pronounced ductility of the PEEK matrix fosters the localized crushing of the plies in compression inducing ductile failure, especially for the orthotropic laminate.

The force-displacement curve of the C8/PEEK orthotropic laminate (Figure III.9(c)) is non-linear even before propagation begins. At room temperature, and at 150°C, the orthotropic C8/PEEK laminate does not exhibit fiber breakage in tension; the fibers all fail in compression (Figure III.10(a)). This can be explained by the absence of plies at ±45°, which limits the transmission of shear forces. At 150°C, the test was stopped before the final break to avoid contact between the notch faces of the specimen, but the specimen was not completely broken (the load does not decrease to 0). This interruption is likely to prevent the development of a tensile crack, observed in quasi-isotropic laminates. The influence of temperature is more pronounced compared to the quasi-isotropic laminates with a reduction of about 50% of the resistance at the initiation of the fracture.

III.5 Experimental estimation of the critical strain energy release rate

The resistance of a laminate to translaminar crack initiation and propagation can be characterized by a resistance curve, called the R-curve. The first point of the R-curve can be defined as the critical strain energy release rate related to crack initiation G_{I_C}, while the propagation values G_{I_C} generally tend towards an asymptote in brittle FRP composites [14, 16-18, 24, 34, 39, 41-42]. Here, the ASTM-399 standard is applied only to determine the value of the critical strain energy release rate at initiation, the critical load associated with crack initiation was identified using digital image analysis. The compliance method is used to monitor the evolution of the strain energy release rate during propagation as well.

The purpose of this section to estimate the critical strain energy release rate associate associated with mode I tensile and compressive failure.

III.5.1 Tensile tests

The mean R-curves obtained for the three laminates are shown in Figure III.11. No value was taken for a crack length greater than 11 mm due to the appearance of a secondary crack (compression crack for the CT test and tensile crack for the CC test), which contributes to dissipation of mechanical energy during fracture, which disturbs the evaluation of the strain energy release rate.

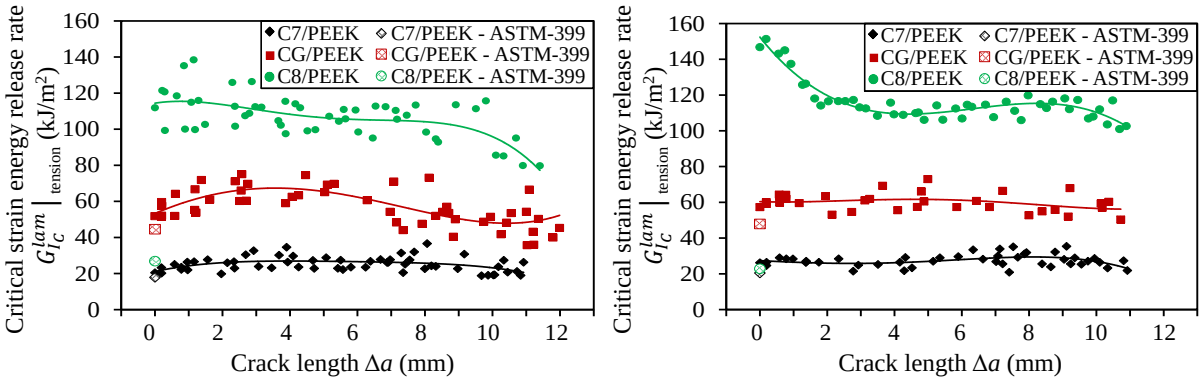

(a) Compact Tension at room temperature

(b) Compact Tension at 150°C

Figure III.11. G-R curves obtained with the compliance method from CT specimen tests: (a) RT and (b) 150°C.

The compliance method makes it possible to monitor the evolution of the strain energy release rate during crack propagation (Figure III.11). The values of $G_{Ic}^{lam}\big|_{\text{tension}}$ at initiation determined from the ASTM-399 standard seem to validate its use for quasi-isotropic woven laminates; the difference observed at the values obtained with the compliance method remains small (Figure III.11, Figure III.15 and Table III.4). For the orthotropic C8/PEEK laminate, the mean value of $G_{Ic}^{lam}\big|_{\text{tension}}$ at initiation calculated from ASTM-399 gives a value at RT of 29.9 kJ/m^2 compared to 117.3 kJ/m^2 for the compliance method. It is reasonable to assume that the higher value of $G_{Ic}^{lam}\big|_{\text{tension}}$ at initiation is due to a very high plasticity at the points of load application accompanied by a greater area of plasticity at the crack tips (Figure III.7). It is worth noting that ASTM-399 is applicable for materials with elastic-brittle behavior, which is not observed for orthotropic laminate (Figure III.6(c)).

Figure III.11 shows that all the R-curves tend to converge for a crack length greater than about 4 to 11 mm depending on the case, this would mean that the size of the FPZ is reached from the beginning and does not change much, as is shown in Figure III.12, where the highly deformed zone is illustrated using a value lower than that of the fiber failure as the limits of the strain field. In quasi-isotropic laminates, it appears that the increase in thickness implies a significant increase in $G_{Ic}^{lam}\big|_{\text{tension}}$ at initiation and during propagation (Figure III.11, Figure III.15 and Table III.4). The presence of two glass-PEEK plies can be considered negligible compared to the proportion of carbon-PEEK plies in the CG/PEEK hybrid laminate, so the large increase observed can be attributed mainly to the increase in the thickness of the laminate [16, 34], which leads to an increase in the size of the damaged areas (Figure III.13). In section IV.6 a study

about the influence of glass fibers of the CG/PEEK laminate on the translaminar failure and the extrinsic toughness is presented. A simple thresholding method applied in the images (Figure III.13) shows that the fracture surface increase with the thickness and with the presence of 45° laminate ply.

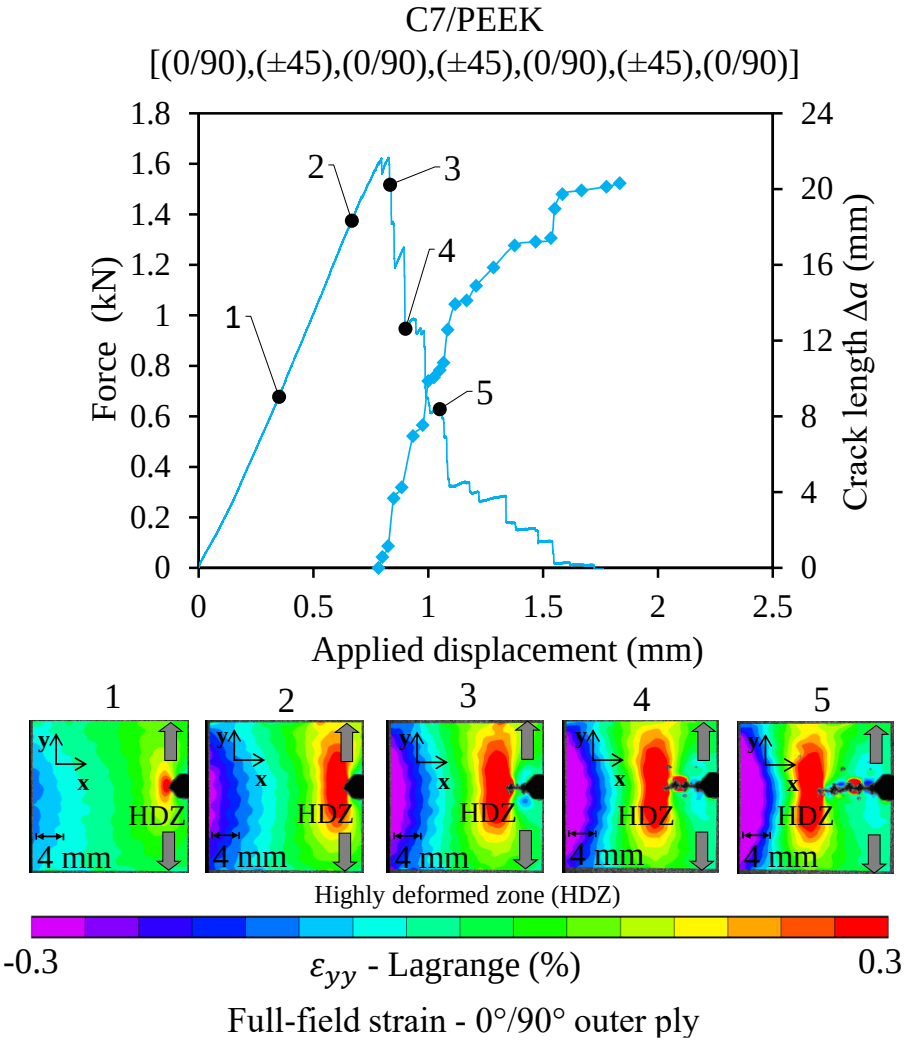

Figure III.12. Evolution of the highly deformed zone (HDZ) and the crack growth in a CT test at RT.

Temperature contributes to a small increase (7% to 10%) in the translaminar fracture toughness of quasi-isotropic laminates at initiation, this trend can also be seen during propagation (Figure III.11, Figure III.15 and Table III.4).

Overall, the C8/PEEK orthotropic laminate has a very high translaminar tensile fracture toughness compared to the quasi-isotropic laminates, while the number of fibers to be broken is lower (Figure III.13). In practice, cutting a 0°/90° ply requires cutting only the fibers at 0°, whereas cutting a ±45° ply requires cutting the fibers at +45° and -45° [34]. The greater toughness of the orthotropic laminate could be due to a zone of extensive plasticity caused by blunting at the initial crack tip (Figure III.7) as well as significant plastic deformations at the load application points, thus inducing energy dissipation, which is added to those due to the crack propagation. However, this calls into question the computation of the critical strain energy

release rate from a global computation using the force-displacement curve (Figure III.6), and must be confirmed by a local computation of the integral J type or infrared thermography [19].

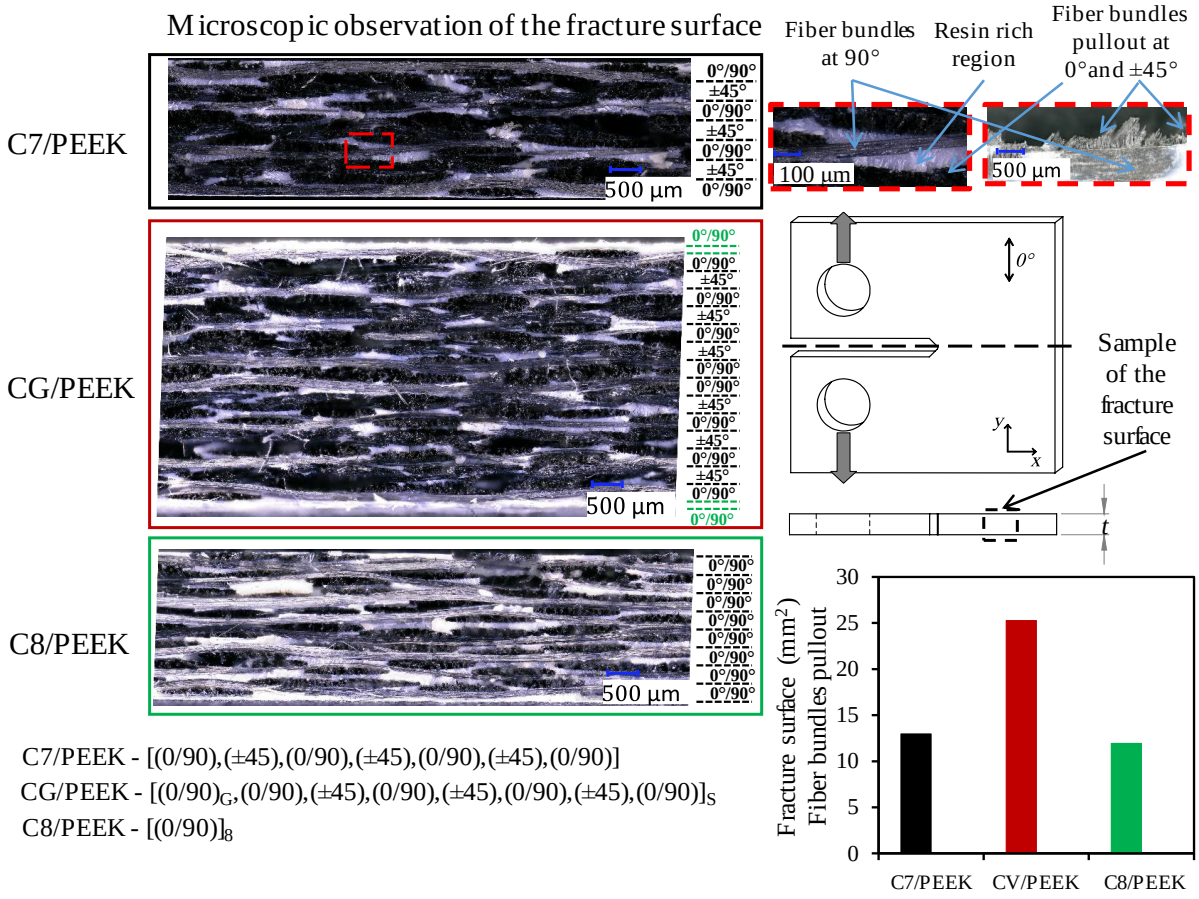

Figure III.13. Microscopic observations of the fracture surface of studied laminates in the case of CT specimens at RT.

III.5.2 Compressive tests

In this case, R-curves were obtained for crack growth values up to about 16 mm (Figure III.14). An increasing trend of $G_{Ic}^{lam}\big|_{\text{compression}}$ during propagation is observed for all laminates. This evolution is due to the fact that after a compressive failure in the form of a kink-band, a crushing stress is transmitted (contrary to the case of a tensile test). Thus the evolution of the critical strain energy release rate during the formation of a kink-band does not accurately describe the absorbed energy, since other modes of damage are present in particular the crushing of the fibers or the delamination (Figure III.10). Thus the values at initiation seem to be the best measure of the critical strain energy release rate associated with the appearance of the kink-band (Figure III.14 and Table III.4). For quasi-isotropic laminates, an increase in translaminar fracture toughness is observed with thickness, but not to the same magnitude as in tension.

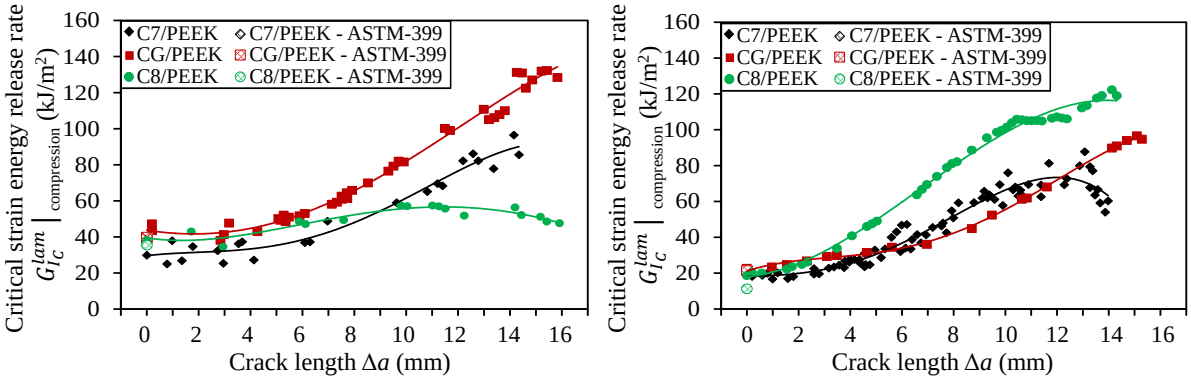

(a) Compact Compression at room temperature

(b) Compact Compression at 150°C

Figure III.14. G-R curves obtained with the compliance method from CC specimen tests: (a) RT and (b) 150°C.

There is also a very marked decrease in translaminar fracture toughness on all the laminates studied at 150°C (Figure III.14 and Table III.4), in contrast to the tensile characterized by a slight increase, suggesting that a test temperature $T>T_g$ contributes to the formation of plastic buckling bands in compression due to increased ductility of the PEEK matrix. At RT, the crushing is more pronounced than the buckling and at 150°C the out-of-plane buckling is more pronounced than the crushing, because the softening of the matrix in the overlapping areas facilitates the out-of-plane displacement of the fiber bundles.

III.5.3 Summary of the translaminar fracture toughness found in this study

The purpose of this section is to summarize the critical strain energy release rate found in this study. The tensile and compressive translaminar fracture toughness for the three woven-ply thermoplastic laminates with the two temperature tested are shown in Figure III.15 and in Table III.4.

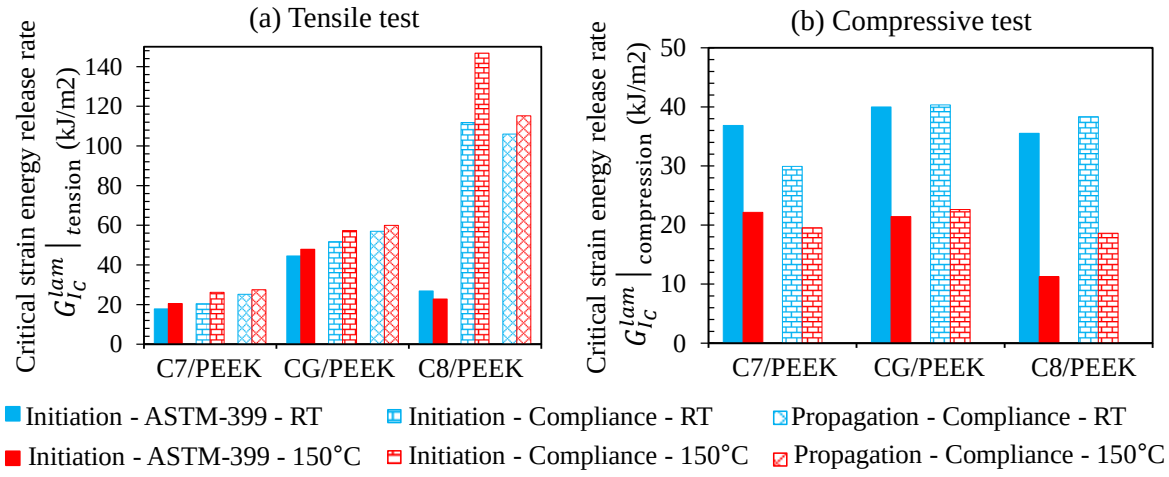

Figure III.15. Influence of the stacking sequence and the temperature on the tensile and compressive fracture toughness.

Laminate type Polymeric resin Fiber reinforcement	Specimen name Laminate lay-up	Method of data reduction	Fracture toughness G_{Ic}^{lam} (kJ/m²)			
			TA		150°C	
			Initiation	Propagation	Initiation	Propagation
Woven ply composite laminate PEEK Carbon HTA40 / E-Glass	Compact Tension					
	C7/PEEK [(0/90),(±45),(0/90),(±45),(0/90),(±45),(0/90)]	ASTM-399	17.81	-	20.48	-
		Compliance	20.44	25.19	26.21	27.47
	CG/PEEK $(0/90)_G$,(0/90),(±45),(0/90),(±45),(0/90),(±45),(0/90)]$_S$	ASTM-399	44.56	-	47.89	-
		Compliance	51.76	56.94	57.33	59.92
	C8/PEEK [(0/90)]8	ASTM-399	26.89	-	22.84	-
		Compliance	111.84	106.00	146.79	115.21
	Compact Compression					
	C7/PEEK [(0/90),(±45),(0/90),(±45),(0/90),(±45),(0/90)]	ASTM-399	36.86	-	22.13	-
		Compliance	29.91	-	19.53	-
	CG/PEEK $(0/90)_G$,(0/90),(±45),(0/90),(±45),(0/90),(±45),(0/90)]$_S$	ASTM-399	39.98	-	21.43	-
		Compliance	40.32	-	22.63	-
	C8/PEEK [(0/90)]8	ASTM-399	35.53	-	11.27	-
		Compliance	38.35	-	18.60	-

Table III.4. Summary of the fracture toughness obtained in this study using CT and CC specimens.

III.6 Conclusion

In the framework of the study the damage tolerance of the high performance TP laminates used for aeronautical applications in high temperature conditions, the quantification of translaminar fracture toughness plays a key role. One of the main objectives of this study was to determine translaminar fracture toughness values for composite woven-ply thermoplastic-based laminates to be used under high temperature conditions. This study was aimed at proposing an in situ crack growth measurement based on a Digital Image Correlation (DIC) technique implemented in a thermal chamber combined with a high intensity light source and a binarization algorithm.

In this chapter, Compact Tension and Compact Compression specimens were used to study the translaminar fracture on three thermoplastic laminates reinforced with woven-ply carbon fiber. Tests at room temperature and at 150°C were carried out to study the effects of temperature when the ductility of the PEEK matrix is exacerbated.

In orthotropic laminates, tensile tests also reveal that the plastic area is very large at the crack tip due to its low shear modulus (intrinsic toughness). Local plasticity also causes an important toughness linked to localized crushing in the area of force application (extrinsic toughness). In quasi-isotropic laminates, thickness contributes to increase the initiation load at fracture and slows the propagation of the crack. Compressive failure by plastic buckling on the edge opposite the notch is facilitated by the ductility of the PEEK matrix at $T>T_g$.

Compression tests show that compressive failure is driven by the fiber breakage at 0° and the formation of a plastic kink-band. As for tension tests, for the orthotropic laminate, the low shear modulus induces an important zone of plasticity, an important extrinsic toughness and makes it difficult the evaluation of the fracture toughness. At high temperature, ductile failure associated with localized crushing of the plies is promoted by the plastic deformation of the PEEK matrix at $T>T_g$.

Toughness evaluation based on ASTM-399 proved to be relevant for quasi-isotropic woven laminates giving similar values compared to the compliance method. For highly orthotropic laminates, the computation of toughness based on an overall behavior (force-displacement curve) is related to energy dissipation at the points of load application accompanied by greater plasticity mechanisms at the crack tip, which are combined with those related to crack propagation. In tension, the R-curves tend to converge towards an asymptote with an almost constant value, while in compression the R-curves tend to increase due to localized crushing which results in constant crushing stress.

Finally, at a temperature (e.g. 150°C) slightly higher than the glass transition temperature of the materials there is a moderate increase in the translaminar fracture toughness in tension. Thickness increases the fiber pull-out length causing an increase in the translaminar fracture toughness in tension. In compression, the thickness does not seem to influence the size of the kink-band (which is associated with the fiber diameter and to the matrix shear mechanical behavior). The compressive translaminar fracture toughness decreases sharply with the temperature, as the softening of the matrix in the overlapping areas facilitates the out-of-plane movement of the fiber bundles. For orthotropic laminates the computation of the translaminar

fracture toughness will have to be confirmed by a local computation of the integral J type or infrared thermography due to the ductile fracture behavior.

To understanding the influence of stacking sequence and the laminate thickness on the fracture toughness is of the utmost important to develop numerical tools capable of capturing the fracture behavior of laminate composites. It is therefore possible to tester fracture parameters (e.g. the critical strain energy release rate, crushing stress, failure strain in tension and in compression) and to simulate the phenomena that induce high plasticity to obtain the valid values for a safe structural design. In Chapter V, a numerical model is developed with the aim to better understand the influence of stacking sequence and laminate thickness on the fracture behavior of woven-ply laminated composites and with the objective of better understanding the CT test, and in particular the CC tests which are more difficult to analyze.

Chapter IV: Fracture mechanics of hybrid composites with ductile matrix and brittle fibers, influence of temperature and constraint effect

Specimens with initial notches induce a local stress concentration and thus favor damage localization. Certain specimen geometries produce a progressive and stable crack growth providing the evolution of the critical strain energy release rate. In this chapter, two specimen geometries with different initial notches were tested in the hybrid laminated composite (CG/PEEK) in order to study the influence of temperature and constraint effect.

In the first part of this chapter, a brief overview of the influence of intrinsic and extrinsic toughness on the estimation of fracture toughness is presented. Then, the main objectives of this chapter are detailed. In the second part, the materials, experimental set-up and data reduction methods are specified. In the third part, the main results of this study are presented and discussed. First, the macroscopic mechanical response and fracture behavior are discussed. Second, the G-R curves for the Single-Edge-Notch Bending specimens with different ratio a/w are computed. Thereafter, a discussion about the influence extrinsic toughness on the fracture behavior is proposed. In the last part of this chapter, the main conclusions are detailed.

The work presented within this chapter has resulted in the following publication:

Vieille, B., Pujols González, J. D., & Bouvet, C. (2019). Fracture mechanics of hybrid composites with ductile matrix and brittle fibers: Influence of temperature and constraint effect. Journal of Composite Materials, Vol. 53 (10), pp. 1361-1376.

Chapter IV outline

IV.1 Introduction

In a material, fracture toughness is classically defined as the energy required to extend a crack, in other words to resist fracture under mechanical loading by means of locally dissipative behaviors (e.g. plastic deformation or damage mechanisms). In notched structures, plastic and damage deformation mechanisms are instrumental in redistributing the overstresses around the notch, and therefore in modifying their fracture behavior [51, 60-61]. Early in the seventies, it was shown that the fracture toughness of engineering materials is improved by introducing tough fibers into a brittle matrix [62], or brittle fibers into a ductile matrix [63]. In polymer matrix composites (PMCs), it is also well accepted that the insertion of a ductile resin-rich layer between laminates layers is found to increase significantly their fracture resistance, without altering its dependence on crack growth rate [64-65]. The fiber/matrix adhesion also plays a major role in fracture toughness as the adhesion rules the overstress profiles near the fiber/matrix interface [66]. In brittle matrices polymer composites, a too strong interface discourages additional energy absorbing mechanisms such that fiber bridging and breakage [51]. In tough matrices polymer composites, the strong fiber/matrix interface is necessary to allow extensive deformation of the matrix in order to fully utilize the intrinsic matrix toughness [67]. When a notched laminate is loaded in tension, a Fracture Process Zone (FPZ) is observed at the notch tip [68], and gradually grows with increasing load (Figure IV.1).

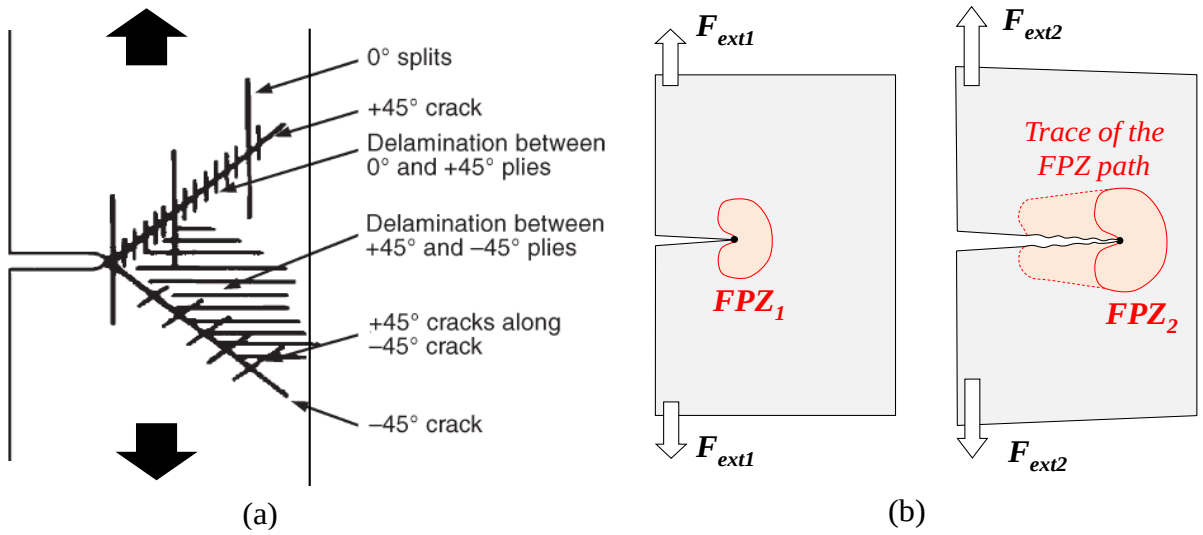

Figure IV.1. Single-Edge-Notch composites loaded in opening mode: (a) Typical fracture process zone at a sharp crack [68] – (b) Trace of the Fracture Process Zone at the crack tip [8]

Depending on stacking sequence and constitutive materials, the crack path observed in fiber-reinforced polymer laminates is often complex. The crack propagates at a critical load, and the translaminar crack growth resulting from an initial transverse notch is usually self-similar (Figure IV.2) in quasi-isotropic brittle laminates [31, 69-71]. Thus, the extension of a self-similar translaminar crack allows a global analysis based on a global strain energy release-rate that is computed from tensile loading [69-72].

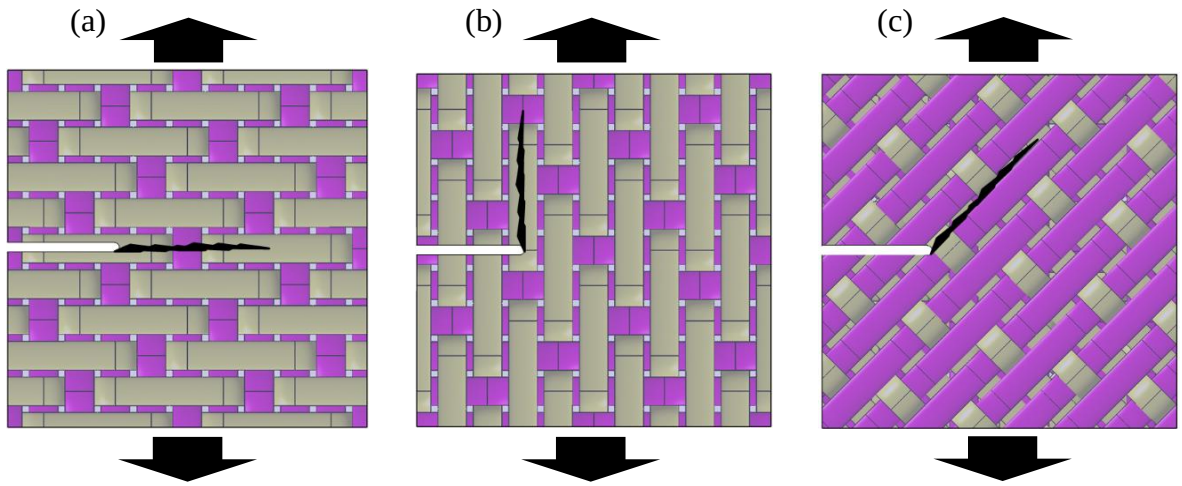

Figure IV.2. Crack growth in single-edge-notch laminates, here the case of a woven-ply laminated (Adapted from Jones [31]): (a) Self-similar and (b) nonself-similar.

IV.1.1 Intrinsic vs extrinsic toughness

In most engineering materials, the fracture resistance depends on their microstructure by means of two primary toughening (intrinsic and extrinsic) mechanisms [43]. As pointed by Launey et al. [51], single-value parameters (such that the mode I critical stress intensity factor K_{Ic}) based on crack initiation are classically used to quantify intrinsic toughness (associated with the nature of the constituents and the reinforcement architecture). However, these parameters cannot always capture the ability of a microstructure to develop toughening mechanisms acting either ahead or behind the crack tip. The fracture toughness of fiber-reinforced composites is improved by increasing both micro- and meso-structural resistances by changing the nature of constituents, the fibers and matrix distribution and/or the interface properties to suppress damage (primarily micro-cracking and fiber breakage) ahead of the crack tip. These changes represent intrinsic toughening and are instrumental in increasing the fracture toughness of ductile materials. On the contrary, the fracture of brittle materials is characterized by micro- and meso-structural mechanisms. These mechanisms result in effectively reducing the crack-driving force at the crack tip by dissipating mechanical energy by means of local plastic deformation, damage mechanisms, and fibers bridging (primarily associated with local debonding and fibers pull-out). These mechanisms represent extrinsic toughening also known as crack-tip shielding [51]. Contrary to intrinsic toughness, extrinsic toughness is often developed primarily during crack growth resulting from crack-tip shielding mechanisms that result in rising R-curve behavior.

IV.1.2 Influence of the temperature on fracture toughness

The modes of energy dissipation are primarily affected by the matrix fracture mode (brittle or ductile). This is mainly determined by the loading rate or temperature conditions in the literature [73-75]. The energy dissipated during controlled crack propagation in fiber reinforced composites is usually evaluated in terms of different source mechanisms: plastic deformation, fiber-snapping, matrix-cracking and fiber pull-out [31, 70, 76]. In composite materials with a

brittle matrix, the energies dissipated during crack initiation and propagation in the composite with a weak fiber/matrix interface are derived principally from the work of fiber pull-out (resulting from the frictional forces that hold a broken fiber in its matrix socket). In ductile matrix composite systems, the local plastic deformation of the matrix also needs to be taken into account in the total fracture toughness [46, 74]. The mechanical behavior of polymer resins exhibits temperature dependence (viscoelastic and viscoplastic behaviors) not only above T_g and also below T_g. Kim et al. have studied the influence of temperature on interfacial debonding on composites with TP coated carbon fibers [46]. In the late eighties, the elevated-temperature dependence of fracture energy mechanisms of hybrid carbon-glass fiber reinforced epoxy composites was studied by Munro et al. [75], who concluded that the work of fracture increased with temperature and glass fiber content. Indeed, the post-debond friction energy term was shown to be dominant, resulting from an extensive frictional work of the post-debond sliding type after glass fiber failure, in addition to that from the glass-fiber pull-out mechanism. Besides, the reinforcement architecture (UD or woven fabrics) also appears to significantly influence the extrinsic toughness of PMCs [33, 77]. The influence of temperature on the interlaminar fracture toughness of thermoplastic-based composites was widely investigated in unidirectional composites as reviewed in previous studies [65-66], and more specifically in the case of woven-ply laminates [46, 65].

IV.1.3 Objectives of this chapter

This study present in this chapter deals with the fracture mechanics of hybrid laminated composites consisting of highly ductile thermoplastic matrix (PEEK) and brittle fibers CG/PEEK. The effect of temperature and constraint effect on the strain energy release rate and crack extension of the laminates are specifically addressed in the case of a mode I translaminar failure mode. On the one hand, tests are carried out at room temperature (RT) and at 150°C (i.e. slightly higher than T_g as the ductile behavior of PEEK matrix is exacerbated) to examine the influence of temperature on fracture energy. On the other hand, tests are conducted on SENT and SENB specimens with different ratio *a/w* to investigate the influence of constraint effect on fracture toughness. The *G-R* curves were derived from the computation of the compliance loss and the crack extension in agreement with the ASTM standard E1820.

IV.2 Specimen description and tests procedures

IV.2.1 Materials

In this chapter, only the composite laminate noted as CG/PEEK will be used to perform this study. All specifications of this composite laminate are given in section III.2.1. The laminated plates CG/PEEK obtained by thermo-compression are made up of carbon (Tenax®-E HTA40 3K)–PEEK 5HS woven plies prepregs and glass–PEEK prepregs. The consolidated laminates consist of 14 inner carbon-PEEK plies and two outer glass-PEEK plies. In addition, the carbon and glass fiber fabrics are balanced in the warp and weft directions. The stacking sequence of laminates is quasi-isotropic (as shown in Figure III.1): $[(0/90)_G,[(0/90),(\pm45)]3,(0/90)]_S$ (with G index for glass fibers ply). The average thickness of laminates is about 4.5 mm.

IV.2.2 Specimen geometries

The Single-Edge-Notch test specimens (tensile and bending) were cut by water jet from 600 × 600 mm^2 plates (Figure IV.3). The machining of the Single-Edge notches was done by means of a precision endless diamond wire saw whose radius is 0.085 mm. The initial notch length to specimen width ratio *a/w* ranges from 0.2 to 0.5 in both SENT and SENB specimens.

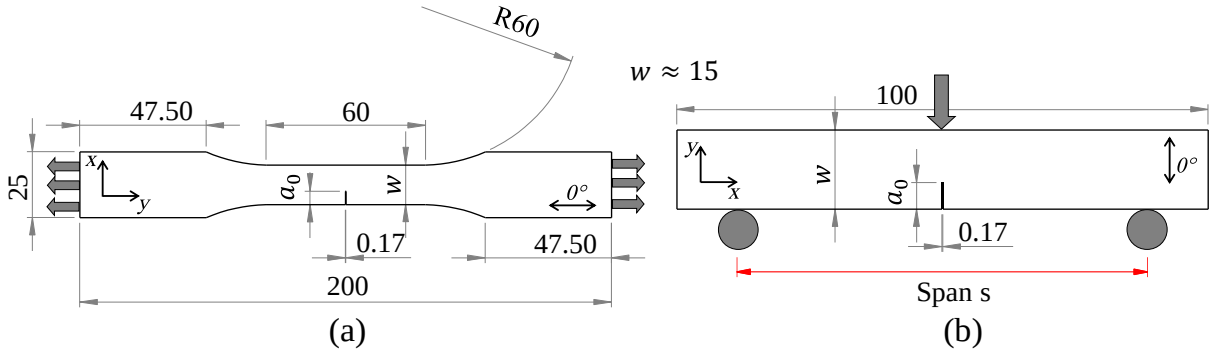

Figure IV.3. Geometry of Single-Edge Notched (in mm): (a) Tensile specimens and (b) Bending specimens.

IV.3 Experimental set-up and methods

IV.3.1 Thermo-mechanical testing

All the tests were performed using the same machine described in section III.3.1. A 100kN capacity load cell of a MTS-810 servo-hydraulic testing machine in displacement-controlled mode and with a temperature control system. Tensile and three points bending loadings were applied to notched specimens at Room Temperature (RT) and 150°C. Three specimens were tested in each configuration to obtain an acceptable average value.

IV.3.2 Data reduction methods

The tensile mechanical properties were determined according to the European standards EN 6035 [78]. In SENT specimens, the longitudinal modulus (E_X) and ultimate strength (σ^u) were calculated from the following definitions:

$$E_X = \frac{\Delta F}{S.\Delta\varepsilon_X} \tag{IV.1}$$

and

$$\sigma^u = \frac{F^u}{S} \tag{IV.2}$$

where ΔF is the difference in the applied tensile loads at $(\varepsilon_X)_2 = 0.25\%$ and $(\varepsilon_X)_1 = 0.05\%$, S is the specimen cross section, $\Delta\varepsilon_X = (\varepsilon_X)_2 - (\varepsilon_X)_1$ is the difference in the longitudinal strains obtained from a blade-extensometer, F^u is the maximum force borne by the specimen at failure. The mechanical properties of C/PEEK and G/PEEK elementary plies are specified in Table III.2.

The mechanical properties in bending were determined according to the European standards EN 2562 [79]. The bending strain and stress are defined as follows:

$$\varepsilon_{bending} = \frac{6\delta w}{s^2} \tag{IV.3}$$

and

$$\sigma_{bending} = \frac{3Ps}{2tw^2} \tag{IV.4}$$

where t is specimen's thickness, s is the span between the support points, and δ is the displacement applied to the upper part of the specimen (Figure IV.1(b)).

The bending stiffness is classically given by:

$$E_{bending} = \frac{P^u s^3}{10tw^3(\delta_1 - \delta_2)} \tag{IV.5}$$

where P^u is the ultimate load, δ_1 and δ_2 are the applied displacement at $P^u/2$ and $P^u/10$, respectively.

IV.3.2.1 Relationship between critical stress intensity factor and critical strain energy release rate

Here, the same relation is used between stress intensity factor and strain energy release rate from section III.3.4.1. Let us call again. In orthotropic materials, the critical strain energy release rate G_I is classically obtained from the critical stress intensity factor K_I and the engineering constants [15, 21, 80]:

$$G_{Ic}^{lam} = C_I K_{Ic}^2 \tag{IV.6}$$

with $C_I = \sqrt{\frac{1}{2E_xE_y}}\sqrt{\sqrt{\frac{E_x}{E_y}} - \nu_{xy} + \frac{E_x}{2G_{xy}}}$ for plane stress conditions.

where E_x, E_y, G_{xy} and ν_{xy} are respectively the Young's modulus in x and y directions, the shear modulus and the Poisson's ratio of the laminate. The properties used for the computation of the orthotropic elastic coefficient of the equivalent laminate CG/PEEK are given in Table III.3, they are obtained from the properties of the elementary ply (Table III.2) using the laminate theory [9, 31]. The estimation of the fracture toughness depends on the geometry, the loading conditions and the characteristic length of the initial notch machined in the specimen to initiate failure [15, 48]. One of the most commonly used specimens are Single-Edge-Notch Bending (SENB) and Single-Edge-Notch Tensile tests (SENT). The ASTM standard E1820 test method covers procedures and guidelines for the determination of fracture toughness of isotropic materials using the following parameters [81]: *K*, *J*, and Crack Tip Opening Displacement (CTOD). The fracture toughness determined in accordance with this test method is for the opening mode (Mode I) of loading. To a first approximation, this method was applied to

evaluate the mode I strain energy release rate from SENT and SENB specimens, as well as the crack growth in SENB specimens.

IV.3.2.2 Critical stress intensity factor

The use of critical stress intensity factor values in engineering applications of fracture mechanics do not require values computed with absolute precision. Different approximations were proposed for K_{I_C} in the literature [15, 20], and the critical stress intensity factor is classically estimated by analytical functions in SEN specimens in mode I:

$$K_{I_C} = \sigma_C \sqrt{\pi a_0}.\, f(a/w) \qquad \text{(IV.7)}$$

where σ_C is the critical remote applied stress ensured at crack initiation, a_0 denotes the length of the initial crack and w is the specimen width (Figure IV.4). $f(a/w)$ is a geometric finite-width-correction (FWC) function calculated from the ratio a/w and empirical formulas. By definition, this FWC function is a scale factor applied to multiply the notched infinite-plate solution to obtain the notched finite-plate result [31].

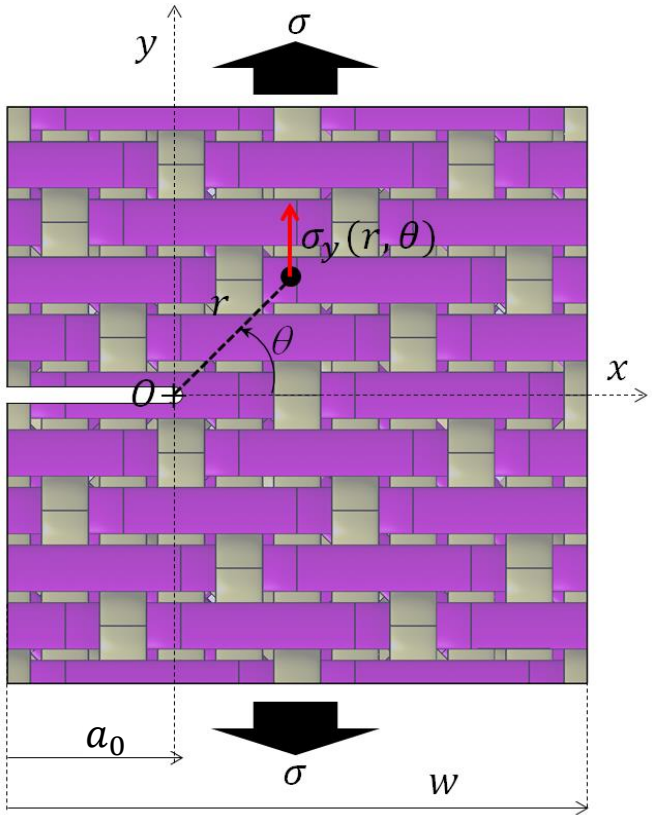

Figure IV.4. Longitudinal stress near the crack tip in QI SEN laminates loaded in mode I.

For SENT specimens, Gross et al. have proposed the following expression [82], whose precision is 0.5% for $a/w \leq 0.6$:

$$f(a/w) = 1.122 - 0.231(a/w) + 10.550(a/w)^2 - 21.710(a/w)^3 + 30.382(a/w)^4 \qquad \text{(IV.8)}$$

As introduced in the case of SENT specimens, the mode I fracture toughness is also estimated from the equation IV.7. The geometric finite-width-correction function $f(a/w)$ is calculated from the ratio a/w and empirical formulas whose precision is 0.5% for any ratio a/w [15]:

$$f(a/w) = \frac{1}{\sqrt{\pi}} . \frac{[1.99 - (a/w)(1 - a/w)(2.15 - 3.93(a/w) + 2.7(a/w)^2]}{(1 + 2(a/w))(1 - a/w)^{3/2}} \qquad \text{(IV.9)}$$

IV.3.2.3 Estimation the crack growth in SENB specimens

In SENB specimens, the ASTM standard E1820 test method gives an estimation of the crack growth versus applied stress [81]. Thus, the crack length on a SENB specimen is normally determined from crack opening compliance. According to the ASTM standard, it is determined from load-line compliance if the correct calibration is available. For a resistance curve test method using an elastic compliance technique (Figure III.5(a)) on single edge bend specimens with crack opening displacements measured at the notched edge, the crack length a_i at each mechanical load is given as follows:

$$a_i/w = [0.999748 - 3.9504u + 2.9821u^2 - 3.21408u^3 + 51.51564u^4 - 113.031u^5] \qquad \text{(IV.10)}$$

where $u = \frac{1}{\left[\frac{twE'C_i}{s/4}\right]^{1/2} + 1}$

t and w are the specimen thickness and width respectively, $E'(E' = 1/C_I)$ is the orthotropic stiffness coefficient of the equivalent laminate at the test temperature (equation III.5),$C_i = (\Delta v_m/\Delta P)$ is the crack opening compliance (the ratio of displacement increment to load increment) obtained from the crack opening displacement at notched edge v_m and the applied load P, s is the specimen span, the distance between specimen supports (Figure IV.3(b)).

The crack opening displacement at notched edge v_m is computed using the plastic hinge model (Figure IV.5) as follows [20, 83]:

$$v_m = \frac{2\Delta_{pl}}{\sqrt{\Delta_{pl}^2 + 4w^2}} \left[r_{pl}(w - a_0) + a_0\right] \qquad \text{(IV.11)}$$

where Δ_{pl} is the plastic component of load point displacement and r_{pl} plastic rotational factor.

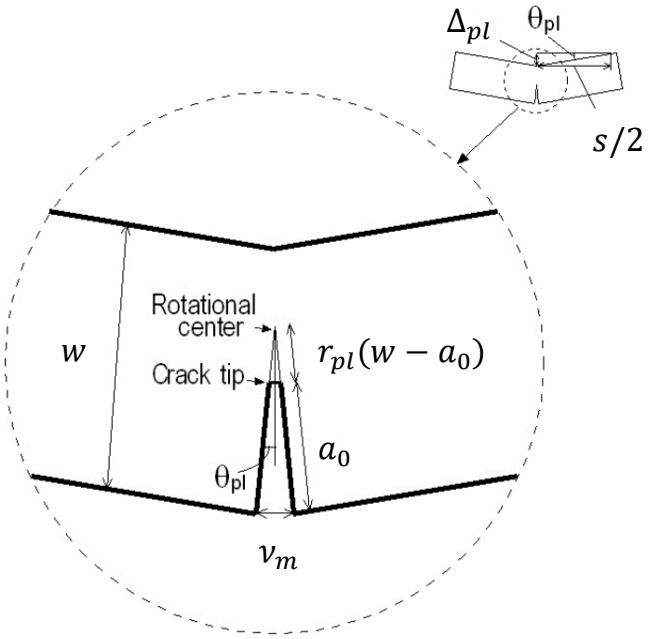

Figure IV.5. Plastic hinge model of a deformed SENB specimen [98].

IV.3.2.4 Stress concentration factor

The expression of σ_y at the crack tip (Figure IV.4) is used to estimate the stress concentration factor K_T for mode I type loading [48]:

$$K_T = \frac{\sigma_y(\theta = 0)\big|_{x=0}}{\sigma} = \sqrt{\frac{a}{2\rho}}.f(a/w) \tag{IV.12}$$

where $\rho = 0.085$ mm is the radius of the notch at the crack tip and σ is the remote applied stress far from the notch.

IV.3.2.5 Evolution of the critical strain energy release rate

According to equation IV.10, the crack length a_i at each mechanical load is computed from the crack opening compliance as described in ASTM standard E1820. Thus, the critical strain energy release rate in opening mode G_{Ic} is classically obtained from the load-line compliance $C = \delta/P$ and the crack length (Figure III.5(b)):

$$G_{I_c}^{lam} = \frac{P^2}{2t}\frac{dC}{da} \tag{IV.13}$$

where δ represents the applied displacement, P the force borne by the specimen and t is the specimen width. In this chapter, a simple method for numerical differentiation of dC/da is used.

IV.4 Macroscopic mechanical response and fracture behavior

From the macroscopic response standpoint, both SENT and SENB specimens exhibit a brittle failure at RT with a tendency to shift towards a quasi-brittle failure (Figure IV.6 and Figure IV.7) as the initial notch length to specimen width ratio *a/w* (typically from 0 to 0.5) and test temperature increase. As the ratio a/w increases, the stress concentration factor computed from equation (IV.8 - IV.9 - IV.12) gradually increases at the crack tip (Figure IV.8). In SENT specimens, the influence of stress concentration is about the same with an 80% decrease in the residual strength at both temperatures (Figure IV.8(a)). In SENB specimens, the constraint effect (quantified by the stress concentration factor K_T) decreases the residual strength by virtually 80% and 70% at RT and 150°C, respectively (Figure IV.8(b)). In both SENT and SENB specimens, the influence of temperature on the residual strength is limited. The decrease in the residual strength along with an increasing a/w ratio appears to be hyperbolic in SENT specimens and linear in SENB specimens.

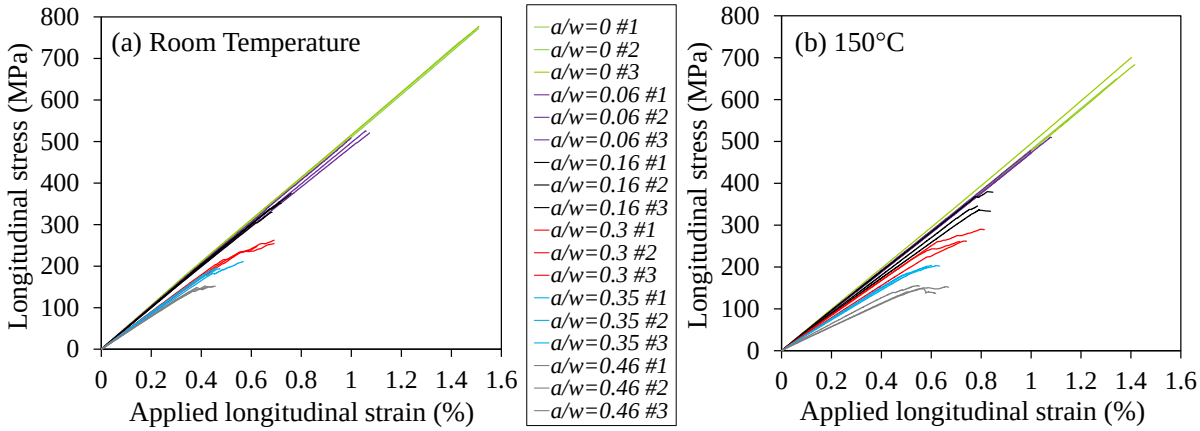

Figure IV.6. Constraint effect on SENT specimens: (a) RT and (b) 150°C.

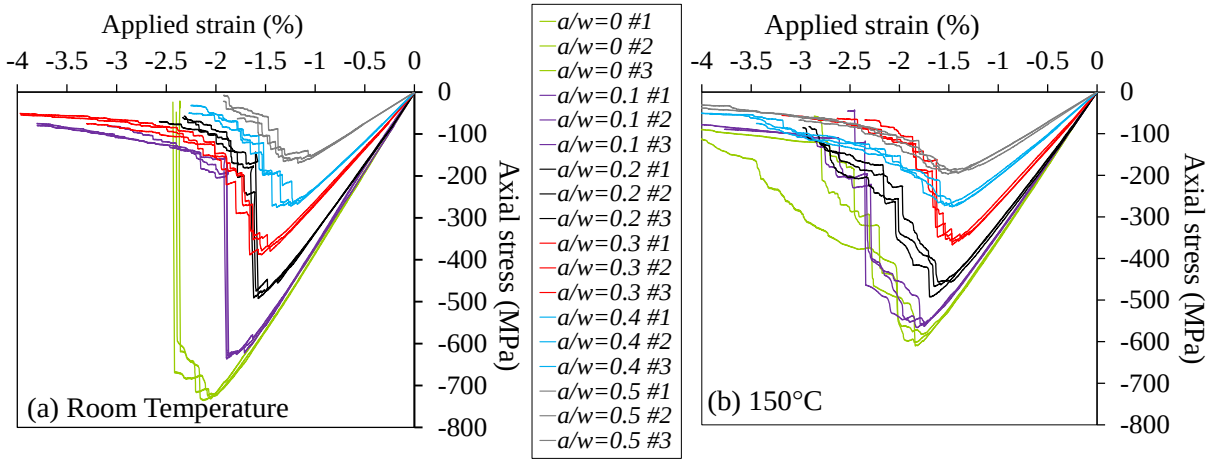

Figure IV.7. Constraint effect on SENB specimens: (a) RT and (b) 150°C.

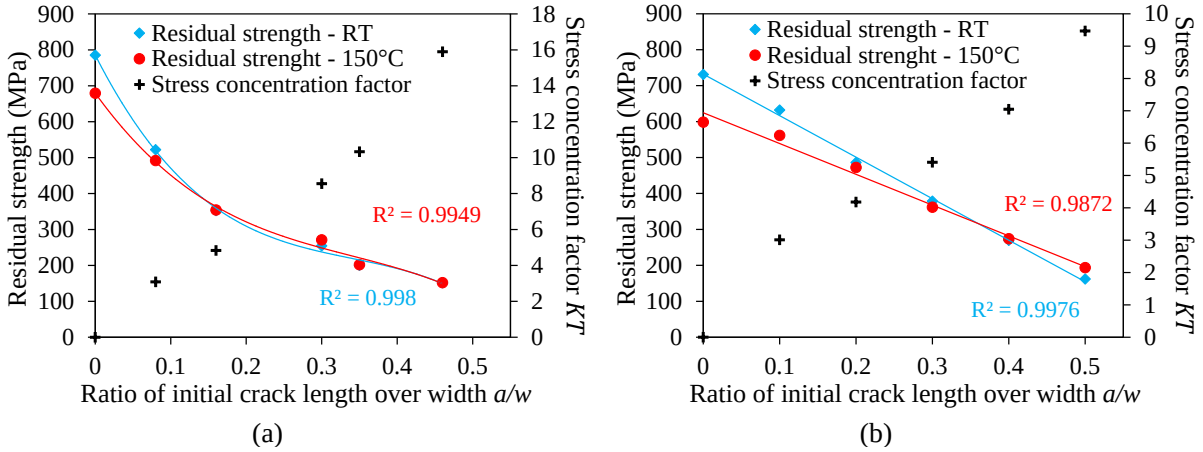

Figure IV.8. Influence of temperature and constraint effect (quantified by the stress concentration factor) on the residual strength of QI laminates: (a) SENT and (b) SENB.

In both SENT and SENB specimens, the microscopic observations of failure surfaces clearly show that fracture is translaminar in mode I loading even at elevated temperature (Figure IV.9 and Figure IV.10) regardless the a/w ratio. At room temperature, translaminar fracture is observed in all specimens. The front views indicate that the macroscopic translaminar crack grows self-similarly with respect to the initial notch in SENT specimens. In SENB specimens with low a/w ratio, the translaminar crack is not self-similar.

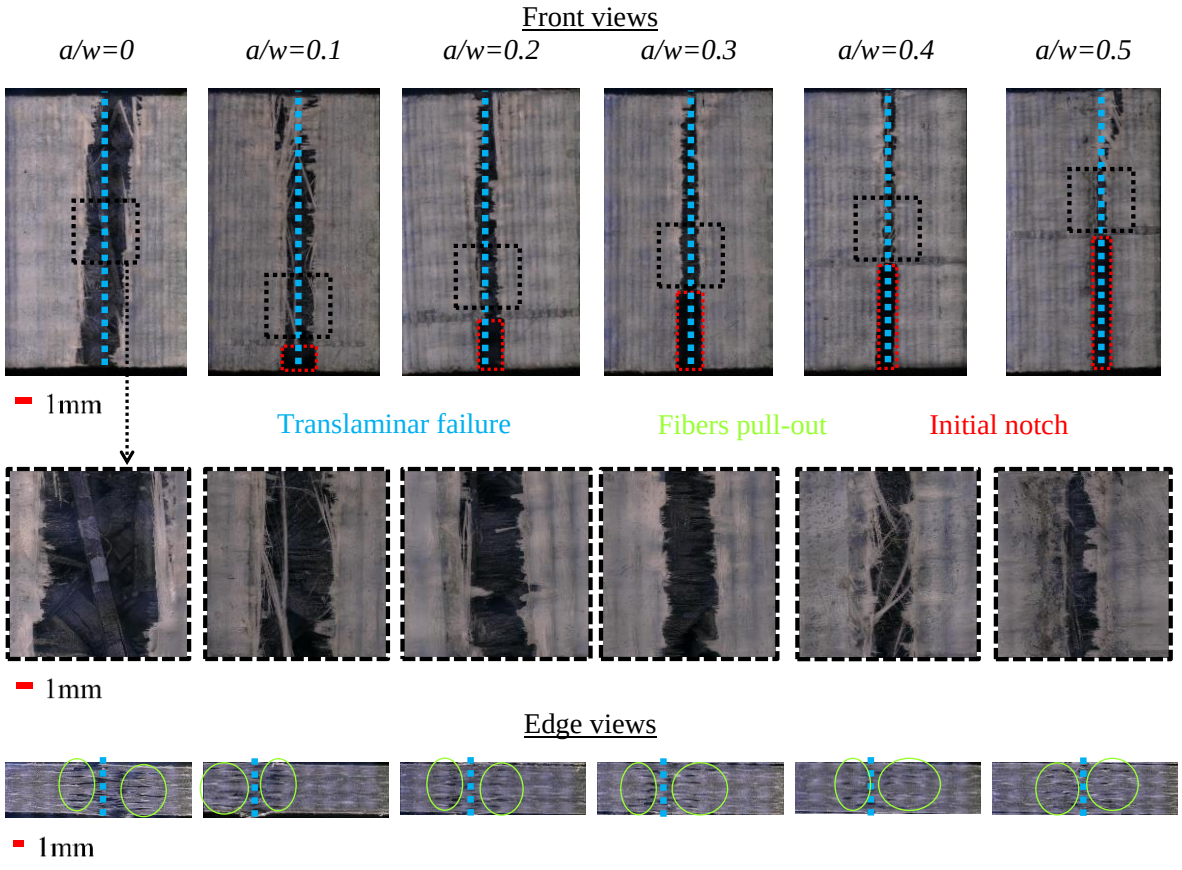

Figure IV.9. Microscopic observations of SENT specimens after failure in mode I at 150°C.

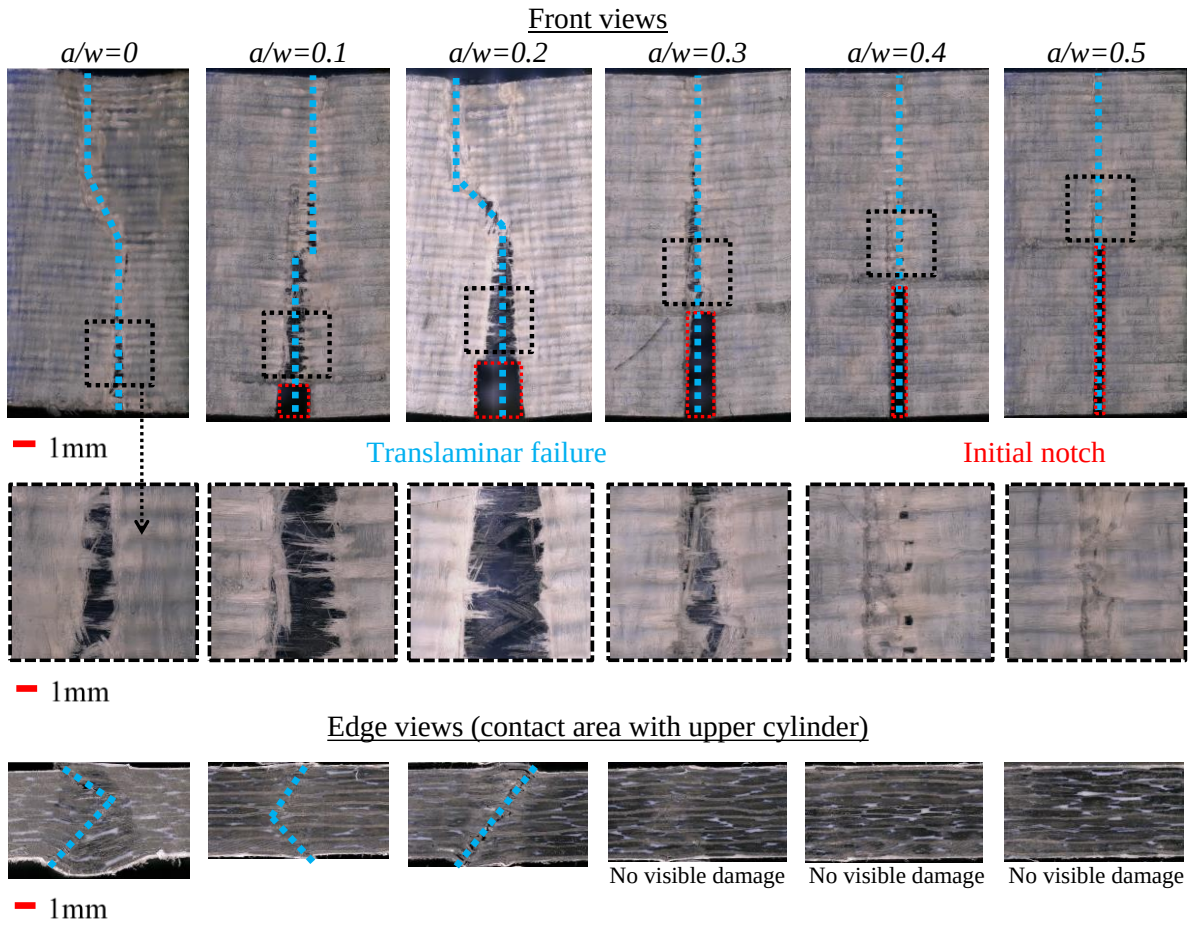

Figure IV.10. Microscopic observations of SENB specimens after failure in mode I at 150°C.

In SENT specimens, failure is primarily dominated by the tensile breakage of 0° carbon fibers, with no visible contribution of the +/-45° plies suggesting that the quasi-brittle failure observed at 150°C is primarily resulting from some fiber/matrix debonding coming along with fibers pull-out (edge views Figure IV.9).

In SENB specimens, failure consists of tensile and compressive breakage of 0° carbon fibers particularly in specimens with low a/w ratio (Figure IV.10). When loaded in bending, the upper part of specimens (above the neutral axis) is subjected to compression whereas the lower part (below the neutral axis) is subjected to tension. In addition, local crushing of the upper edges is observed in the contact area. As a/w ratio increases (typically from a/w=0.3), the stress concentration factor K_T increases as well (Figure IV.8(b)), and promotes a translaminar failure dominated by the tensile breakage of 0° carbon fibers. No visible damage is observed on upper edges of these specimens as the bending stress is lower than the crushing stress [84]. The gradual failure observed at 150°C is primarily associated with glass fibers bridging at the outer surfaces of specimens (Figure IV.11). The ultimate strength of G/PEEK plies being lower than C/PEEK plies, glass fibers cannot take up the load transferred to neighboring fibers when carbon fibers fail. Thus, glass fiber bridging results from the debonding at the glass fiber/matrix interface as is observed on the microscopic observation. As carbon fibers breakage comes along with the crack mouth opening, gradual glass fibers pull-out may be observed behind the crack tip. In addition, temperature promotes local crushing (resulting from compression) in the

contact area, and exacerbates ductility at $T>T_g$ [70, 85]. It therefore contributes to the retardation of the crack extension and the increase in the fracture toughness as will be further discussed in section IV.5.1.

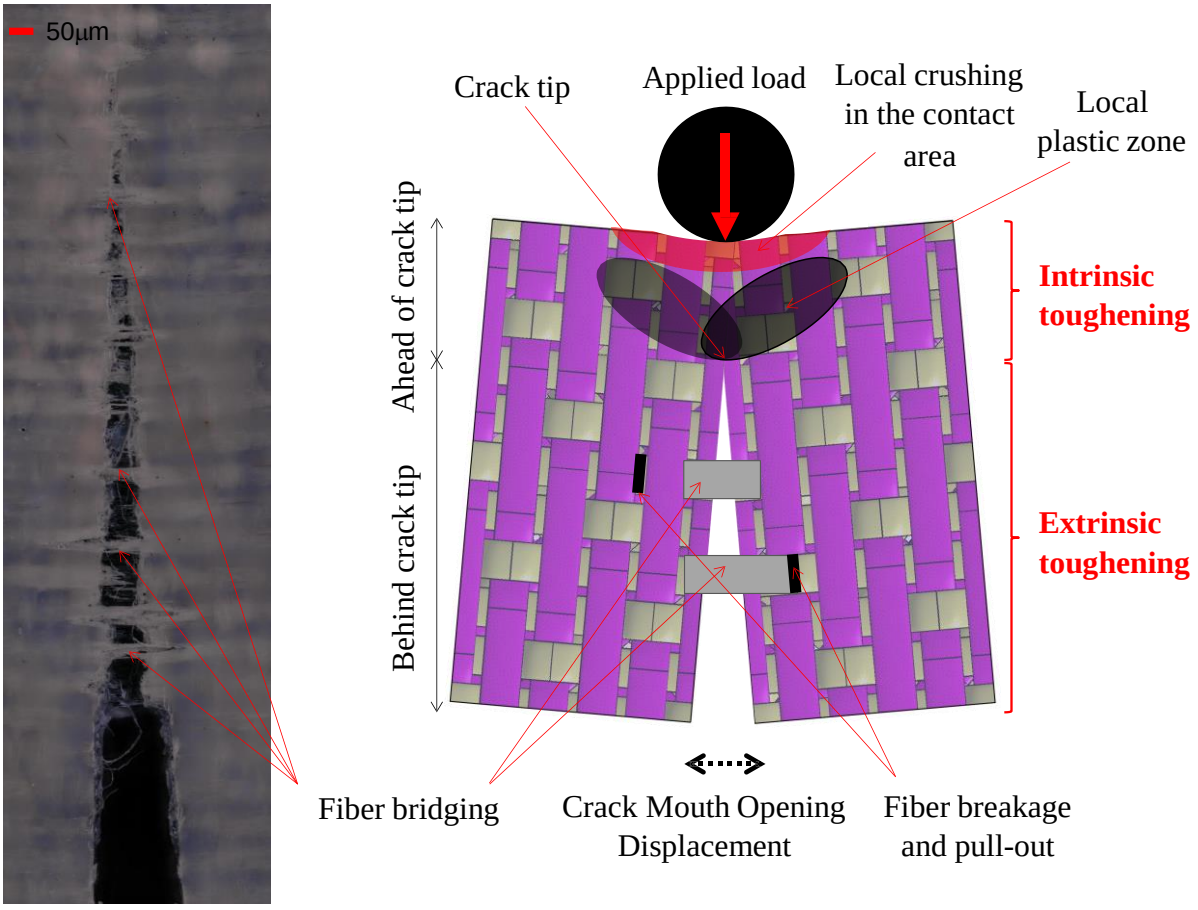

Figure IV.11. Illustration of crack extension and crack mouth opening displacement in SENB specimens at 150°C ($a/w = 0.3$): influence of fiber bridging on extrinsic toughness.

IV.5 Experimental estimation of the G-R curves on SENB

IV.5.1 Influence of temperature on G-R curves

Depending on the specimen's geometry and the loading mode, fiber-reinforced composites are generally characterized by an observable stable crack growth before instability [14, 16-18, 24, 34, 39, 41-42, 86] and the fracture toughness (or critical strain energy release rate) usually increases with crack extension before reaching a plateau value. Thus, the critical fracture toughness $K_{I_C|\text{tension}}$ is not sufficient to characterize the whole fracture behavior and the concept of crack resistance curves (described as G-R curves) has to be adopted [87]. Within the framework of LEFM, the determination of G-R curves is therefore the key point to quantify fracture in terms of energy required to grow a crack in quasi-isotropic laminates. In the present chapter, the idea was first to build equivalent G-R curves based on the evaluation of fracture toughness for different ratios a/w and different loadings (e.g. tensile and bending). From Eq. (IV.7 - IV.8 - IV.9), it is possible to compute the value of the critical fracture toughness $K_{I_C|\text{tension}}$ in SENT and SENB specimens (Figure IV.12). As failure is primarily driven by

carbon fibers breakage in tension (SENT) and in tension/compression (SENB), it turns out that a temperature increase has very little influence on the critical translaminar fracture toughness though the ductility of PEEK matrix is exacerbated at $T>T_g$. It also appears that the constraint effect has very little influence on the critical mode I fracture energy as SENT and SENB specimens have virtually the same mean value (about 45MPa.$\sqrt{m}$). With increasing ratio a/w, the critical translaminar fracture toughness gradually in SENT specimens (Figure IV.12(a)), whereas it slowly increases and gradually decreases in SENB specimens, resulting from less contribution of compressive failure (Figure IV.12(b)).

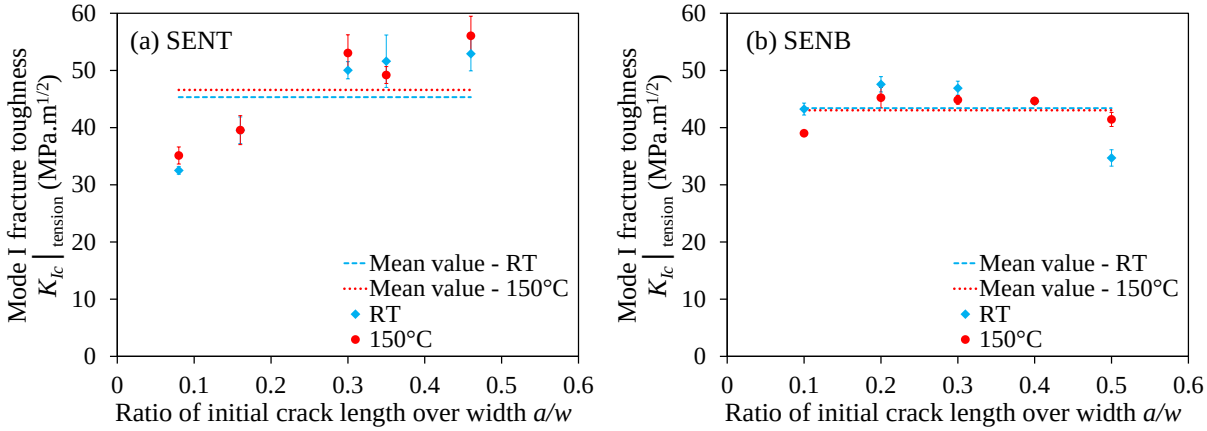

Figure IV.12. Influence of temperature and constraint effect on the mode I fracture translaminar toughness of QI laminates: (a) SENT and (b) SENB.

The G-R curves are drawn using the equation IV.13 from the translaminar crack extension calculated with the equation IV.10 (Figure IV.13). This technique was applied to the tests conducted at both temperatures in SENB specimens. As will be discussed in section IV.6.1, the gradual failure observed at high temperature is associated with glass fiber bridging. This contributes to the increase in the extrinsic toughness, hence slowing down the crack extension (Figure IV.11). The equivalent G-R curves built from equation IV.6 and the fracture toughness at crack initiation $K_{I_C|\text{tension}}$ corresponding to different ratio a/w (Figure IV.12) is reported in Figure IV.13 in terms of critical strain energy release rate in both tests temperatures. It is therefore possible to compare the evolution of the strain energy release vs crack propagation with the values of $G_{I_C}^{lam}|_{\text{tension}}$ at crack initiation computed from different ratio a/w. The values at initiation computed from LEFM equations [15] are in agreement with the values obtained during propagation from the compliance loss (ASTM standard E1820). As indicated previously, a temperature increase to temperatures higher than T_g has little influence on the translaminar fracture toughness, and the mean value of $G_{I_C}^{lam}|_{\text{tension}}$ (computed from equation IV.6) slightly increases at 150°C (from 44.65 kJ/m² to 47.37 kJ/m² hence a 7% increase) because the mechanical properties of the equivalent orthotropic material slightly change between RT and 150°C resulting from the softening of the PEEK matrix (Table III.3).

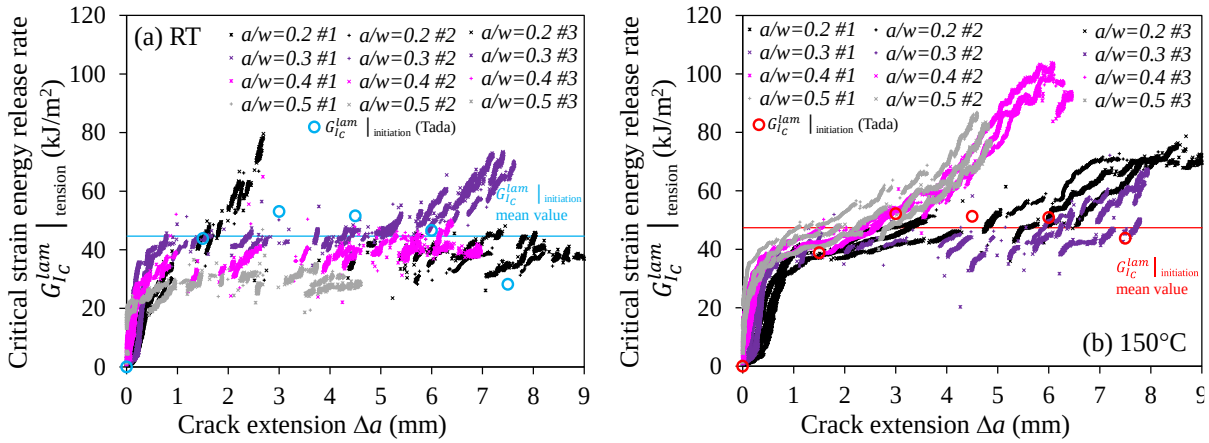

Figure IV.13. Evolution of strain energy release rate along with the crack growth in SENB specimens with different ratio a/w: (a) RT – (b) 150°C.

IV.5.2 Influence of constraint effect on G-R curves

In PMCs, Mahmoud [36] have studied the influence of the constraint effect during fracture toughness tests by means of Single-Edge-Notch Bending specimens in order to define a valid plane strain fracture toughness value $K_{Ic}|_{\text{tension}}$. The influence of crack tip constraint effect (depending on the specimen geometries and the loading conditions) and stress triaxiality (depending on the initial notch length to specimen width ratio *a/w)* on ductile and brittle fracture is of major importance for the assessment of structural integrity. The loss of constraint effect is related to the position and the size of the plastic zones. Indeed, the deeper the notch and the higher the test temperature; the greater are the plastic zone and constraints (resulting from the triaxial stress state). Therefore, the higher the loading force must be to deform the sample [61]. As a consequence, it is usually observed that the decrease in crack tip constraint (the stress concentration at the notch root is offset by plastic deformation) leads to an increase of the fracture toughness (corresponding to a ductile failure).

IV.6 Influence of glass fiber on the translaminar failure of SENB specimens

IV.6.1 Translaminar failure in SENB specimens

As pointed in section IV.4, the fracture mechanisms are modified at $T>T_g$ because of glass fiber bridging behind the crack tip and local plastic deformation in matrix-rich areas ahead of the crack tip as translaminar crack grows (Figure IV.11). It appears that both mechanisms are enhanced when matrix ductility increases. Indeed, instead of the sudden breakage of 0° carbon fibers at RT, the ductile behavior of the PEEK matrix at the fiber/matrix interface contributes to the dissipation of a portion of the mechanical energy during the load transfer between a broken fiber bundle and the neighbor fibers.

In order to investigate more specifically the contribution of the 0° and +/-45° oriented plies in quasi-isotropic CG/PEEK laminates, X-Rays tomographic observations were conducted in SENB specimens with a ratio $a/w = 0.3$ (Figure IV.14). In 0° plies, a clear translaminar crack is observed suggesting the catastrophic failure of 0° carbon fiber bundles initiated from the

stress concentration near the initial notch. A local crushing (or compressive failure) of laminates' upper edges in the contact area with the upper cylinder is also observed. In +/-45° oriented plies, the fracture surface reveals the breakage of +/-45° carbon fibers in shearing. In QI laminates, the macroscopic failure is primarily dominated by 0° fibers resulting in a virtually temperature-independent behavior (even at $T>T_g$) as the +/-45° oriented plies do not significantly contribute to bear the mechanical loading. From the fracture mechanics standpoint, the translaminar failure is initiated when the stress intensity factor in tension reaches its critical value $K_{I_C|\text{tension}}$.

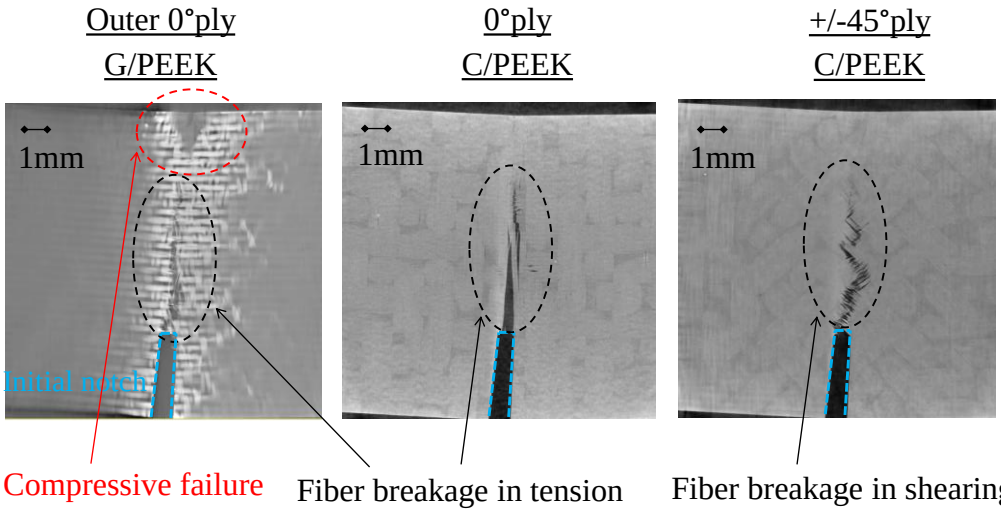

Figure IV.14. Tomographic observations of SENB specimens ($a/w = 0.3$) at 150°C.

A brittle interface allows crack advance by sudden breakage of 0° carbon fibers, while a ductile interface forms a well-defined glass fiber-bridged crack potentially leading to divert the crack front and to reduce crack growth [86]. After the failure of carbon fibers, the broken glass fiber locally debonds from the matrix, and the matrix surrounding the broken fiber ends is stressed at a significantly higher level than prior to the fiber failure. The resulting temporary and local plastic deformation of the matrix in this area comes along with a gradual pull-out of 0° glass fibers at 150°C as the translaminar macroscopic crack grows, therefore leading to glass fiber-bridging that reduces the crack mouth opening. At RT, pull-out is reduced as sudden breakage of 0° carbon fibers does not allow the matrix to dissipate the mechanical energy by means of inelastic deformation and does not imply significant interface debonding in the outer G/PEEK plies. These mechanisms are instrumental in ruling the mechanical energy released during fracture. More specifically, the strain energy release rate increases at macroscopic scale resulting from enhanced ductility of the PEEK matrix at microscopic and mesoscopic scales as temperature increases. In addition, a larger number of glass fibers bridge the crack as it grows. Ultimately, such fiber-bridging results in increasing the mode I translaminar fracture toughness during the last stage of fracture.

IV.6.2 Influence of glass fibers on extrinsic toughness

SENB specimens are characterized by a gradual failure (particularly at 150°C as explained in section IV.6.1). G-R curves were derived from equation IV.13 and the corresponding gradual crack growth in agreement with the ASTM standard E1820. It is therefore possible to observe a sigmoid evolution of crack extension vs time (Figure IV.15). Until crack initiation at maximum stress (about 350MPa for a 1.7% axial strain, see Figure IV.7(b)), the crack length is virtually unchanged. Therefore, it suddenly increases and jumps is clearly observed on the curves obtained from the ASTM standard E1820 method. These jumps are associated with the breakage of 0° carbon fibers. The stress redistribution to the neighboring fibers was described in details in section IV.6.1. Both glass fiber bridging and local plastic deformation of the PEEK matrix at the interface and at the crack tip contributes to the momentary stabilization of the crack growth. At the end of loading, when the stress borne by specimens tends to low values (typically less than 100MPa as shown on Figure IV.7(b)), it appears that there are no jumps (because all the 0° fibers are broken), and the crack extension gradually slows down as there are lots of bridged glass fibers behind the crack tip reducing the crack mouth opening (microscopic observations on the left on Figure IV.11). Thus, the Fracture Process Zone consists of two zones (behind and ahead of the crack tip) resulting from the damage mechanisms taking place during translaminar cracking [87-88]:

1. The damage zone ahead of the advancing crack tip where matrix cracking, interfacial debonding and post-debonding friction occurs;

2. The glass fibers bridging zone or tied zone at the wake of the crack tip where glass fibers bridge the opposite fracture surfaces and pull-out.

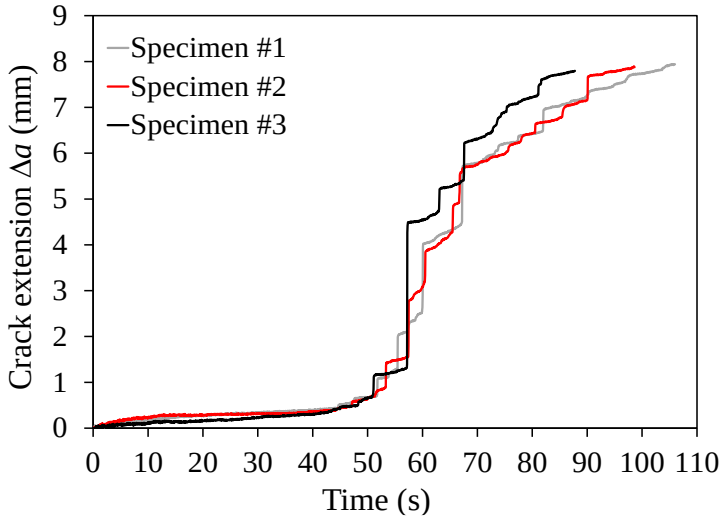

Figure IV.15. Evolution of the crack growth estimated by the ASTM standard E1820 test method applied to SENB specimens ($a/w = 0.3$) at 150°C.

These two zones are closely associated with both intrinsic and extrinsic fracture toughness. In the present case, the highly ductile behavior of the PEEK matrix at $T>T_g$ provides good intrinsic toughness to quasi-isotropic hybrid laminates, whereas the bridging of macroscopic translaminar crack by the glass fibers at the outer surfaces of laminates contributes to the

increase in its extrinsic toughness. This evolution of the G-R curve is in agreement with the observations proposed in previous studies [51, 62-63, 75, 88]: extrinsic toughness primarily contributes to the increase in the fracture energy during crack growth by means of crack-tip shielding mechanisms that result in rising R-curve behavior.

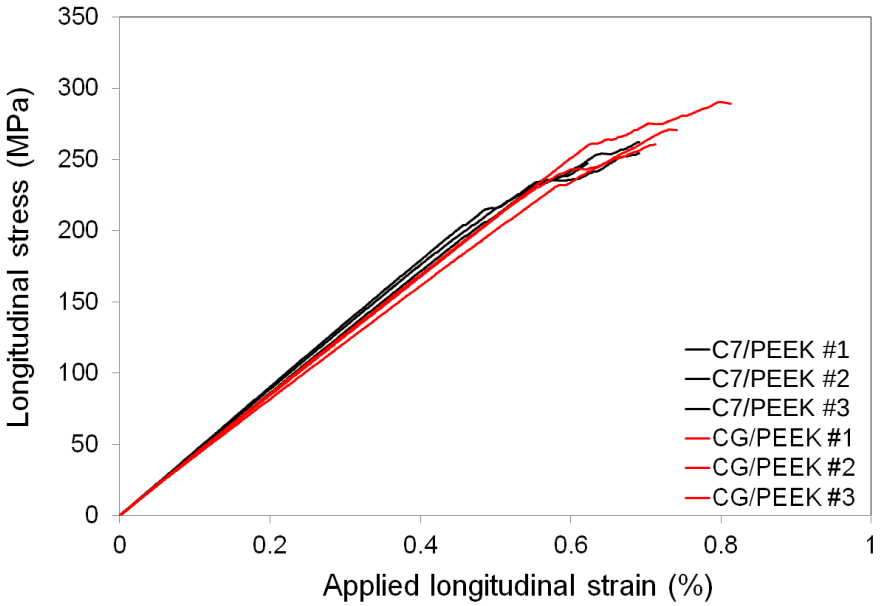

Figure IV.16. Influence of outer glass fibers/PEEK laminates on the tensile response of SENT specimens ($a/w = 0.3$) at 150°C.

Indeed, the effect of the extrinsic toughening by the glass fibers is expected to be small, as was shown also in Chapter III. For quantification purposes, the extrinsic toughening by the glass fibers is evaluated from tests on SENT specimens (with a ratio $a/w = 0.3$) consisting of carbon fiber reinforced PEEK matrix laminated composites one the one hand, and glass and carbon fiber reinforced PEEK matrix composites one the other hand (Figure IV.16). From the macroscopic mechanical standpoint, the outer glass fiber PEEK plies have a moderate influence.

IV.7 Conclusion

Tensile and bending tests were conducted at room temperature and 150°C ($T>T_g$) on single edge notched specimens consisting of hybrid carbon glass reinforced PEEK composite materials. In the studied quasi-isotropic laminates, the translaminar crack is dominated by the breakage of 0° carbon fibers and appears to be self-similar in both SENT and SENB specimens.

Equivalent G-R curves are obtained from SENT and SENB specimens with different initial notch length to specimen width ratio *a/w* (typically from 0.2 to 0.5). As failure is primarily driven by carbon fibers breakage in tension (SENT) and in tension/compression (SENB), it turns out that a temperature increase has very little influence on the mode I critical translaminar fracture toughness $K_{I_C}\big|_{\text{tension}}$ though the ductility of PEEK matrix is exacerbated at $T>T_g$. It

also appears that the constraint effect has very little influence on $K_{I_C}\big|_{\text{tension}}$ as SENT and SENB specimens have virtually the same mean value (about 45 MPa.$\sqrt{\text{m}}$).

G-R curves were derived from the computation of crack growth and compliance loss in agreement with the ASTM standard E1820. After reaching a plateau value, the critical strain energy release rate in mode I gradually increases as the translaminar crack ultimately grows. The late increase in translaminar toughness results from both intrinsic and extrinsic toughness that are specifically enhanced at $T>T_g$. The fracture energy is associated with the brittle failure of carbon fibers leading to gradual fiber bridging of glass fibers (contributing to a reduced extrinsic toughness), whereas the highly ductile PEEK matrix provides the composite material its intrinsic toughness by means of local plastic deformation at the crack tip and around the broken fibers ends.

Chapter V: Translaminar cracking modelling on woven-ply thermoplastic laminates in tension and in compression

The experimental tests and fractographic analysis carried out in Chapter III and Chapter IV allowed the identification of the main failure mechanics responsible for the dissipation of mechanical energy during the translaminar cracking on woven-ply thermoplastic laminated composites. In this chapter, a numerical model is developed and tested. The purpose is twofold: what about the influence of (1) the stacking sequence and (2) the laminate thickness on the tensile and compressive translaminar cracking. Only the simulations at RT will be performed; the influence of temperature is not covered in this chapter.

In the first part of this chapter, a bibliographical review about the modelling of translaminar cracking is introduced. Then, the main objectives of this chapter are detailed. In the second part, the principle and description of the numerical model is presented. First, the mesh description and boundary conditions are indicated. Subsequently, the behavior laws and material properties are detailed. In the third part, the numerical model is tested and validated with the experimental test. In the last part of this chapter, the main results are summarized.

The work presented within this chapter should be submitted to journal as a paper entitled: "Translaminar cracking modelling on woven-ply thermoplastic laminates in tension and in compression".

Chapter V outline

V.1 Introduction

Fiber Reinforced Polymer (FRP) composites are extensively used in the aeronautical industry thanks to their high strength-to-weight ratio. However, the estimation and the quantification of the failure modes on composite materials play a fundamental role in the damage tolerance of a composite structure. During their life cycle, composite structures are subjected to tensile and compressive loads. In notched composite laminated structures the critical failure mode is the translaminar fracture. Translaminar failure of a composite laminate is defined by the emergence of a crack that covers the entire thickness, leading to structural collapse. In the case of composite laminates subjected to tensile and compressive loads, fibers are responsible for transferring most of the loads. The translaminar fracture of a laminated ply manifests itself at a mesoscopic scale by the fiber breakage in tension due to fiber bundles pull-out at 0° and by fiber breakage in compression linked to kink-band plastic formation [14-33]. Therefore, the study of translaminar fiber cracking is of the utmost importance to determine the damage tolerance of composite laminates.

V.1.1 About the modelling of translaminar cracking

Consequently, many authors have studied the translaminar fiber cracking of unidirectional laminated composites, as well as the stacking sequence and the ply thickness effects, both experimentally [14, 16, 18, 33-34] and numerically [14, 33, 89-94]. However, it is still necessary to better understand the translaminar fiber cracking in woven-ply laminated composites [19, 33, 95], as well as to simulate the damage evolution [95]. Analytical, semi-analytical models and formulations based on the drop of the mechanical properties have been used to represent the changes in damage during crack propagation [33, 89-91, 95]. Though these approaches are efficient, they do not describe the behavior of the composite material. The Finite Element method based on an energy approach in association with the fracture toughness (or critical strain energy release rate) is a relevant approach to characterize the translaminar fracture [14, 92-94] and to provide information on the fracture behavior of composite structures. Energy-based models ensure that effective stress and strain tensors are set so that the correct amount of energy is dissipated through damage formation. In order to have a faithful and reliable behavior of Finite Element method, the translaminar fracture of the woven-ply laminated composites must be evaluated by experimental procedures [19, 33, 50, 95].

CT and CC are usually used to quantify the translaminar fracture toughness in FRP composites [14, 16, 18, 33-34, 94-95]. These specimens allow inducing a progressive and stable crack growth. This notion of stability of the macroscopic transverse cracking is fundamental to plot the evolution of the critical strain energy release rate as a function of the crack increment, Δa, in the form of the fracture resistance curve (R-curve). On the one hand, many studies have shown a more or less constant value of the critical strain energy release rate using CT tests, the R-curve often tends towards an asymptote during the crack growth [14, 16, 18, 33-34]. On the other hand, CC tests have shown an artificial positive trend in the R-curves, and only initiation values seem to be the relevant measurement of the critical strain energy release rate associated with kink-band [14, 33]. Based on these results, many modelling approaches to account for Mode I translaminar fracture assume a constant translaminar fracture toughness value during

fracture propagation [92-94, 96-101]. Ranging from discrete to continuum, these models attempt to capture the complex and multi-scale physics of damage formation in FRP composites.

Compared to the number of reported numerical models for unidirectional composites [14, 33, 89-94, 96-98], very few woven-ply damage models have been developed [95, 99-101]. Several numerical models to predict damage in unidirectional fiber reinforced thermosetting (TS) composites, more specifically in unidirectional carbon-fiber reinforced epoxy resin composites, are available in the literature [92-93, 96-98]. Experimental studies have shown that woven fabric reinforced composite structures exhibit higher interlaminar strengths and damage tolerance than unidirectional composite structures, what motivated the growing interest in woven composites [10]. As with unidirectional composites, most numerical woven damage models have been developed for woven-ply carbon fiber-reinforced epoxy resin composites [95, 99], but models have been recently developed to simulate the behavior of woven-ply carbon fiber-reinforced composites consisting of high performance thermoplastic (TP), PEEK and PPS [100-101]. Indeed, semi-crystalline TPs resins offer a number of advantages over conventional TS resins (such as epoxies): a high degree of chemical resistance, excellent damage and impact resistances, and they may be used over a wide range of temperatures. Lastly, there are numerous engineering reasons why TP composites are attractive as aerostructures: increased toughness compared to TS resins, inherent flame retardancy, and they are associated with low-cost manufacturing processes like thermofolding, stamping, welding or co-consolidation, and present a better recycling capacity. The increasing utilization of woven composites requires the development of corresponding numerical models, due to the complex and multi-scale nature of the damage formation in laminated composites. It is well admitted that there is no unique model applicable to a variety of loading conditions and geometries [102].

Iannucci and Willows [99] proposed an energy-based damage mechanics approach to model impacts in woven composite materials. Their numerical model was elaborated from five damage variables for in plane damage per ply layer to predict the fiber failure in warp and weft directions in both tensile and compressive failure modes, with an additional variable to determine the degradation of the fiber-matrix interface and with an interface modelling to predict delamination. The authors used constant energy dissipation to prevent mesh-dependent solutions by linked the characteristic length of the element to the translaminar fracture toughness. The values of the critical translaminar fracture toughness used by the authors were taken in the literature for a unidirectional carbon fiber-epoxy laminate. Failure in both warp and weft directions was formulated in a similar manner. Tensile failure in the local warp and weft directions was modelled with a single damage variable in each direction using a fracture mechanics approach based on energy release rates; when damage is equal to 1, complete tearing or failure of the warp or weft has occurred at the ply level. In their formulation, compressive failure was modelled similarly to the tensile failure mode, in compression when damage variable reaches a value of 1, the residual strength and stiffness of the crushed tows was used until complete failure at a specified strain occurs at the ply level. A simple non-linear shear stress–strain behavior was considered to account for the in-plane shear response. Shear damage was associated with debonding of the fiber–matrix interface. After model validation under

different loading conditions (tensile, tension-shear and double cantilever beam), the proposed numerical model was used to simulate impact behavior.

Ortega et al. [95] proposed an inverse method for obtaining the translaminar Cohesive Law with the use of an analytic model capable of predicting the load–displacement curve of a CT specimen for any arbitrary Cohesive Law shape. The authors used two woven fiber-reinforced epoxy prepreg composites to obtain the softening law, one laminate made of woven glass fabric plies (LG) and the other made of woven glass fabric and woven carbon fabric plies (LCG). They noted that the fracture toughness (G_c) measured from the area under Cohesive Law curve is nearly identical regardless the number of points used in the fitting. In the first laminate (LG), the Cohesive Law can be adjusted with a trilinear piecewise function and with a tensile G_c of 78.6 N/mm. In the second laminate (LCG), the Cohesive Law can be adjusted with piecewise constant-stress function followed by an exponential decrease of the stresses and with a tensile G_c of 105.0 N/mm. Using the second laminate (LCG), the authors were capable to predict the force-displacement curve of the CT specimen. With the obtained softening function, the authors predicted the nominal strengths of a Center Cracked Specimen and an Open Hole specimen for a wide range of specimen sizes.

More recently, a few experimental and numerical studies on woven fabric reinforced thermoplastic composites have considered open hole specimens, under compression [100] and tension [101]. Liu et al. [100] have developed a mesoscale damage model for predicting damage in woven carbon-fiber-reinforced PEEK prepreg composites under compressive loading. Using a combination of interlaminar and intralaminar damage models implemented in Abaqus/Explicit [103], the authors were able to capture different composite failures modes, such as fiber fracture and matrix cracking as well as delamination. A strain-based damage criterion was employed by the authors to evaluate the fiber failure in warp/weft directions, due to tensile and compressive loading respectively. This criterion combines the ultimate strains of the fiber to the translaminar fracture toughness, strength and characteristic length of the element. The translaminar fracture toughness values associated with fiber-dominated tensile and compressive failure are 109 kJ/m^2 and 52 kJ/m^2 respectively; these values were measured using Modified Compact Tension (MCT) and CC testing methods. The non-linear shear response was obtained from standard V-notched Rail Shear (VRS) and was expressed by an exponential function. A good agreement was observed between experimental and numerical results for both the open hole and the pinned open-hole.

Jebri et al. [101] have tested three-dimensional finite element model implemented in Abaqus/Explicit [103] to reproduce the mechanical behavior of 5-harness satin weave carbon/PPS composite with different fiber orientations (warp, diagonal and weft) under tension. Fiber failure and matrix cracking were modelled using the Hashin failure criterion and a damage evolution law. Delamination was simulated using cohesive zone elements between composite layers. The non-linear shear response was taken into account using an exponential function, where the constants were obtained by a tensile test of the laminate oriented at 45°. The damage evolution was calculated from classical strain-stress relationships and the fracture toughness associated with the fiber failure in tension and compression. A good agreement was achieved between the experimental and simulation results in terms of load–displacement curves and

strain fields. Fiber breakage is the dominating failure mechanism, the presence of a centered hole affects the translaminar fracture as fiber breakage grows from the vicinity of the hole to the laminate edges.

V.1.2 Objectives of this chapter

Aiming at understanding the translaminar fracture in woven-ply thermoplastic laminates, a numerical model developed in Abaqus is proposed. This model is based on experimental observations of CT and CC specimens used to induce the translaminar fracture in tension and in compression, and on the three main physical phenomena responsible to dissipate the mechanical energy: fiber failure, in-plane shear plasticity and crushing plasticity. Three stacking sequences like those described in section III.2 (an orthotropic laminate and two quasi-isotropic laminates) were considered in both configurations (CT and CC).

One of the main objectives of this chapter is to use the numerical model to investigate translaminar failure based on CT and CC tests, CC tests are more difficult to analyze due to the combination of several physical phenomena at the same time, which imply kinking, crushing and fiber breakage. It is also very difficult to separate overall plasticity, which induces an overall energy dissipation, called extrinsic toughness, from the energy dissipated by the crack tip, which is the true energy dissipation, called intrinsic toughness [50, 60]. Firstly, tensile tests are simulated in order to understand how the energy is dissipated. The influence of stacking sequence and the laminate thicknesses on the tensile translaminar failure is also investigated. Secondly, compressive tests are simulated in order to better understand the crack kinking and crushing phenomena.

V.2 Numerical modelling of the translaminar cracking: Principe and description

A numerical model consisting of a failure criterion based on fracture mechanics is tested to take into account for the dissipation of the critical strain energy release rate in opening mode (mode I) due to fiber breakage. This model is implemented with user-defined VUMAT subroutine and runs with Abaqus/explicit solver [104]. A focus on translaminar cracking and damage evolution on woven-ply laminated composites is realized, wherefore CT and CC tests were chosen to be simulated. The damage model is based on ply failure mechanisms at a ply level.

V.2.1 Mesh description

Mesh maker in the propagation damage area is written and compiled in Fortran 90 language. Positions of nodes are uniformly stacked in row and column to respect the orientation plies. Square shaped elements C3D8 are used in 0°/90° plies and in ±45° plies in order to follow the fiber direction and to have coincident nodes between adjacent plies (Figure V.1). Elements wedge shape C3D6 is used so that it is adapted to the mesh.

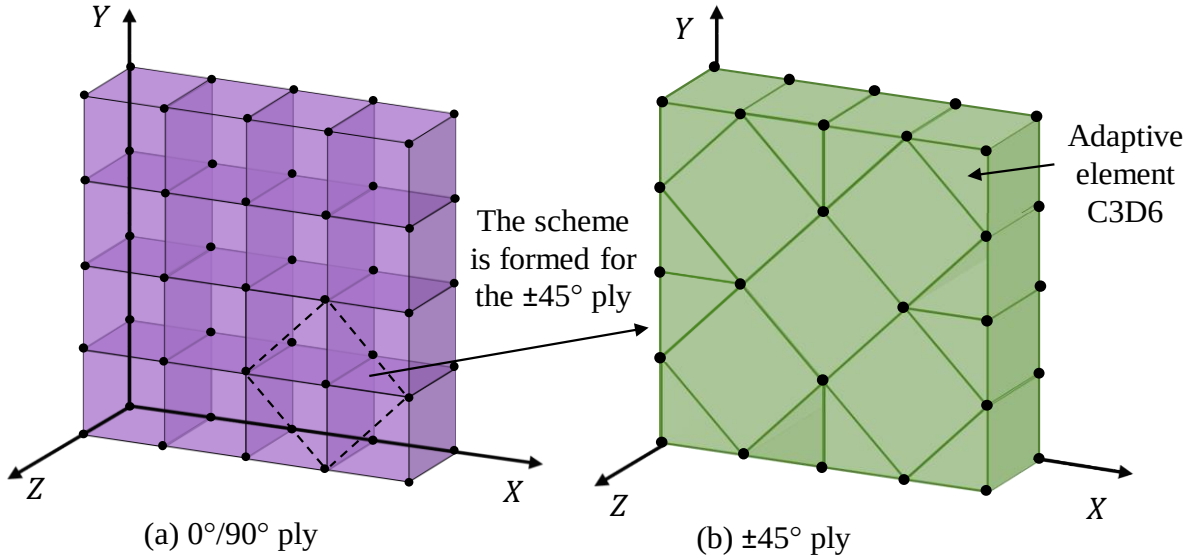

Figure V.1. Mesh shape in each oriented ply.

The delamination between plies is driven using a contact algorithm and cohesive contact law based on fracture mechanics [104]. In section V.2.3.2, the modelling of delamination will be detailed. The size of the square shaped elements used in the propagation damage area is approximatively 0.625 mm for the 0°/90° plies and 0.886 mm for the ±45°plies. The average ply thickness of the laminates is 0.31 mm.

V.2.2 Boundary conditions

CT and CC translaminar fracture tests are modeled using the same specification given as in the experimental test (section III.2). The loading in the fixing holes is applied by means of semi-spherical analytical rigid cylinders (Figure V.2).

The mesh used in the damaged area being done with finite elements aligned in the fiber direction (Figure V.1), it is difficult to mesh the loading holes and the notch shape. Then a simple mesh generated by Abaqus/CAE [103] is done in this area (Figure V.2). Consequently, the fiber damage is not simulated in this zone, which does not induce problem because no fiber failure is observed in this area. Conversely, plane shear plasticity is observed in this area and is then taken into account in this area.

Considering three stacking sequences, the mechanical response of both CT and CC specimens was simulated. Two laminates with the same ply ratio at 0°/90° and ±45°, but with different thicknesses qualified as quasi-isotropic and one orthotropic laminate (see section III.2). The total number of elements used in the simulations varies between 50,000 and 100,000 elements for each lay-up configuration.

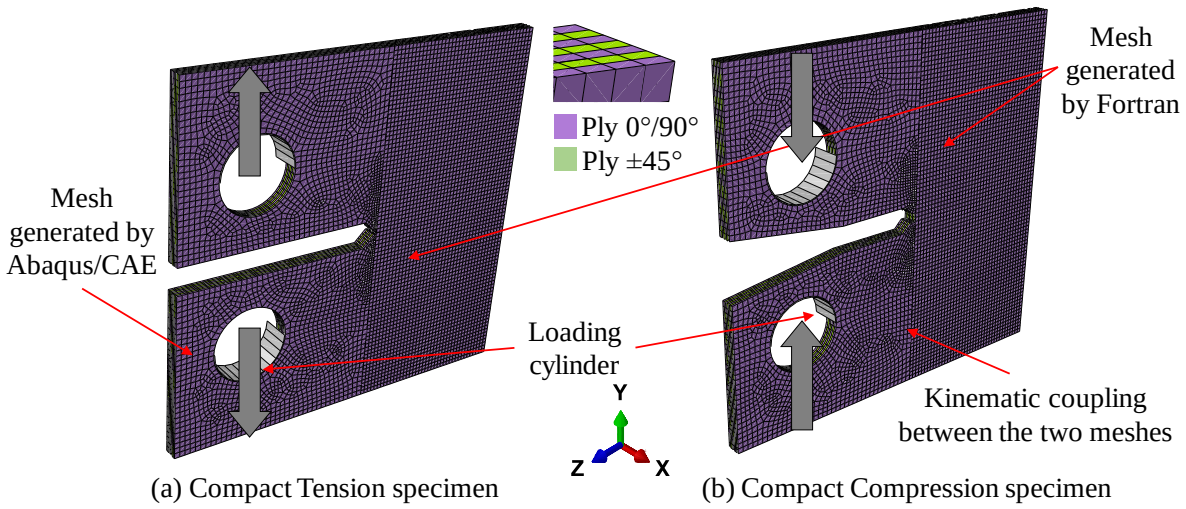

Figure V.2. Mesh and boundary conditions used in the numerical model for a seven-ply laminated.

V.2.3 Behavior laws

V.2.3.1 Modeling fiber failure

CT tests show that fiber failure and crack growth is mainly related to fiber bundle breakage at 0° (Figure V.3(a)). CC tests show that several physical phenomena (fiber breakage, kinking, crushing) occur at the same time making the translaminar cracking analysis more complex (Figure V.3(b)). Based on these experimental observations, three main physical phenomena were found as those responsible to dissipate the mechanical energy: fiber failure, in-plane shear plasticity and crushing plasticity. The behavior laws implemented in this numerical model and presented below are based on these physical phenomena.

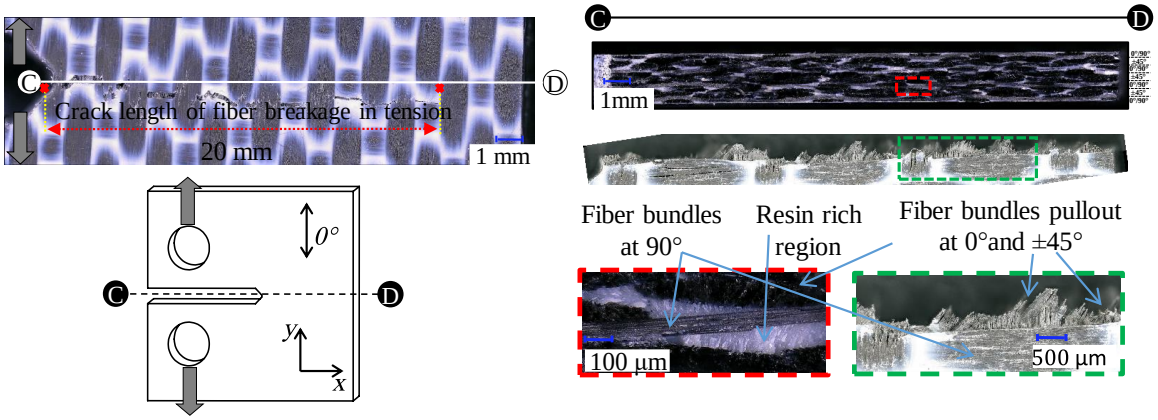

(a) Compact Tension - C7/PEEK - [(0/90),(±45),(0/90),(±45),(0/90),(±45),(0/90)]

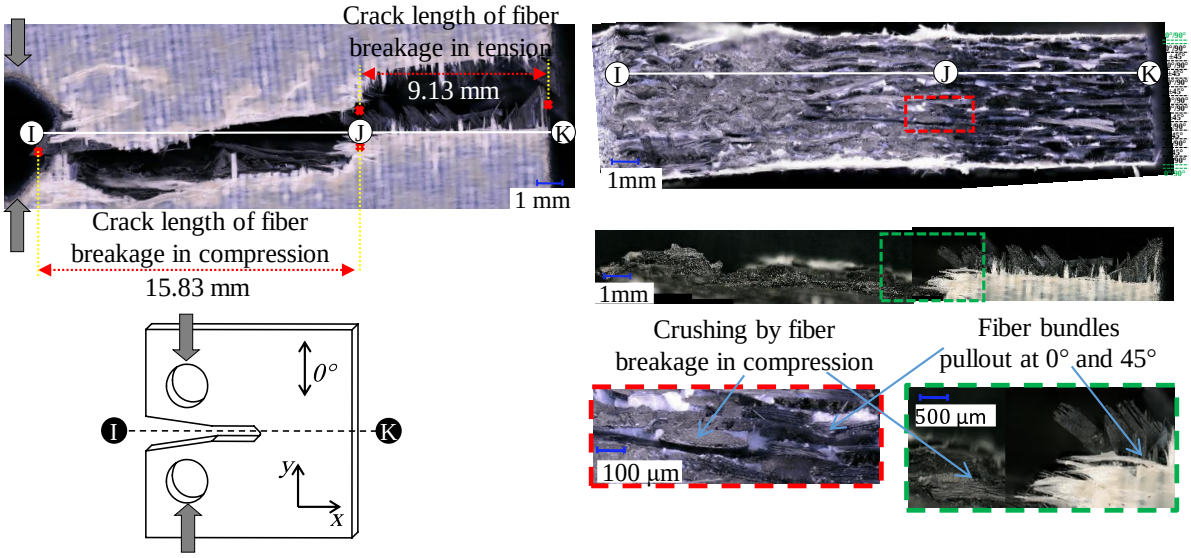

(b) Compact Compression - CG/PEEK - $[(0/90)_G,(0/90),(\pm45),(0/90),(\pm45),(0/90),(\pm45),(0/90)]_S$

Figure V.3. Microscopic observations of the fracture surface after the mechanical test: (a) tensile test and (b) compressive test

Fiber failure is taken into account using a failure criterion written inside the volume elements (Figure V.4). This criterion based on fracture mechanics is built to dissipate the critical strain energy release rate in opening mode (I) due to fiber fracture in the volume elements whatever the size of the element. Then a classical formulation between the integration points of the elements allows producing a constant energy release rate per unit area [105]:

$$\int_V \left(\int_0^{\varepsilon_1} \sigma d\varepsilon \right) . dV = S . G_{I_c}^f \tag{V.1}$$

where $G_{I_C}^f$ is the critical strain energy release rate in mode I, σ and ε are the stress and strain in fiber direction, and ε_1 is the strain in fiber direction at final failure. As seen in Figure V.5, this formulation is applicable either in tension ($G_{I_c}^{f,T}$ and ε_1^T), as in compression ($G_{I_c}^{f,C}$ and ε_1^C), and in longitudinal, as in transverse fiber direction. In compression, crushing phenomenon is also simulated, as further described. *V* and S are the volume and the surface of the element (Figure

V.4), they can be reduced in terms of a characteristic internal length L_C to avoid the mesh dependent solution [105].

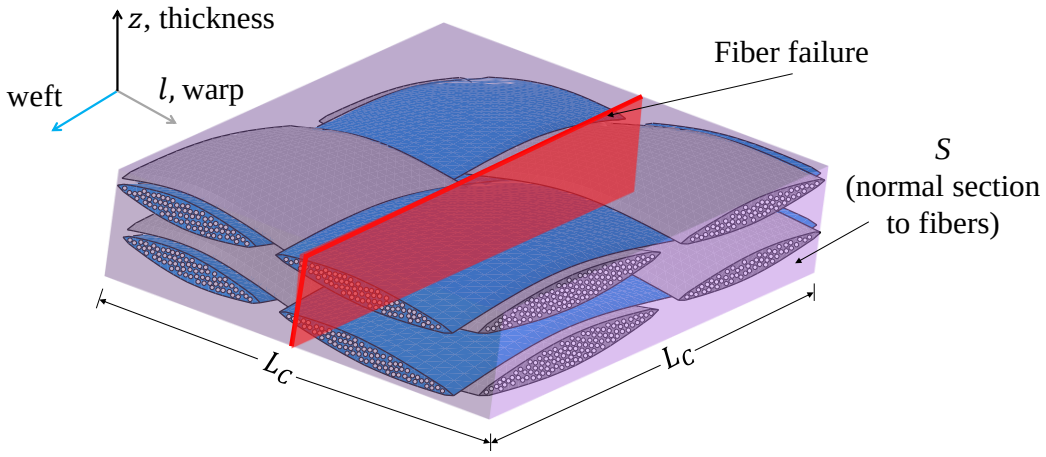

Figure V.4. Representation of fiber breakage at the level of the volume element.

When the failure strain in tension (ε_0^T) or in compression (ε_0^C), according to longitudinal or transverse direction is reached, a damage variable (d) relaxing linearly is used to calculate the stress representing the fracture toughness dissipation for the opening mode I (Figure V.5). It can be noticed in this figure (Figure V.5), that the curve being represented in the stress / strain plane, the area of the triangle (healthy phase + damage propagation phase) represents the fracture toughness divided by the characteristic length of the element, $G_{I_c}^f/L_c$. Consequently the strain at finale failure, ε_1^T or ε_1^C, depends on the finite element size [105].

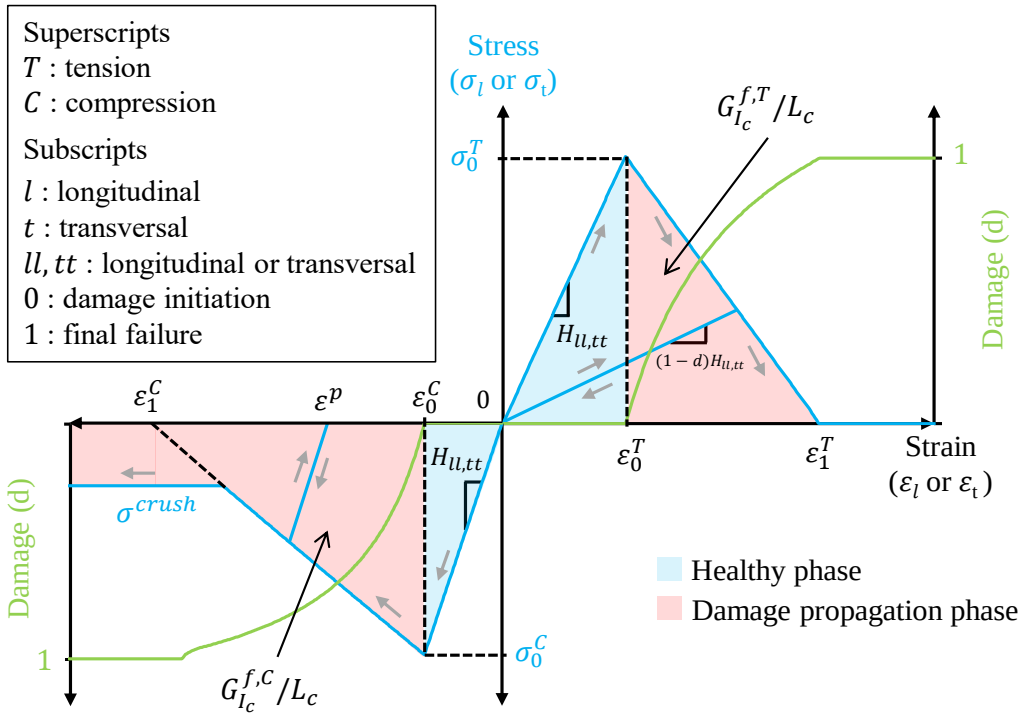

Figure V.5. Overall fiber failure behavior law with damage initiation and damage propagation under tension and compression, in longitudinal and in transverse fiber direction.

Then the tensile stress is calculated using the orthotropic stiffness coefficients as:

- For the longitudinal direction, $\varepsilon_l > 0$:

$$\sigma_l = (1-d)[H_{ll}\varepsilon_l + H_{lt}\varepsilon_t + H_{lz}\varepsilon_z] \quad \text{(V.2)}$$

- For the transverse direction, $\varepsilon_t > 0$:

$$\sigma_t = (1-d)[H_{tt}\varepsilon_t + H_{lt}\varepsilon_l + H_{tz}\varepsilon_z] \quad \text{(V.3)}$$

Where H_{ij} is the ij component of the Hooke's matrix and d is evaluated in order to obtain a linear decreasing of the stress versus strain (Figure V.5) in dissipating the fracture toughness (equation V.1). Moreover, the damage d is considered strictly increasing.

Once the critical energy release in compressive fiber failure is dissipated, a plastic behavior (ε^p) should be considered and a crushing stress σ^{crush} should be applied according to a plateau, in order to simulate the crushing behavior. Moreover in order to avoid a discontinuity between the fracture toughness dissipation phase and the crushing phase (Figure V.5), this plastic behavior is also considered to dissipate the fracture toughness. Thus, the compressive stress is calculated using the plastic strain and the orthotropic stiffness coefficients as:

- For the longitudinal direction, $\varepsilon_l < 0$:

$$\sigma_l = H_{ll}\left(\varepsilon_l - \varepsilon_l^p\right) + (1-d)[H_{lt}\varepsilon_t + H_{lz}\varepsilon_z] \quad \text{(V.4a)}$$

Such that:

$$f_l = |\sigma_l| - \sigma^{crush} \leq 0 \quad \text{(V.4b)}$$

Where f_l is a plastic function, σ^{crush} the crushing stress and a coupling between plasticity and damage is considered in order to link the damage and the plastic strain:

$$\left(\varepsilon_l - \varepsilon_l^p\right) = (1-d)\varepsilon_l \quad \text{(V.4c)}$$

$$\Rightarrow d = \frac{\varepsilon_l^p}{\varepsilon_l} \quad \text{(V.4d)}$$

This coupling allows to obtain a continuity of behavior in compression between the damage zone (the zone where the fracture toughness) and the crushing zone (the zone of constant stress charactering the crushing of the material). This coupling induces the plastic strain ε_l^p can only decrease (or increase in absolute value), which means that damage by crushing can logically only increase.

- For the transverse direction, $\varepsilon_t < 0$:

$$\sigma_t = H_{tt}\left(\varepsilon_t - \varepsilon_t^p\right) + (1-d)[H_{lt}\varepsilon_l + H_{tz}\varepsilon_z] \quad \text{(V.5a)}$$

Such that:

$$f_t = |\sigma_t| - \sigma^{crush} \leq 0 \quad \text{(V.5b)}$$

with a similar coupling plasticity/damage, as in the longitudinal direction:

$$\left(\varepsilon_t - \varepsilon_t^p\right) = (1-d)\varepsilon_t \quad \text{(V.5c)}$$

$$\Rightarrow d = \frac{\varepsilon_t^p}{\varepsilon_t} \tag{V.5d}$$

Then, a failure criterion is applied to ensure the coupling of the energy dissipation associated with mode I in tension/compression and in longitudinal/transverse directions:

$$\frac{G_I^{l,T} + G_I^{t,T}}{G_{I_C}^{f,T}} + \frac{G_I^{l,C} + G_I^{t,C}}{G_{I_C}^{f,C}} = 1 \tag{V.6}$$

This relation means that a failure in the longitudinal direction induces failure in the transverse direction (and vice versa). This hypothesis is tricky and should be confirmed using bi-axial failure experimental tests. Unfortunately, this type of experiment is difficult to perform and no standard test exists, then the hypothesis was admitted and used for this study.

In addition, the plane shear strain (γ_{lt}) is computed from a plasticity law:

$$\tau_{lt} = G_{lt}(\gamma_{lt} - \gamma_{lt}^p) \tag{V.7}$$

Such that:

$$f_{lt} = |\tau_{lt}| - \tau_{lt}^0 - \lambda\left(\gamma_{lt}^p\right)^\eta \leq 0 \tag{V.8}$$

Where τ_{lt} is the plane shear stress, τ_{lt}^0 is the shear yield stress, λ is the strength index, G_{lt} is the plane shear stiffness, f_{lt} is the in-plane shear plastic function, γ_{lt}^p is the plastic plane shear strain and η is the strain hardening exponent.

Finally, the stress in out-of-plane direction is calculated as:

$$\sigma_z = H_{zz}\varepsilon_z + (1-d)[H_{lz}\varepsilon_l + H_{tz}\varepsilon_t] \tag{V.9}$$

$$\tau_{lz} = G_{lz}\gamma_{lz} \tag{V.10}$$

$$\tau_{tz} = G_{tz}\gamma_{tz} \tag{V.11}$$

H_{zz}, G_{lz} and G_{tz} are considered without damage to avoid too distorted elements and because these damages are considered of second order compared to the damage in the (l, t) plane.

V.2.3.2 Modelling of delamination

The delamination is taken into account by the interaction between surfaces with a contact algorithm and cohesive contact law based on a hard pressure-overclosure relationship, which is coded in the constitutive library of material models provided in ABAQUS [103].

A damage criterion to simulate the degradation and possible breakage of the liaison between the surfaces is defined from the constitutive library of material models provided in ABAQUS [103]. At first, a quadratic tension-interaction criterion based in the ultimate strength of the resin in transverse (σ_t^d) and in shear (σ_{lt}^d) direction is used. Then, the damage evolution is defined by a power law fracture criterion based in the fracture toughness in mode I ($G_{I_c}^d$) and mode II ($G_{II_c}^d$) of the resin. An initial stiffness value of 500 GPa/mm was chosen for the delamination interfaces.

V.2.4 Material properties used in the model

The properties used in the simulation are classified in three parts: elastic properties, plastic properties and fracture properties. All those properties have been investigated and identified from experimental tests realized in the laminated composites described in Figure III.1.

V.2.4.1 Elastic properties

Elastic properties are defined in the elementary laminate ply of PEEK thermoplastic matrix reinforced with a continuous carbon fiber fabric (Tenax®-E HTA40 3K) arranged in a 5-harness satin weave (Table V.1). Glass fabric (5-harness satin weave) and PEEK matrix is used only in the outer plies of the CG/PEEK laminate to evaluate if these plies have a significant influence on the translaminar cracking behavior.

Woven carbon fibers reinforced PEEK				
E_l^T (GPa)	E_l^C (GPa)	E_t^T (GPa)	E_t^C (GPa)	E_z (GPa)
65	59	65	59	6.73
ν_{lt}	ν_{lz}	G_{lt} (GPa)	G_{lz} (GPa)	G_{tz} (GPa)
0.04	0.3	4.83	2.59	2.59
Woven glass fibers reinforced PEEK				
E_l^T (GPa)	E_l^C (GPa)	E_t^T (GPa)	E_t^C (GPa)	E_z (GPa)
22	22	22	22	6.73
ν_{lt}	ν_{lz}	G_{lt} (GPa)	G_{lz} (GPa)	G_{tz} (GPa)
0.04	0.3	4.83	2.59	2.59

Table V.1. Elastic properties of the elementary ply used in the simulation [49, 106-107].

V.2.4.2 Plastic properties

A plastic behavior is observed when all the fibers of the laminated composites are oriented at an angle of ±45° with respect to the loading direction (Figure V.6). To take into account this plastic behavior, the implementation of in-plane shear plasticity according to the Ludwik's hardening model [108] was implemented into the behavior law (equation V.8).

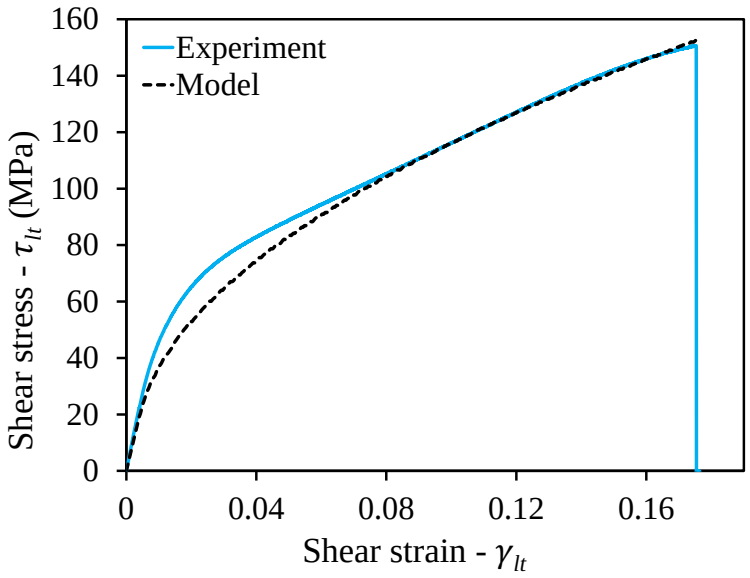

Figure V.6. Experimental and numerical shear stress-strain curve of angle-ply C8/PEEK laminate showing the elastic-plastic behavior.

The parameters of the plastic law (Table V.2) were identified from the experimental stress-strain curve of angle-ply C8/PEEK in tension (Figure V.6).

τ_{lt}^{0} (MPa)	λ (MPa)	η
20	350	0.5

Table V.2. Plastic properties used in the simulation.

The predictions of the plane shear plasticity implemented in the behavior law of the numerical model prove to be satisfactory with the experimental test (Figure V.6).

V.2.4.3 Fracture properties

Fracture properties given in Table V.3 were obtained from the experimental tests carried out on three different stacking sequences (Figure III.1).

In Chapter III, experimental tests carried out on woven-ply thermoplastic laminates with CT and CC specimens have shown that the increase in thickness implies a significant increase of the translaminar fracture toughness for a quasi-isotropic laminates, C7/PEEK and CG/PEEK (Figure V.7). In CT, the G-R curves for the quasi-isotropic laminates (C7/PEEK and CG/PEEK) are approximately constant, with a tendency towards an asymptote during crack growth. For the orthotropic C8/PEEK laminate, the CT test is characterized by a higher value of $G_{I_C}\big|_{tension}$, which is caused by an extended plasticity zone at the crack tip. In CC test, the G-R curves show an artificial positive trend and the values related to the ASTM analysis seem more consistent. In addition, it is difficult to separate overall plasticity (extrinsic toughness) from the energy dissipated by the crack tip (intrinsic toughness); and to separate the energy dissipated by the different damage mechanisms. Numerical simulations provide information on energy dissipative mechanisms as a function of the plies orientation. Therefore, the contribution of

each failure mechanism to the overall failure energy can be quantified. As a result, the values of $G_{I_c}^{f,T}$ and $G_{I_c}^{f,C}$ used in the numerical model presented in Table V.3 were chosen and adapted based on experimental observations with the objective of better understanding the failure experimental tests. As was mentioned previously the CC tests are more difficult to analyze due to the combination of several physical phenomena at the same time implying kinking, crushing and fiber breakage.

	C7/PEEK	CG/PEEK		C8/PEEK
		C14/PEEK	V2/PEEK	
	Fiber failure			
$\boldsymbol{\sigma^{crush}}$ (MPa)	100	100	100	100
ε_0^T	0.016	0.016	0.02	0.016
ε_0^C	-0.0115	-0.0115	-0.0115	-0.0115
$G_{I_c}^{f,T}$ (N/mm)	15	40	20	40
$G_{I_c}^{f,C}$ (N/mm)	25	40	20	26
	Delamination			
σ_t^d (MPa)	50			
σ_{lt}^d (MPa)	90			
$G_{I_c}^d$ (N/mm)	0.7			
$G_{II_c}^d$ (N/mm)	2			

Table V.3. Fracture properties of the materials used in the simulation.

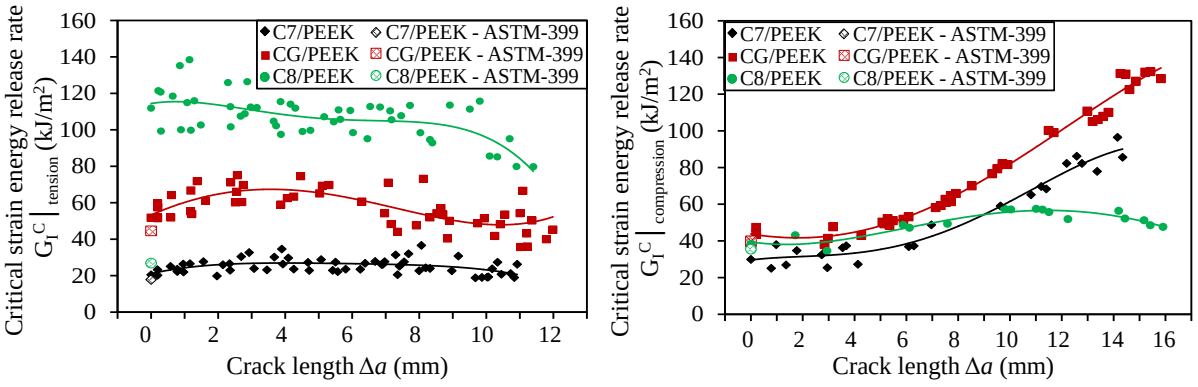

(a) Compact Tension (b) Compact Compression

Figure V.7. Experimental G-R curves obtained with the compliance method and the standard ASTM-399 at RT from: (a) CT tests and (b) CC tests.

V.3 Numerical approach of the translaminar cracking applied to woven-ply laminated composites

CT and CC tests were considered to induce translaminar fracture in tension and in compression. Three types of woven-ply laminated composites were tested, as described in section III.2. The Digital Image Correlation technique was applied during mechanical loading and the crack propagation was measured using an algorithm of binarization implemented in the Scilab code [56]. To validate the numerical model and the values of the translaminar fracture toughness identified from experimental tests, three different stacking sequence woven-ply thermoplastic laminates and two loading conditions (CT and CC) were simulated. Thus, the objective of these simulations is to better understand the failure experimental tests, and in particular, the crack kinking phenomenon in CC tests which is more difficult to analyze due to the combination of complex physical phenomena at the same time.

The simulations presented in this chapter was performed using HPC resources of CALMIP (CALcul en Midi-Pyrénées, https://www.calmip.univ-toulouse.fr) supercomputing center under the allocation p1026.

V.3.1 Tensile tests

Tensile tests were carried out on three woven-ply laminated composites using CT specimens, two quasi-isotropic laminates (C7/PEEK and CG/PEEK) with different thicknesses and one orthotropic laminate (C8/PEEK). By means of a Digital Image Correlation, the crack propagation and the full-field strains in the 0°/90° outer ply are monitored during mechanical loading. The crack propagation in the numerical model was measured from the damage variable. The full-strain field at the crack tip is also displayed at two different loading times, just before crack initiation (state 1) and during crack propagation (state 2) (Figure V.8). In order to show the highly deformed zone, a value of $3000\ \mu\varepsilon$ lower than that of the fiber failure was chosen as the limits of the strain field. To validate the numerical model, the force-displacement curves, the crack length (Δa)-displacement curves and the strain fields were compared to the experimental data.

V.3.1.1 Experimental validation

V.3.1.1.1 Quasi-isotropic laminates - C7/PEEK and CG/PEEK

In Figure V.8 and Figure V.9, force-displacement-crack length curves for C7/PEEK and CG/PEEK laminates are shown. Two different loading times - before crack initiation (state 1) and during crack propagation (state 2) - show that the size of the highly deformed zone at the crack tip is reached from the beginning and does not change much during the crack propagation. It suggest that the mechanical dissipation energy should be more or less constant and a value of the critical strain energy release rate can be defined, as was discussed in the Chapter III.

A representative experimental test was chosen for comparison purposes with the numerical model. The difference in stiffness at the beginning of the test between experimental and numerical curves shown in Figure V.8 and Figure V.9 should be due to the contact deformation

between the specimen and the testing machine, resulting in additional displacement in the experimental curves.

From the curves shown in Figure V.8 and Figure V.9, it appears that the simulation of the quasi-isotropic laminates (C7/PEEEK and CG/PEEK) shows relatively good agreement from the macroscopic responses standpoint. The force-displacement-crack length simulation curves are characterized by a quasi-linear force-displacement curve before reaching maximum load and a load drop as the crack starts propagating, which is in agreement with the experimental results. In the simulation, a small crack appears before the maximum load, indeed the volume elements that are close to the crack tip reach the failure strain in tension (ε_0^T) early and the energy dissipation starts with fracture. This small early crack is not critical as it does not prevent the laminate from reaching a maximum load on the CT numerical model.

The longitudinal strain is also shown in Figure V.8 and Figure V.9, the first loading time was taken before crack initiation and the second loading time was taken during crack propagation in both CT experimental/numerical test. Acceptable correspondence between numerical simulation and experimental test is presented based on the shape of the strain field of the outer ply for quasi-isotropic laminates.

As shown in Figure V.3, and according to the discussion in Chapter III, the tensile fiber breakage is the primary damage mechanism ruling the dissipation of the mechanical energy. The simulation of C7/PEEK laminate was done using an approximate value of the translaminar tensile fracture toughness $G_{I_c}^{f,T}$ of 15 N/mm (Table V.3) obtained from experimental investigation (Figure V.7). Then a good agreement was found between experimental and simulation for the force-displacement-crack length curves and the strain fields (Figure V.8). The simulation of CG/PEEK which is almost twice as thick of C7/PEEK was done using an approximate value of the translaminar tensile fracture toughness of 40 N/mm found in the experimental test (Table V.3 and Figure V.7) and the model also turns out to be well predictive (Figure V.9). The values used for the simulation of the quasi-isotropic laminates (C7/PEEK and CG/PEEEK) suggest that the translaminar tensile fracture toughness in woven-ply thermoplastic laminates is a thickness-dependent value. After the validation in the case of quasi-isotropic laminates, the numerical model is tested in the case of orthotropic laminates (C8/PEEK).

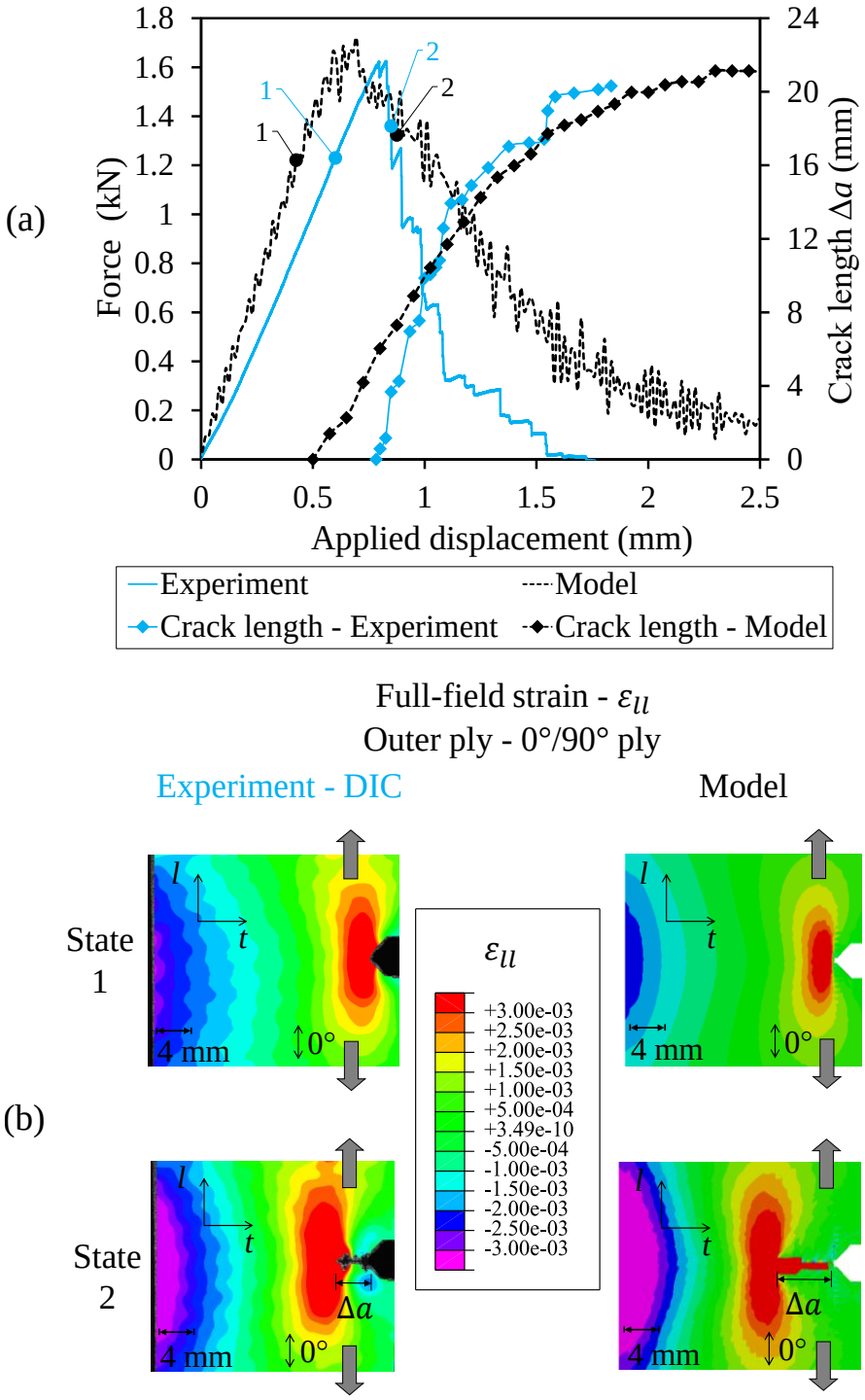

Figure V.8. CT experimental test and CT numerical model in the case of C7/PEEK laminates: (a) force/displacement curves – (b) strain fields, comparison at two different loading times, before crack initiation (state 1) and during crack propagation (state 2).

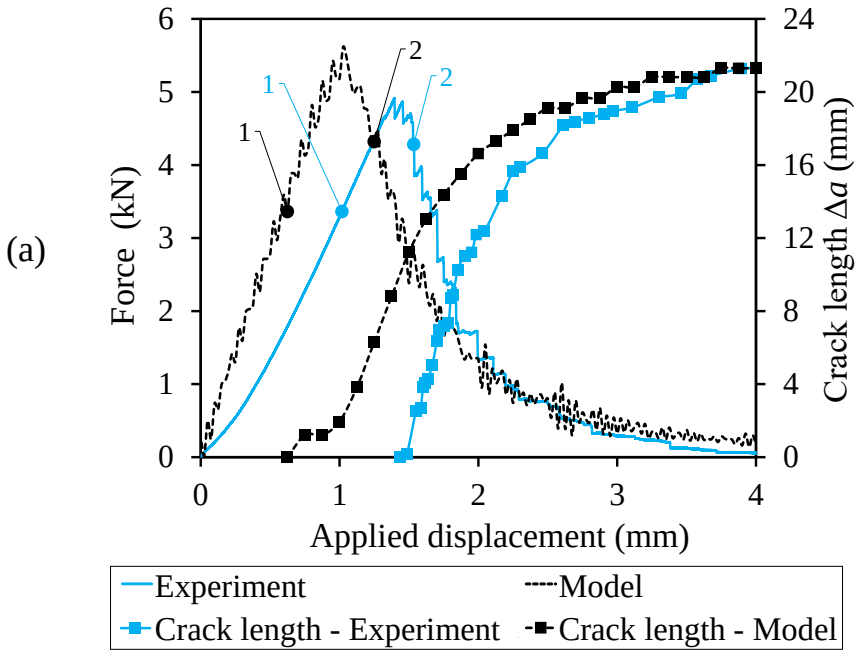

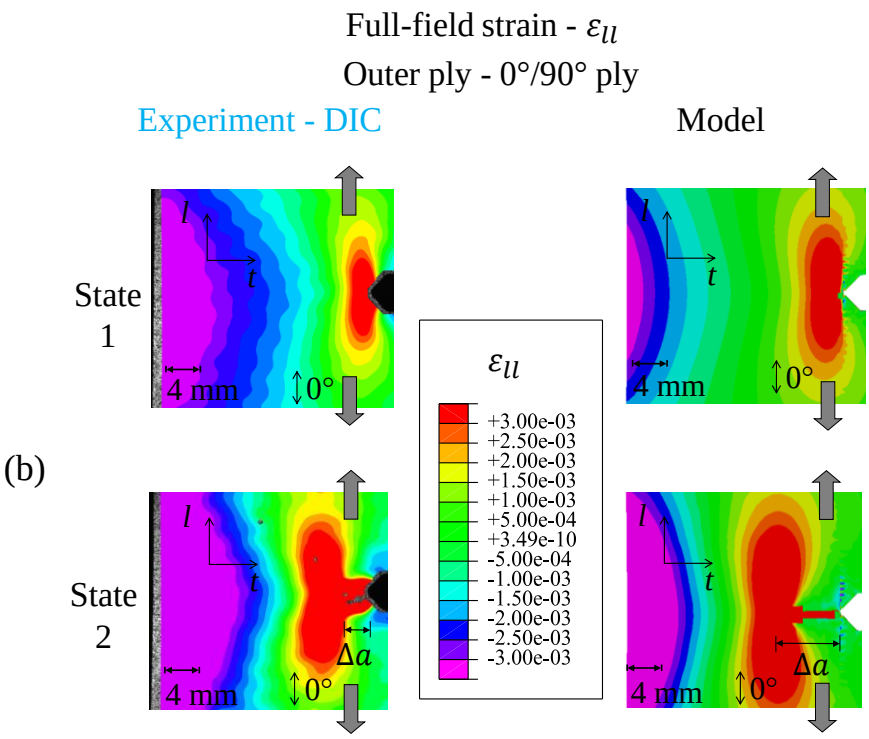

Compact Tension CG/PEEK
$[(0/90)_G,(0/90),(\pm45),(0/90),(\pm45),(0/90),(\pm45),(0/90)]_S$ - 4.5 mm thick

Figure V.9. CT experimental test and CT numerical model in the case of CG/PEEK laminate: (a) force/displacement curves – (b) strain fields, comparison at two different loading times, before crack initiation (state 1) and during crack propagation (state 2).

V.3.1.1.2 Orthotropic laminate - C8/PEEK

As indicated by the experimental force-displacement-crack length curves in Figure V.10, the C8/PEEK laminates exhibit an elastic ductile behavior before the maximum load and a ductile fracture translaminar as the translaminar crack propagates. The CT tests show that the fiber breakage in tension and the plastic shear deformation are the main phenomena dissipating mechanical energy. The non-linearity observed on the C8/PEEK curve is due to the shear plasticity developing at the crack tip but also near the loading cylinders and in the overall specimen (Figure V.11). Indeed, contrary to the quasi-isotropic laminates, the orthotropic laminate has no ±45° ply to withstand the in-plane shear stress, and a low shear loading can induce important area of plastic shear deformation. This phenomenon is also visible on the G-R curve calculation.

For example, the computation of the R-curve presented in Figure V.7 was done from the global force-displacement curve. A high translaminar tensile fracture toughness value of the C8/PEEK orthotropic laminate was computed. This high value results from the formation of a zone of extensive plasticity in the overall specimen (Figure V.11) leading to which both a significant energy dissipation. This plastic deformation comes along with the crack propagation contributes to the computation of the fracture toughness. Then the value of the translaminar tensile fracture toughness, used for the C8/PEEK laminate, was adapted to obtain an appropriate answer of the simulation in order to understand where the energy is dissipated and what area of the laminates is damaged. The simulation of the C8/PEEK laminates was conducted using a value of the translaminar tensile fracture toughness of 40 N/mm (Table V.3). As far CT tests are concerned, a good agreement between the force-displacement-crack length curves of CT experimental test and CT numerical model was observed, proving the capability of the numerical model to describe the plastic behavior of C8/PEEK laminates by using the plastic law presented in equation V.7.

The experimental longitudinal strain field is not very clear, contrary to the numerical one (Figure V.10), and in particular a dissymmetry of the strain field appears that it is not predicted by the numerical model. Of course, the numerical model is very symmetric and is not able to simulate this phenomenon. In experiments, this dissymmetry could be explained by a dissymmetry of the loading set up exacerbated by the high value of shear strains, in particular under the loading cylinders. This point should be confirmed by additional investigations.

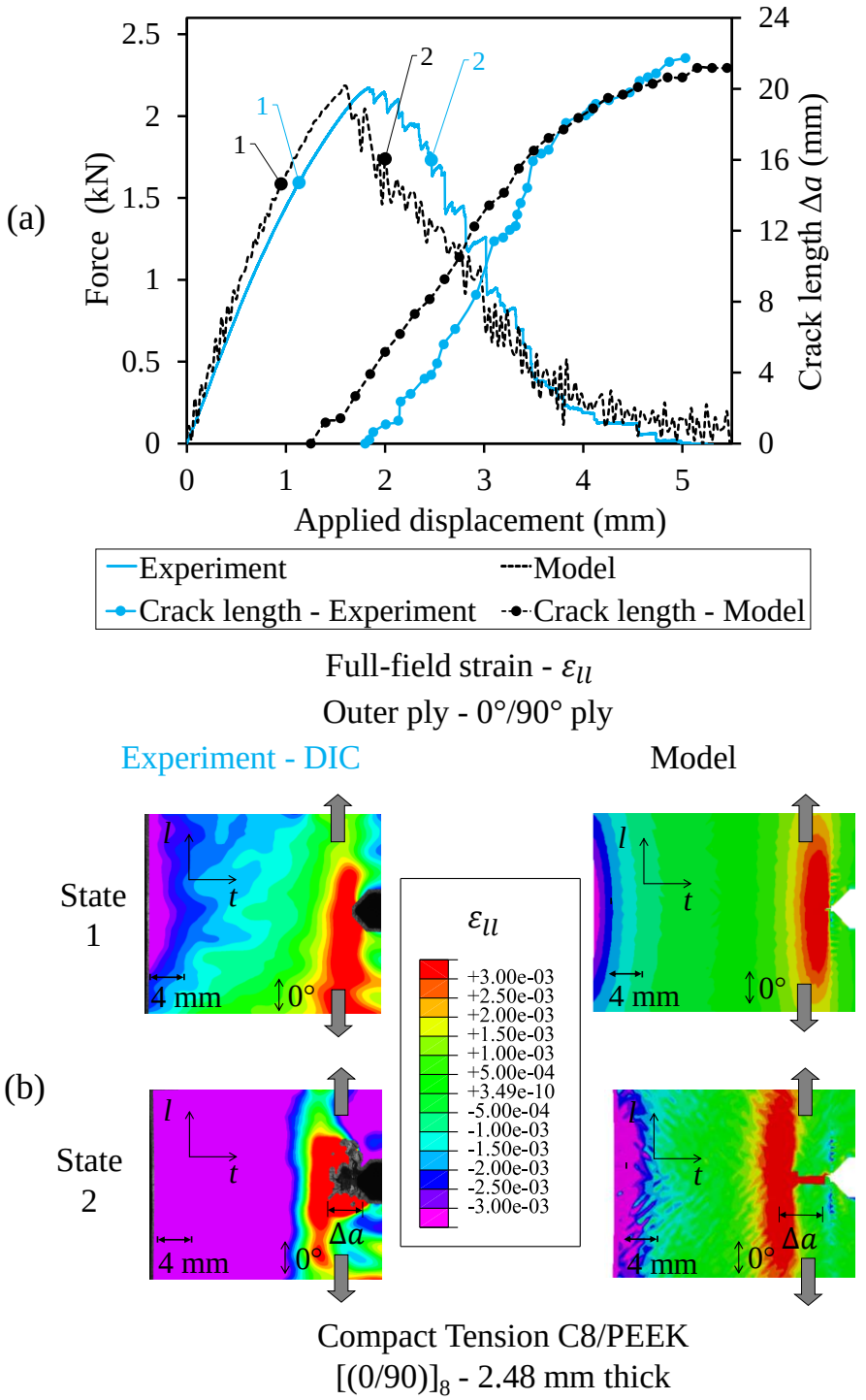

Figure V.10. CT experimental test and CT numerical model in the case of C8/PEEK laminates: (a) force/displacement curves – (b) strain fields, comparison at two different loading times, before crack initiation (state 1) and during crack propagation (state 2).

V.3.1.2 Influence of the thickness and plasticity on the translaminar cracking

In order to compare the mechanical responses of the laminates with different thicknesses, the force was normalized by laminate thickness and the in-plane shear strain fields of the 0°/90° outer ply are represented (Figure V.11).

From the experimental curves shown in Figure V.11, it appears that quasi-isotropic laminates (C7/PEEK and CG/PEEK) are characterized by similar macroscopic mechanical responses with quasi-linear force-displacement curve. The increase in thickness results in an increase of the force and then of the translaminar tensile fracture toughness (Figure V.7). In order to account for this effect, the simulations of the quasi-isotropic laminates shown in Figure V.8 and Figure V.9 were done using a value of $G_{I_c}^{f,T}$ 15 N/mm for C7/PEEK and 40 N/mm for CG/PEEK (Table V.3). These simulations are relatively in good agreement with experimental observations and the influence of thickness in the translaminar fracture toughness is significant.

One way to evaluate the plastic energy resulting from the lower shear behavior of the orthotropic laminate is to visualize the in-plane shear strain field. In Figure V.11 the in-plane shear strain fields of the 0°/90° outer ply are compared for the three laminates. The simulations give a very well predictive shape of the shear strain field. A very significant shear plasticity is observed for the C8/PEEK laminates compared to quasi-isotropic ones. It suggests that the use of a plasticity behavior law in the numerical model is essential to describe the translaminar cracking of this type of composite material.

Finally a value of $G_{I_c}^{f,T}$ of 40 N/mm was used for C8/PEEK (Table V.3) in order to correlate the experimental results (Figure V.10). This value is in total contradiction with the value higher than 100 N/mm obtained using the compliance method (Figure V.7); the difference is of course mainly due to the energy dissipated by shear plasticity, which is integrated in the calculation of the compliance method. Moreover, this value is similar to the fracture toughness evaluated for the CG/PEEK, which is twice thicker. Unfortunately it is difficult to directly compare the thickness of the orthotropic laminate, which only includes 0/90 plies, with the one of the quasi-orthotropic laminate, which induces series of 0/90 and ±45 plies. However, in first approximation it seems logical that the damage zone of an orthotropic laminate is higher than this one of a quasi-isotropic laminate and that the induced fracture toughness is higher. Of course, the present study with only two different thicknesses and three different draping sequences is not sufficient to conclude and additional experimental tests are necessary to conclude.

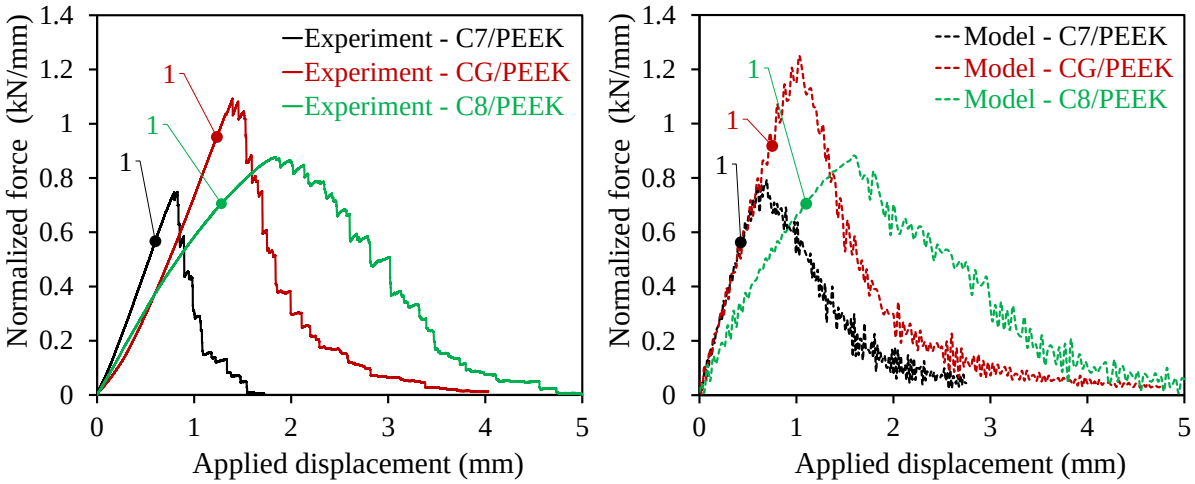

C7/PEEK: [(0/90),(±45),(0/90),(±45),(0/90),(±45),(0/90)] - 2.17 mm thick
CG/PEEK: $[(0/90)_G,(0/90),(\pm45),(0/90),(\pm45),(0/90),(\pm45),(0/90)]_S$ - 4.5 mm thick
C8/PEEK: $[(0/90)]_8$ - 2.48 mm thick

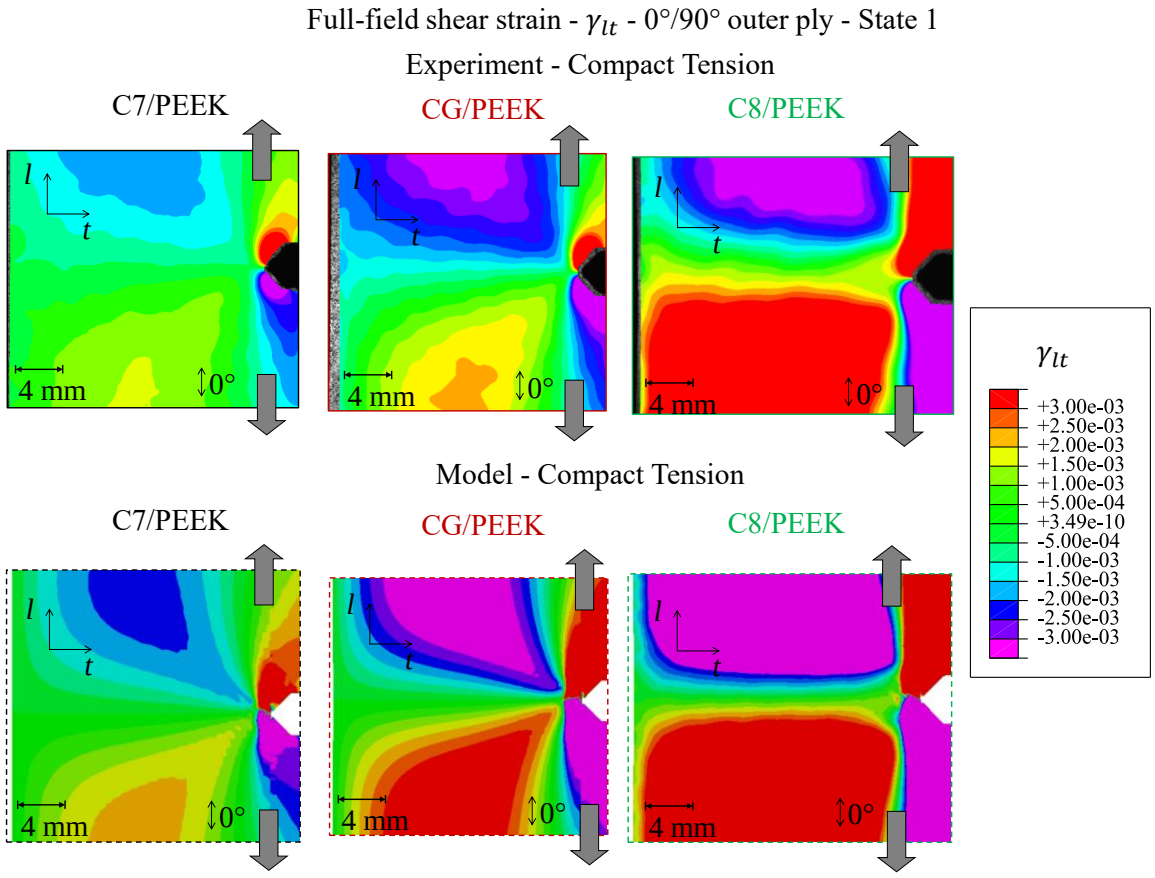

Figure V.11. Experimental/numerical comparison of the three laminates in the case of CT specimens: curves of the force normalized by the thickness as a function of displacement and in-plane shear strain field at laminate surface before crack initiation (state 1).

V.3.2 Application to compressive tests

Compressive tests were carried out on the three woven-ply laminated composites. In CC specimens, crack growth is mainly related to micro-buckling of the plies at 0°, which results in fiber breakage in compression and the formation of kink-bands [14-33]. Using the same protocol as for CT specimens, the crack propagation and the full-field strain were recorded during mechanical loading in CC specimens. The purpose of modeling the CC tests is to verify if the translaminar cracking in compression can be described by the three types of physical phenomena (fiber failure, plane shear plasticity and crushing plasticity) or if additional mechanisms should be considered.

V.3.2.1 Testing with experimental data

V.3.2.1.1 Quasi-isotropic laminates - C7/PEEK and CG/PEEK

A representative experimental test was chosen for comparison purposes with the numerical model. Contrary to tensile testing, the correspondence between the increase in crack length and the jumps observed on the force-displacement curve is not obvious when it comes to compressive loadings. This is because the fiber breakage in compression is more gradual than in tension, and that after the failure in compression a crushing stress continues to be transmitted.

From the curves shown in Figure V.12, it appears that the simulation of the macroscopic mechanical response of C7/PEEK laminates is in relatively good agreement with the experimental results. The onset cracking is observed before maximum load, as for experiment as for numerical modelling, and the load continues to increase for some time before starting to decrease. This is due to the fact that in compressive fiber failure, a plastic behavior is observed as well as a crushing stress (Figure V.5). This phenomenon highlights the main interest of the model, it makes possible to separate the part of the dissipated energy due to the compressive fiber failure from the crushing phenomenon. This confirms it is impossible to obtain the evolution of the compressive fracture toughness versus the crack length using only the global force-displacement curve (Figure V.7) [14, 16, 33-34]. In the present case an artificial increasing of the G-R curve is obtained while the model seems to show a more or less constant value of the compressive fracture toughness.

The longitudinal strain shown in Figure V.12 reveals a very well defined plastically highly deformed zone at the crack tip when considering the shape of the strain field before crack initiation (state 1 in Figure V.12). From state 2, the development of the highly deformed zone at the crack tip in compression is observed. During propagation, the shape of the strain field of the experimental test is not very well defined, probably due to out-of-plane displacements resulting from specimen kinking and from asymmetry of the loading system. The good agreement between the experimental/numerical curves suggests that the specimen's kinking is not very pronounced and a single value of the translaminar compressive fracture toughness ($G_{I_c}^{f,C}$) is enough to describe the translaminar cracking in compression for C7/PEEK laminates.

From the comparison of experimental/numerical results in CG/PEEK laminates (Figure V.13), it appears that the present numerical model is not able to describe the macroscopic mechanical

response in compression. As shown in Figure III.1, the differences between the two quasi-isotropic laminates (C7/PEEK and CG/PEEK) are mainly thickness and the presence of two outer glass-PEEK plies. The mechanical contribution of these outer plies is assumed negligible considering the fraction of carbon-PEEK plies in hybrid CG/PEEK laminates about 10% of the total number of plies. That means that a similar macroscopic response could be expected as in the case of the tensile tests, with a simple increase of the fracture toughness versus the thickness of the laminate between C7/PEEK and CG/PEEK. But in the experimental representative curve shown in Figure V.13, a plateau is observed from the onset of cracking to ultimate failure. This plateau could be explained by an R-curve effect that changes the strain energy release rate along with the crack propagation, as can be seen in the R-curve (Figure V.7), or by an out-of-plane effect, which is not present in the C7/PEEK CC test, nor for the numerical model of the CG/PEEK. Even though different values of $G_{I_c}^{f,C}$ are considered, the numerical model failed to predict the macroscopic mechanical response of CG/PEEK laminates. The current numerical model considers only one value of $G_{I_c}^{f,C}$ and no R-curve effect is taken into account, moreover the fracture toughness is considered constant in the thickness of the laminate but its value could be higher at the mi-thickness than near the outer surface. Finally, the out-of-plane shear effects should also be considered. Indeed the kink bands developing during the compressive fiber failure induce out-of-plane shear strain resulting in the asymmetry of the test; this is probably this effect which partly explains the asymmetry of the highly strain zone observed at the crack tip (Figure V.12 and Figure V.13). It can be also noticed that for the CC tests an anti-buckling system was used in order to avoid the global buckling of the sample. Of course this buckling is not numerically obtained because the out-of-plane shear strain generated by the kink band is not taken into account; additional work is necessary to clarify this point and to explain the effect of this out-of-plane shear on the appearing of the force plateau during the CC test (Figure V.13).

Nevertheless, as in tension, an increase of the fracture toughness is already observed versus the thickness of the laminate, with a value of 25 N/mm for the C7/PEEK and of 40 N/mm for the CG/PEEK; even if regarding the poor correlation of the CG/PEEK CC test, this result should be considered with caution.

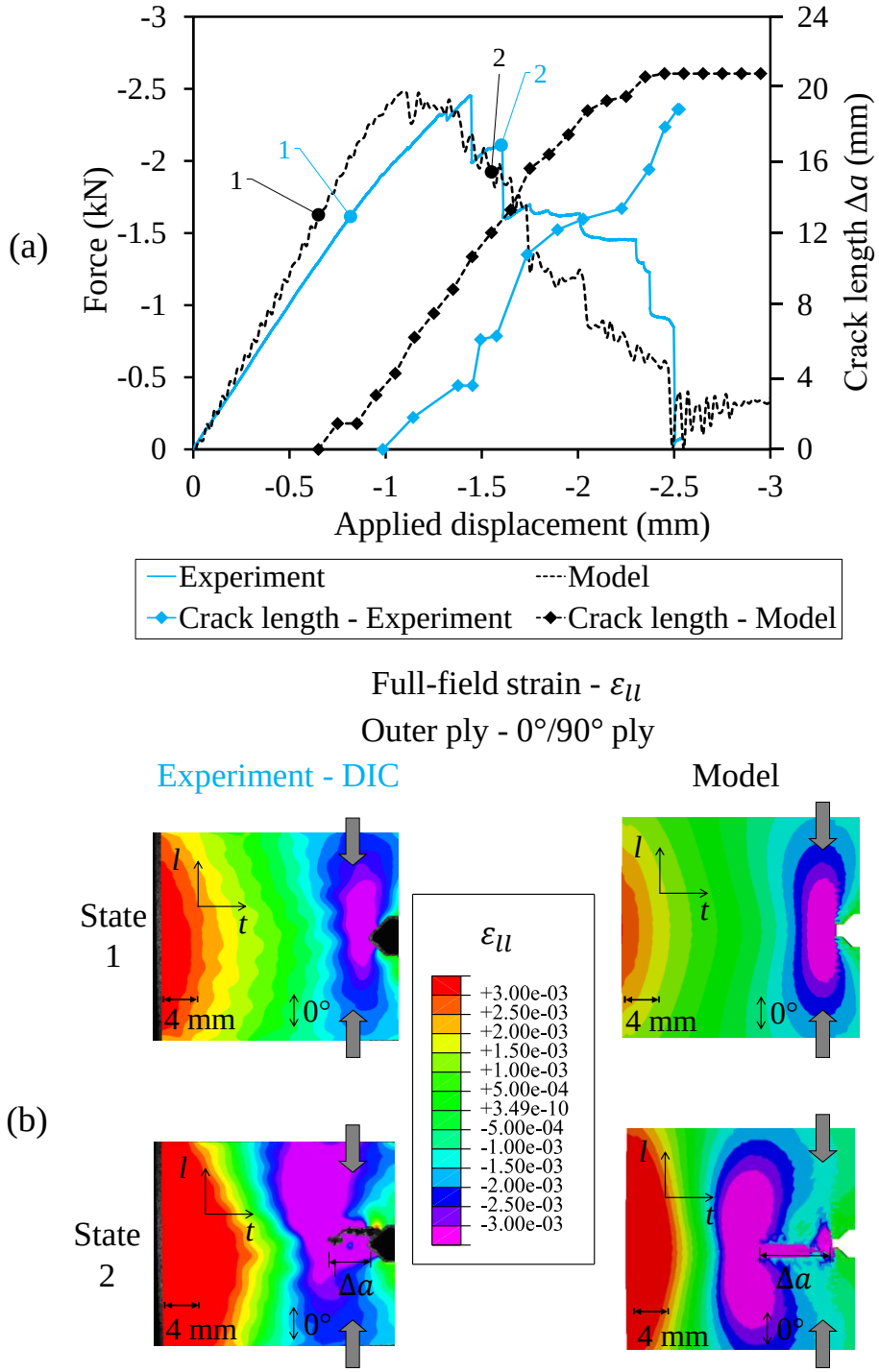

Figure V.12. CC experimental test and CC numerical model in the case of C7/PEEK laminates: (a) force/displacement curves – (b) strain fields, comparison at two different loading times, before crack initiation (state 1) and during crack propagation (state 2).

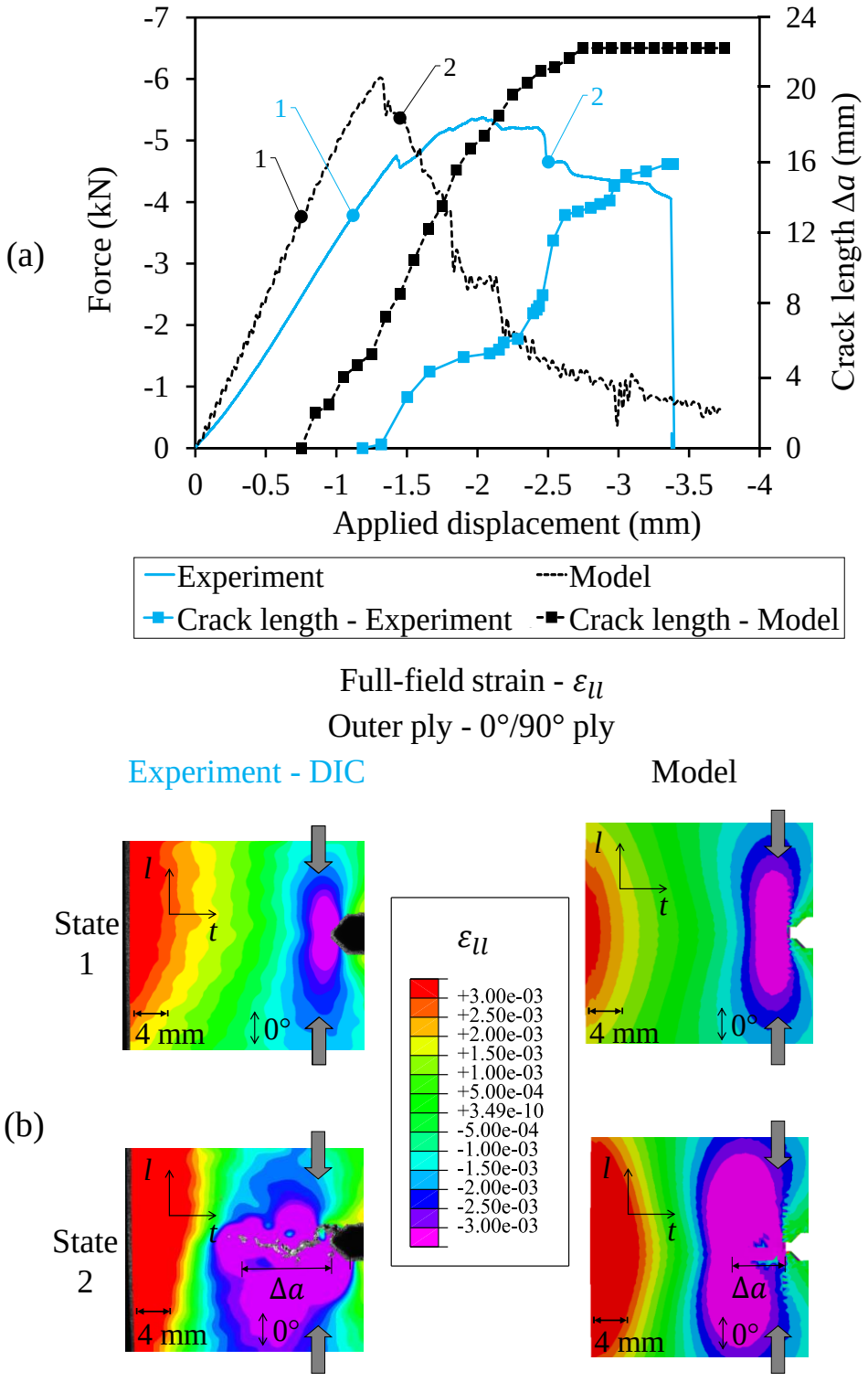

Figure V.13. CC experimental test and CC numerical model in the case of CG/PEEK laminates: (a) force/displacement curves – (b) strain fields, comparison at two different loading times, before crack initiation (state 1) and during crack propagation (state 2).

V.3.2.1.2 Orthotropic laminate - C8/PEEK

In orthotropic laminates subjected to compressive loadings, the force-displacement curves are non-linear, as they are characterized by an elastic ductile behavior before maximum load. In the experimental study, the value of the translaminar compressive fracture toughness for the C8/PEEK laminate was not clearly evaluated due to the non-linearity observed in the force-displacement curve. A value of 26 N/mm was used in the simulation in order to determine if the model is capable to reproduce the macroscopic behavior of the laminates (Table V.3).

From the comparison of experimental/numerical curves in Figure V.14, it appears that the simulation only partially describes the elastic ductile behavior of the laminate before the crack propagation. This discrepancy could be due to the plasticity model of the in-plane shear, which is not efficient (Figure V.6). Moreover, the crack initiation predicted by the model is far too early; this point tends to confirm that the shear plasticity is underestimated by the model and should be improved.

When the first load drop appears for the numerical curve, a plateau at constant load is observed some time before the load starts decreasing again. This plateau in the simulation curve comes from the crushing modelling.

The shape of the experimental strain field is not good, a dissymmetry of the strain field (state 1 in Figure V.14) appears, probably due to very pronounced out-of-plane displacements resulting from specimen´s kinking. The kink-bands induce a more or less important out-of-plane shear effect, which is not considered by the model.

Finally, the main interest of the model was to separate the energy dissipated by the compressive fiber failure and by shear plasticity, but in the present case the bad correlation with the numerical modelling makes it not predictive. Then it is difficult to conclude concerning the value of the compressive fracture toughness and the effect of the shear plasticity on the overall dissipated energy.

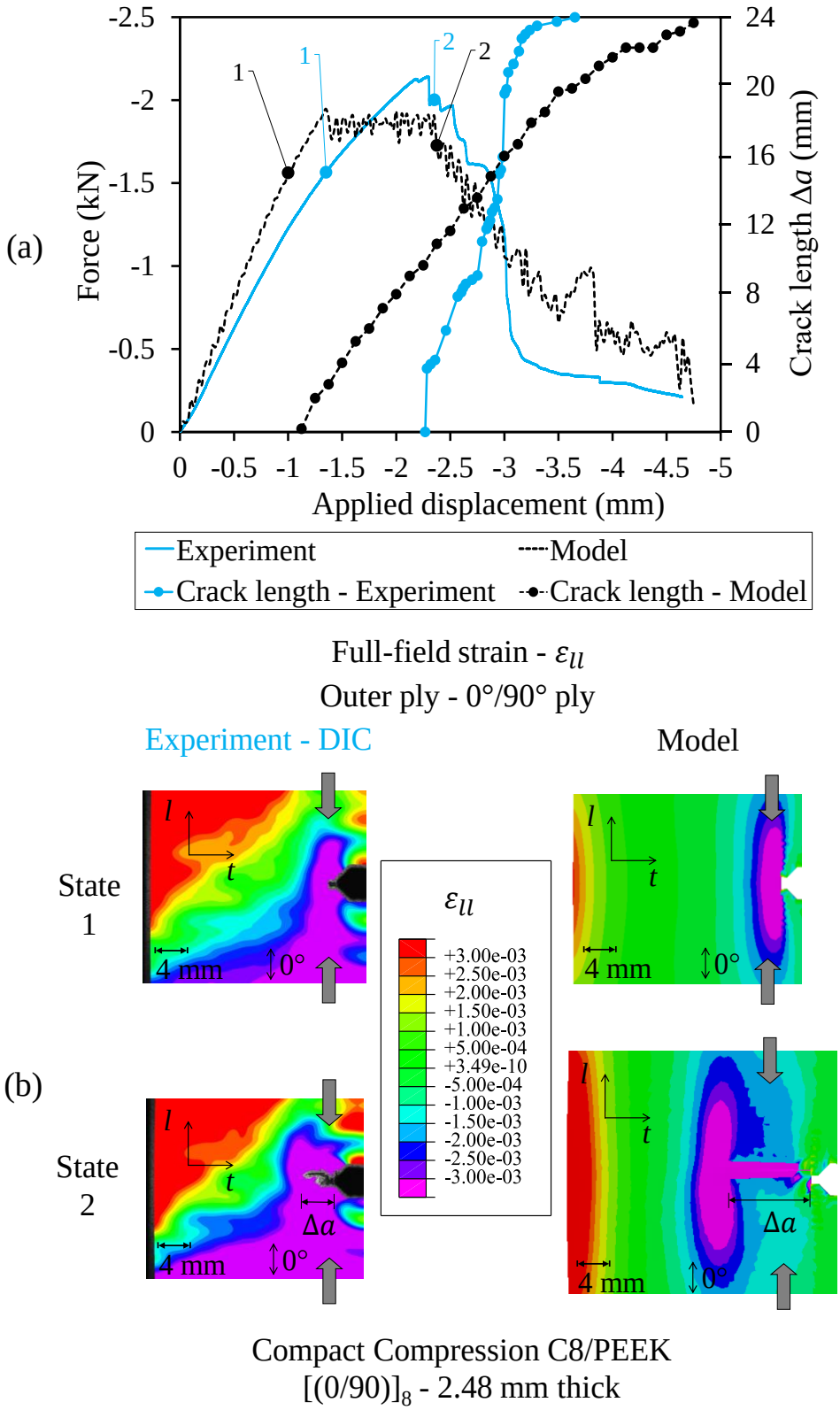

Figure V.14. CC experimental test and CC numerical model in the case of C8/PEEK laminates: (a) force/displacement curves – (b) strain fields, comparison at two different loading times, before crack initiation (state 1) and during crack propagation (state 2).

V.3.2.2 Influence of the thickness and plasticity on the translaminar cracking

Numerical modelling of the compressive tests requires the understanding of the various physical phenomena occurring at the same time when the mechanical energy starts dissipating in CC specimens. The mechanisms ruling the mechanical response of the laminates in compression will be further detailed in the next section. To better understand the influence of the laminate lay-up and thickness, the force was normalized by the corresponding thickness of each laminates and the in-plane shear strain fields of the 0°/90° outer ply are shown (Figure V.15).

From the experimental curves shown in Figure V.15, it appears that the quasi-isotropic laminates (C7/PEEK and CG/PEEK) are characterized by a quasi-linear behavior just before crack initiation. The larger thickness of CG/PEEK laminates results in a plateau that can be explained by a R-curve effect. The simulations on the quasi-isotropic laminates (Figure V.15) were performed with a value of $G_{I_c}^{f,C}$ of 25 N/mm for C7/PEEK and 40 N/mm for CG/PEEK (Table V.3). Only the simulations of C7/PEEK laminates show a relatively good agreement with experimental results. The simulations of CG/PEEK laminates are not satisfactory as the R-curve effect is not taken into account as the laminate thickness increases.

In the case of C8/PEEK laminates, large plastic deformations can be observed from the in-plane shear strain fields in comparison with the quasi-isotropic laminates (Figure V.15). It appears that the simulation on C8/PEEK laminates under compression only partially describes the elastic ductile behavior of the laminate.

The experimental strain field are characterized by a dissymmetry; probably due to out-of-plane displacements, resulting from specimen's kinking which is not taken into account by the numerical model. The numerical model predicts a symmetrical longitudinal strain field, the compressive failure model and crushing model only act along in-plane directions (σ_{LL}, σ_{TT}) under compression, when it should also act along out-of-plane directions (τ_{LZ}, τ_{TZ}).

The simulations of the compressive tests for the three laminates investigated in this study provide an insight into the physical phenomena implied in compressive translaminar failure. They also open prospects on other physical phenomena that need to be considered in the current numerical model to improve its predictive capacities. The R-curve effect should be considered to take into account the laminate thickness, but also the volume variation to account for the out-of-plane strains and in particular its coupling with the crushing phenomenon.

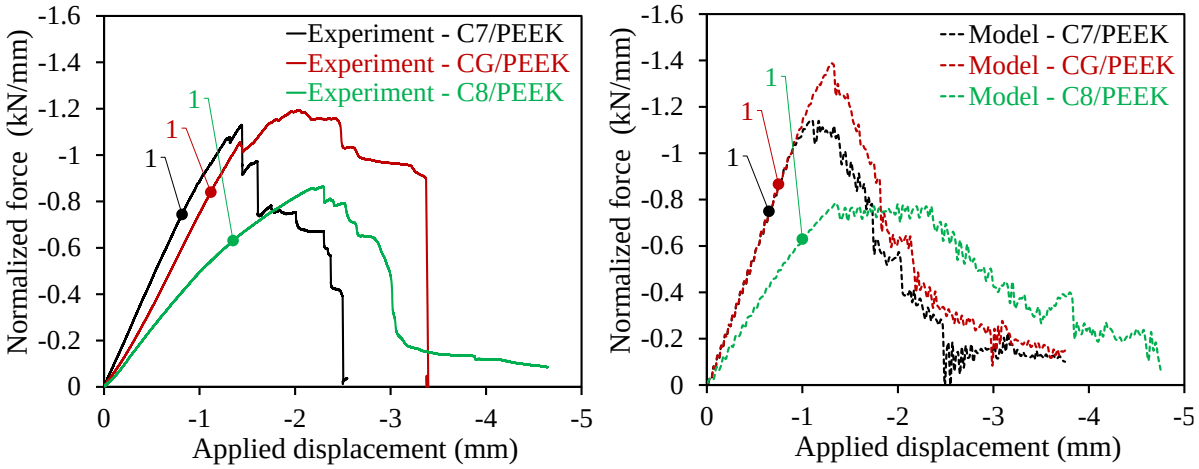

C7/PEEK: [(0/90),(±45),(0/90),(±45),(0/90),(±45),(0/90)] - 2.17 mm thick
CG/PEEK: $[(0/90)_G,(0/90),(\pm45),(0/90),(\pm45),(0/90),(\pm45),(0/90)]_S$ - 4.5 mm thick
C8/PEEK: $[(0/90)]_8$ - 2.48 mm thick

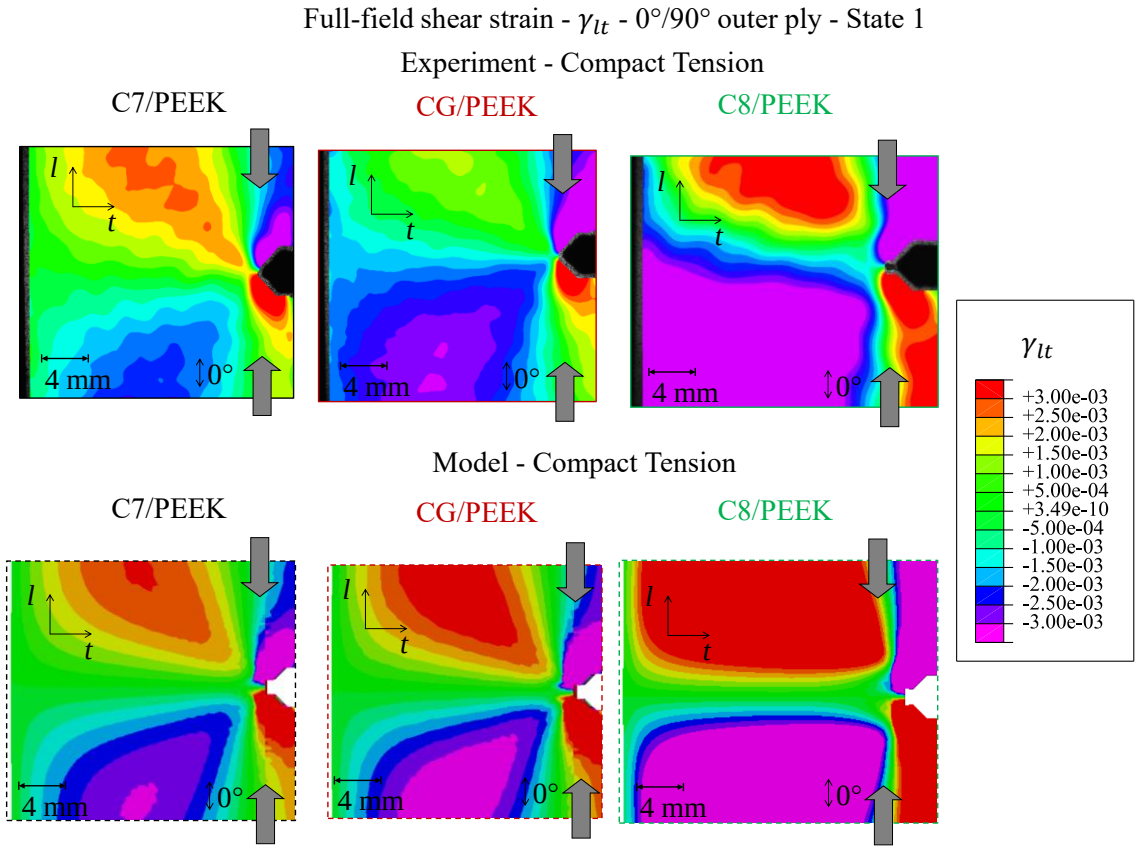

Figure V.15. Experimental/numerical comparison of the three laminates in the case of CC specimens: curves of the force normalized by the thickness as a function of displacement and in-plane shear strain field at laminate surface before crack initiation (state 1).

V.3.2.3 Improvement of the model predictive capacities under compression loading

The difficulty of inducing a failure mode in pure compression (where all the fibers in the different plies break in compression) is associated with buckling at the local scale (microbuckling) which can be generalized at the macroscopic scale (macrobuckling). In laminate composites, the compression failure modes are complex and generally result from the combination of different damage mechanisms. This is why an anti-buckling device is often necessary to limit out-of-plane displacements and therefore promote compression failure of the fibers. However, the use of this type of device is not a sufficient condition. Thus different compressive failure mechanisms are observed: crushing, shearing, kinking or plastic buckling.

In UD-ply laminates under compressive loading, the damage is mainly characterized by fiber bundle breakage and the formation of kink-bands [109]. The "kink-bands" formed in the longitudinal fiber bundles are connected by different damage mechanisms including matrix cracking and delamination between fiber strands. Increasing the compressive load can initiate the failure of the fibers aligned with the loading direction resulting from shear driven fiber failure, or fiber kinking. The corresponding failure mode depends on the presence of shear stresses that can arise from localized fiber misalignment. As compressive load increases an instability appears in misaligned areas, leading to fiber breakage in bending. Then a transition to the fiber kinking failure occurs with the formation of kink bands.

In woven-ply laminates, when the crimp regions are aligned through the thickness, it provides additional support to limit the out-of-plane displacements at the weaving points caused by the compression [110]. As a result, the laminate has better resistance to compression because the local micro-buckling of fiber bundles is delayed. On the contrary, if the crimp regions are in opposition, the out-of-plane displacements are facilitated at weaving points resulting in interlaminar cracking and macroscopic buckling.

In compression the crack-tip stress field does not tend towards infinity and a crushing stress continues to be transmitted during the closing of edge cracks. It is then impossible to evaluate the strain energy release rate during crack growth due to the formation of kink-bands, because other damage modes (delamination, crushing) will develop, as kink-bands broaden [111], and will continue to dissipate energy. It is therefore necessary to separate the energy dissipated by macroscopic crack growth from the one dissipated by other damage modes (produced by the contact stresses in the faces of the kink band). In practice, this is very complicated, the numerical simulation is promising as it provides a few answers.

In this chapter, the modelling of CC tests on woven-ply laminates with different stacking sequence (an orthotropic laminate and two quasi-isotropic laminates) was performed in order to better understand the translaminar failure under compression. Only three types of physical phenomena have been considered: fiber failure, plane shear plasticity and crushing plasticity. The objectives of these simulations were to understand how the energy is dissipated during the translaminar crack propagation under compression and to better understand the kinking phenomenon. The discussion in the previous sections made it possible to verify the partial predictive capacities of the numerical model under compression loading. The longitudinal strain field of the experimental test revealed a dissymmetry of the strain field, probably due to very

pronounced out-of-plane displacements resulting from the specimen kinking, inducing a more or less out-of-plane shear effect which is not taken into account by the numerical model. The numerical model predicts a symmetrical longitudinal strain field, the failure compressive model and crushing model only act along the in-plane directions (σ_{LL}, σ_{TT}) under compression loading, when it should also act along the out-of-plane directions (τ_{LZ}, τ_{TZ}). On the experimental force-displacement curves, a plateau is observed after the onset of cracking, suggesting a change in the translaminar fracture toughness as crack propagates. So far, the numerical model is inefficient to predict the compressive macroscopic mechanical behavior using a constant value of $G_{I_c}^{f,C}$ and a R-curve effect should be implemented to account for this behavior.

V.4 Conclusion

A numerical model developed in FE code Abaqus/Explicit has been used in order to simulate the translaminar fracture and the damage propagation due to fiber breakage in woven-ply thermoplastic laminates. CT and CC tests have been modeled and the primary physical phenomena responsible for the dissipation of mechanical energy during translaminar fracture have been simulated: fiber failure, in-plane shear plasticity and crushing plasticity. The main goal of this study was to develop a numerical simulation capable of reproducing the macroscopic mechanical behavior of laminates with different stacking sequence and thicknesses. The objective was twofold: to highlight the dependence of the translaminar fracture on these parameters and to understand how the mechanical energy is dissipated. Ultimately, the proposed numerical model allows a better understanding of the translaminar fracture behavior in tension and particularly in compression, which is more difficult to analyze due to the combination of complex physical phenomena at the same time.

In the first part of this chapter, CT tests were simulated to investigate the translaminar fracture in tension. The simulations of the CT tests show a good agreement with experimental tests for all the laminates. When simulating the fracture behavior of quasi-isotropic laminates, different values of translaminar tensile fracture toughness were used. A macroscopic mechanical response with quasi-linear behavior is observed. Therefore, it validates the experimental observations suggesting that the translaminar tensile fracture toughness is a thickness-dependent value. The simulations of the orthotropic laminates show that the elastic-ductile behavior is associated with the significant energy dissipation resulting from in-plane shear plasticity. This suggests that a value of translaminar tensile fracture toughness from a global calculation based on the force-displacement curves is not satisfactory.

After the validation in tension, CC tests were simulated to verify if translaminar cracking in compression can be described by the same model. For quasi-isotropic laminates, only C7/PEEK laminates show a good agreement with experimental data from the macroscopic mechanical response standpoint. The larger thickness of CG/PEEK laminates results in a plateau leading to a R-curve effect due to a significant volume variation during crushing. The present numerical model is not able to capture this effect. The simulation of the C8/PEEK laminates under compressive loading only partially describes the elastic-ductile behavior. When the first load drop appears, a plateau at constant load is observed until load starts decreasing again. This

suggests that the out-of-plane displacements are not well taken into account by the numerical model.

Finally, the model presented in this work proves to be effective to study the tensile translaminar cracking in woven-ply laminated composites, this model is characterized by the following specifications: respect of the fiber direction in the laminate lay-up, a relatively limited number of material parameters, and a damage variable that reflects the crack propagation. To improve the predictive capacities of this model in the case of compressive loadings, other physical phenomena such as R-curve effect and out-of-plane displacement still need to be taken into account in the model formulation.

Chapter VI: Conclusions and future works

The principle of a composite material is to combine the advantages of two different materials, most often resistant and brittle fibers, with a less resistant and more ductile polymer matrix. In laminated composites, the thermo-mechanical behavior is primarily driven by the laminates stacking sequence that allows the mechanical role of each constitutive elements to be modulated. When the polymer matrix is ductile (as it is observed in PEEK thermoplastics), its contribution to the mechanical response and the fracture behavior is enhanced at temperatures higher than the glass transition temperature of the composite. Thus, TP-based laminates are characterized by their intrinsic fracture toughness (one of their main advantages over thermosetting composites). Such intrinsic toughness is associated with specific damage mechanisms that are energy dissipative processes ruling their extrinsic fracture toughness. Both intrinsic and extrinsic fracture toughness contribute to the increase in the fracture energy of TP composites. This is the true originality of the investigations presented in these PhD works.

VI.1 Conclusions

The literature review has demonstrated that the fracture mechanics theoretical approaches applied to composite laminates were still opened questions that must be considered with caution. Composite structures are indeed heterogeneous and anisotropic materials. They already have structural characteristics at the ply level, structural effect that is enhanced in woven-ply laminates. Damage that develops during translaminar failure is therefore complex and induces many secondary damages. The application of the Linear Elastic Fracture Mechanics (LEFM) concepts, which were mainly developed in the context of homogeneous and isotropic materials, is therefore often at the limit of its scope of application. After a brief reminder of the characteristic quantities of LEFM, and in particular the strain energy release rates associated with mode I failure, the various tests allowing the assessment of these quantities were critically described.

In Chapter III, an experimental characterization of the translaminar fracture behavior of three composite laminates, based on PEEK thermoplastic matrix reinforced by carbon fibers woven plies, has been carried out by means of Compact Tension (CT) and Compact Compression (CC) tests. An orthotropic laminate and two quasi-isotropic laminates, have been tested at room temperature (RT) and 150°C (i.e. for a temperature slightly higher than the glass transition temperature). The different damages occurring during translaminar failure have been investigated depending on loading conditions (tension and compression). CT tests showed that the temperature influence on the overall mechanical response remains low. The failure of orthotropic laminates is elastic-ductile in tension. It is driven by the breakage of 0° carbon fibers and significant shear-induced plasticity at the crack tip. Quasi-isotropic laminates are characterized in tension by an elastic-brittle mechanical response. CC tests show a decrease in the mechanical resistance as temperature increases. At high temperature, the ductile failure associated with the localized crushing of the plies is promoted by the plastic deformation of the PEEK matrix at $T>T_g$. Finally, a few characteristic values of PEEK-based laminates fracture toughness were discussed. In tension, there is an increase in the translaminar fracture toughness

with the laminate thickness and a slight improvement in this one due to the influence of temperature. In tension, one can observe that the translaminar fracture toughness for quasi-isotropic laminates increases with thickness about (19 to 50 kJ/m^2). Orthotropic laminates, the computation of toughness based on an overall behavior (force-displacement curve) is related to energy dissipation at the points of load application accompanied by greater plasticity mechanisms at the crack tip. In compression, the temperature strongly decreases the translaminar fracture toughness due to the softening of the matrix in the overlapping areas, which facilitate the out-of-plane displacement of the fiber bundles. Thus, the values at initiation seem to be the most accurate measurement of the critical strain energy release rate associated with the formation of kink-bands. The translaminar fracture toughness in compression is about 30 to 40 kJ/m^2, with a dramatic decrease with temperature.

Compared to conventional structural TS-based composite laminates, these values are of around 50 to 150 kJ/m^2 in tension and 20 to 80 kJ/m^2 in compression. These values are obviously only orders of magnitude and may vary according to the type of studied material. They can be compared with the ultimate strength values of polymer matrix (matrix cracking or delamination) of polymer resins between 0.2 and 3 kJ/m^2; the translaminar fracture of fibers obviously requires much more energy than PEEK matrix cracking!

Chapter IV was aimed at studying the influence of temperature and constraint effect on the measurement of translaminar fracture toughness. Single-Edge-Notch Tensile (SENT) tests and Single-Edge-Notch Bending (SENB) tests with different initial notches have been conducted at RT and at 150°C on quasi-isotropic hybrid carbon-glass fiber reinforced PEEK laminates. The translaminar crack is dominated by the breakage of 0° carbon fibers, and appears to be self-similar in both SENT and SENB specimens. In both SENT and SENB specimens, the influence of temperature on the residual strength was limited. In SENB specimens, failure consists of tensile and compressive breakage of 0° carbon fibers particularly in specimens with low *a/w* ratio. A local crushing (resulting from compression) in the contact area was exacerbated at $T>T_g$. It also appears that the constraint effect has very little influence on translaminar fracture toughness as SENT and SENB specimens have virtually the same mean value (about 47 kJ/m^2).

In the last chapter, a numerical model developed in Abaqus was used to better understand the translaminar fracture in woven-ply thermoplastic laminates. Only simulations at RT were performed; the influence of temperature was not covered. This numerical model consists of a failure criterion based on fracture mechanics to take into account for the dissipation of the critical strain energy release rate in opening mode (mode I) due to fiber breakage. The three most common physical phenomena responsible for the dissipation of mechanical energy during translaminar fracture are simulated: fiber failure, plane shear plasticity and crushing plasticity. Three types of composites have been considered for simulation purposes: an orthotropic laminate and two quasi-isotropic laminates. The simulations of the CT tests showed a good agreement with experimental results for all the laminates. Therefore, it validates the experimental observations suggesting that the translaminar tensile fracture toughness is a thickness-dependent value. The simulations of the orthotropic laminates showed that the elastic-ductile behavior is associated with the significant energy dissipation resulting from in-plane shear plasticity. The simulations of the CC showed that the predictive capacities of the

numerical model under compression is not satisfactory, so far as only the simulations are partially in agreement with the experimental results. The numerical model renders a symmetrical longitudinal strain field, the failure compressive model and crushing model only act in in-plane directions (σ_{LL}, σ_{TT}) under compressive loading, when it should also act in out-of-plane directions (τ_{LZ}, τ_{TZ}) as in experimental response.

Beyond the comparison with the experimental results in terms of G_{I_C} values and G-R curves, this numerical model is complementary to the experimental database and knowledge of the damage mechanisms. Indeed, it provides an insight regarding the role played by different damage mechanisms as well as the contribution of the plies orientation into energy-dissipative processes.

Fracture mechanics and finite elements modeling provide a very efficient framework for better understanding the fracture behavior of woven-ply PEEK-based laminated composites as well as the origin of their damage tolerance. However, the characteristics values of fracture toughness and corresponding G-R curves can be difficult to determine and to interpret. Ultimately, the present work also emphasized the limitations of fracture mechanics concepts applied to laminated composite structures.

VI.2 Future works

The results (experimental and numerical) obtained from this PhD open many interesting prospects for future works as follows:

- Utilization of the surface measurement of displacements and strain fields provided by the Digital Image Correlation (DIC) technique to compute the strain energy release rate
- Simulation of Single-Edge-Notch Bending (SENB) tests
- Improvement of the numerical crushing model to take into the out-of-plane displacements during compressive failure
- Implementation of a viscoplastic model to account for the influence of temperature and viscosity on both initiation and propagation of translaminar failure

During CT and CC tests, DIC data are relevant to establish the R-curve from the surface measurement of the displacements and strain fields. The J-integral being a contour integral that surrounds the crack tip, its calculation is based on the evaluation of the strain and stress fields in the vicinity of the crack, which could be obtained from full-field measurements. Such technique would be of particular interest to quantify the fracture toughness of [±45°] angle-ply laminates, which have a highly ductile fracture behavior, particularly at high temperature.

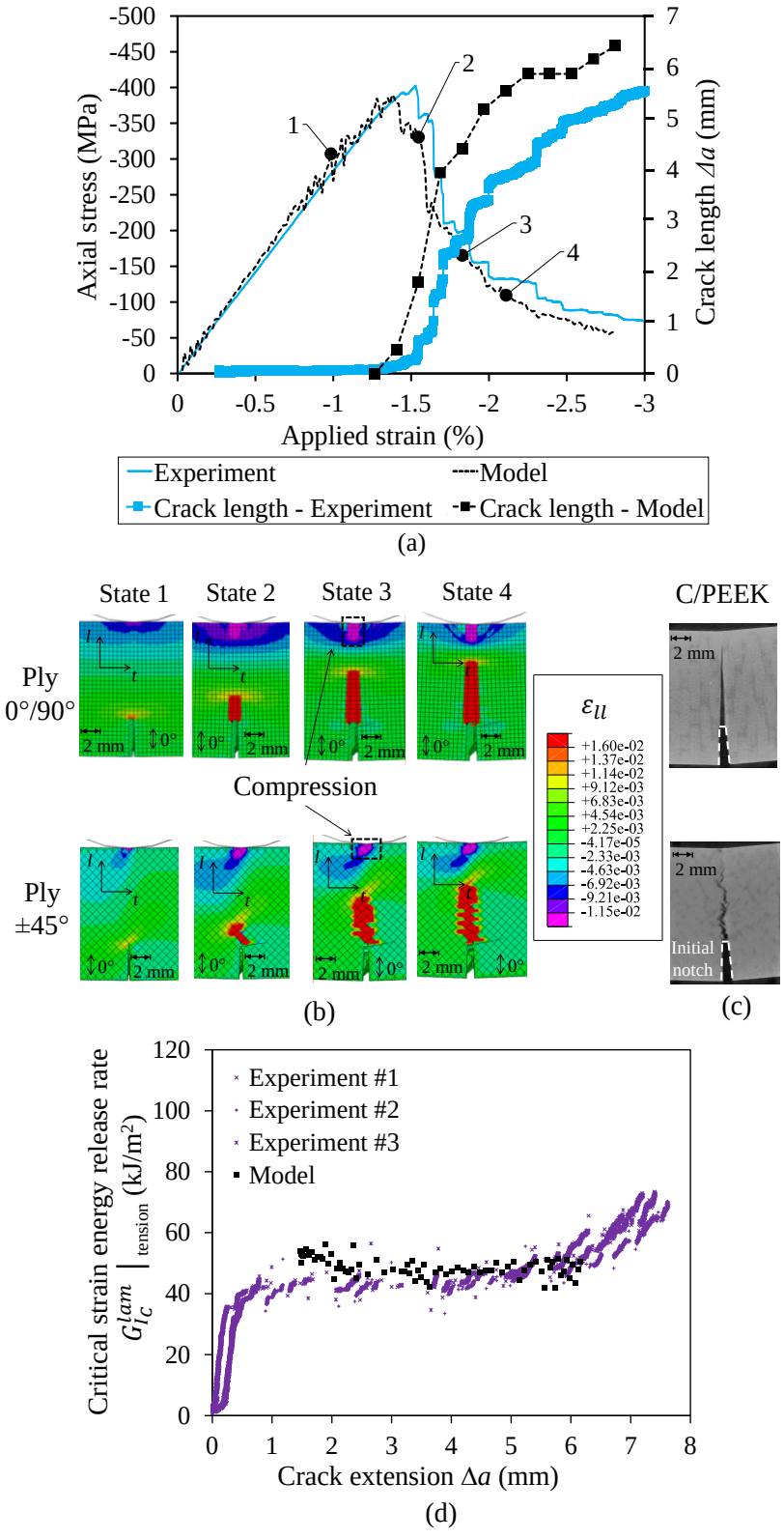

SENB CG/PEEK – $a/w = 0.3$
$[(0/90)_V,(0/90),(\pm45),(0/90),(\pm45),(0/90),(\pm45),(0/90)]_S$ - 4.5 mm thick

Figure VI.1. Numerical simulation of SENB tests (ratio $a/w = 0.3$) at RT: (a) Comparison with experimental tests - (b) Evolution of the Fracture Process Zone in the different plies of the laminate - (c) Post-mortem X-ray tomographic observations of SENB specimens - (d) Evolution of strain energy release rate along with the crack growth

The numerical model proved to be predictive in the case of CT test, but is not accurate enough in CC. It should be interesting to simulate SENB tests that imply both tensile and compressive failure. As was shown in the experimental part of this work, SENB tests are characterized by a gradual and stable crack growth. Moreover, in these loading conditions a combination of local crushing of the upper edges in the contact area and compressive fiber failure is observed during translaminar crack propagation. Simulation of SENB tests are representative of complex stress states within the laminates. Thus, they are relevant to validate the predictive capacity of the numerical model, but also as an additional insight into the translaminar failure of woven-ply TP-based composites. The preliminary results show that the numerical model is able to describe the macroscopic mechanical behavior of SENB tests (Figure VI.1). Besides X-ray tomography observations allow the validation of the model at the ply scale as crack patterns are very well predicted.

The numerical crushing model should be improved. Simulations of CC tests reveal the weakness of the model to account for out-of-plane displacement resulting from the kink-bands formation. The out-of-plane shear effect (τ_{LZ}, τ_{TZ}) needs to be taken into account in the plasticity/damage constitutive laws when it comes to compressive loadings.

In order to account for the time-dependent behavior of the PEEK matrix at $T>T_g$, a viscoplastic model should also be implemented into the model formulation.

Ultimately, these different prospects should allow a better understanding of the translaminar failure of woven-ply thermoplastic laminated composites that are expected to be used for applications in aeronautics under high temperature conditions ($T>T_g$).

Annex A: Translaminar fracture toughness tests and crack growth

Tensile tests:

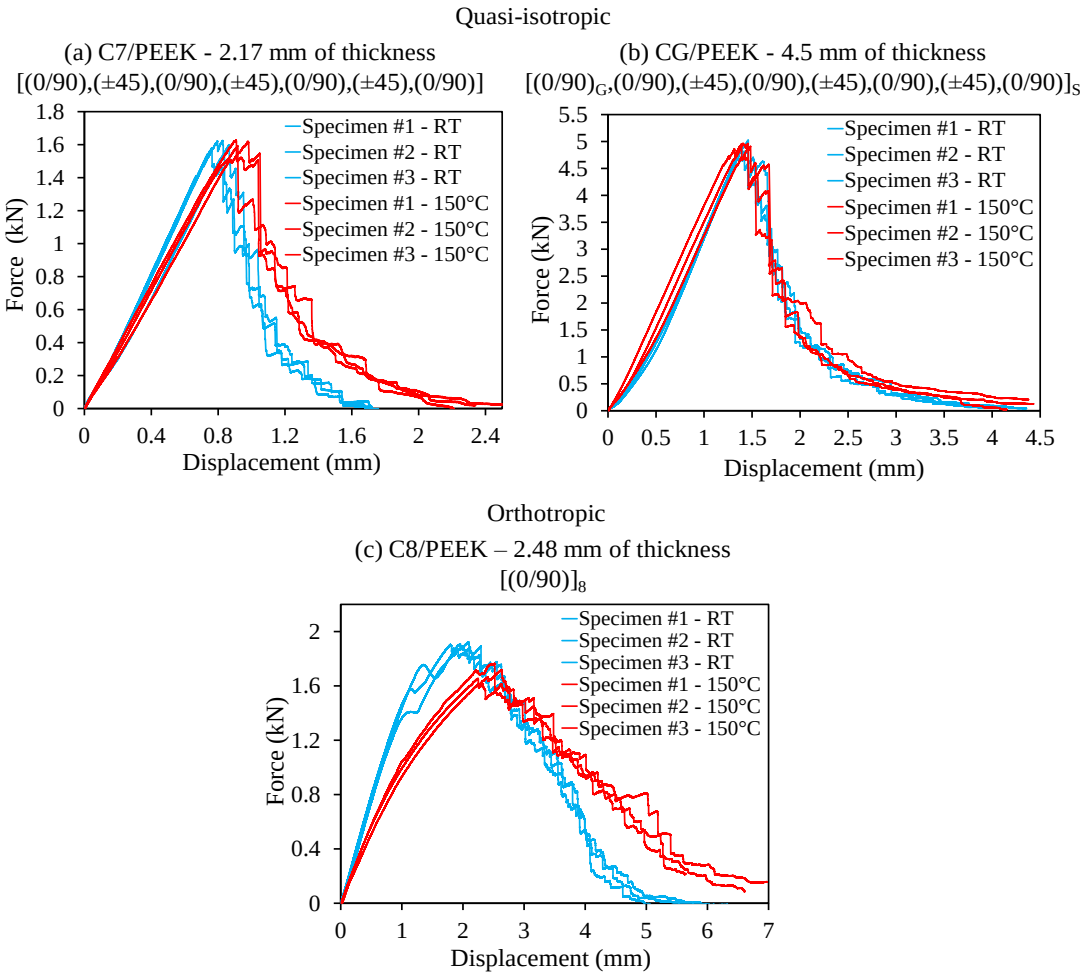

Figure A.1. Force-displacement curves in the case of Compact Tension specimens at RT and at 150°C: (a) and (b) quasi-isotropic laminates. – (b) Orthotropic laminate.

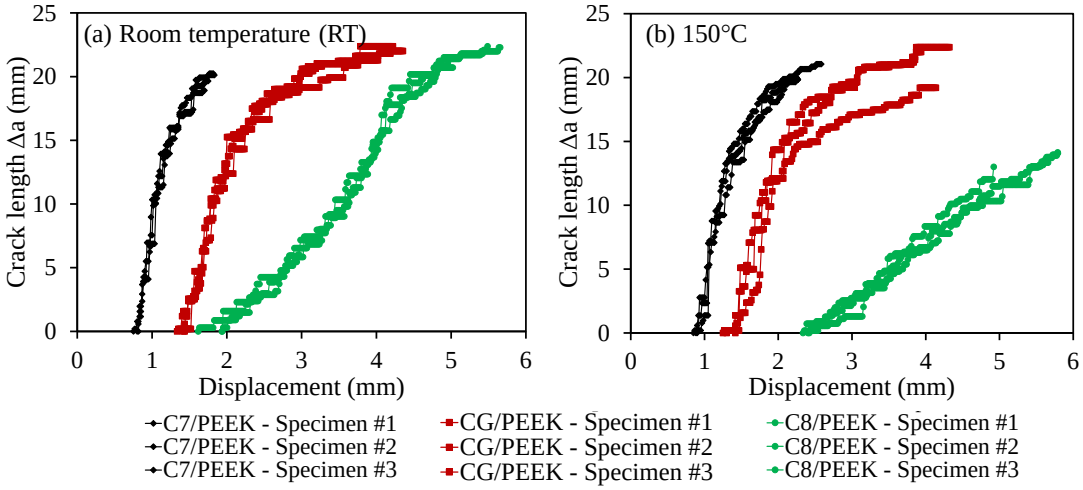

Figure A.2. Crack propagation measurement by means of a Digital Image Correlation (DIC) technique in the case of CT specimens at RT and at 150°C. No secondary crack is shown for better visualization.

Compressive tests:

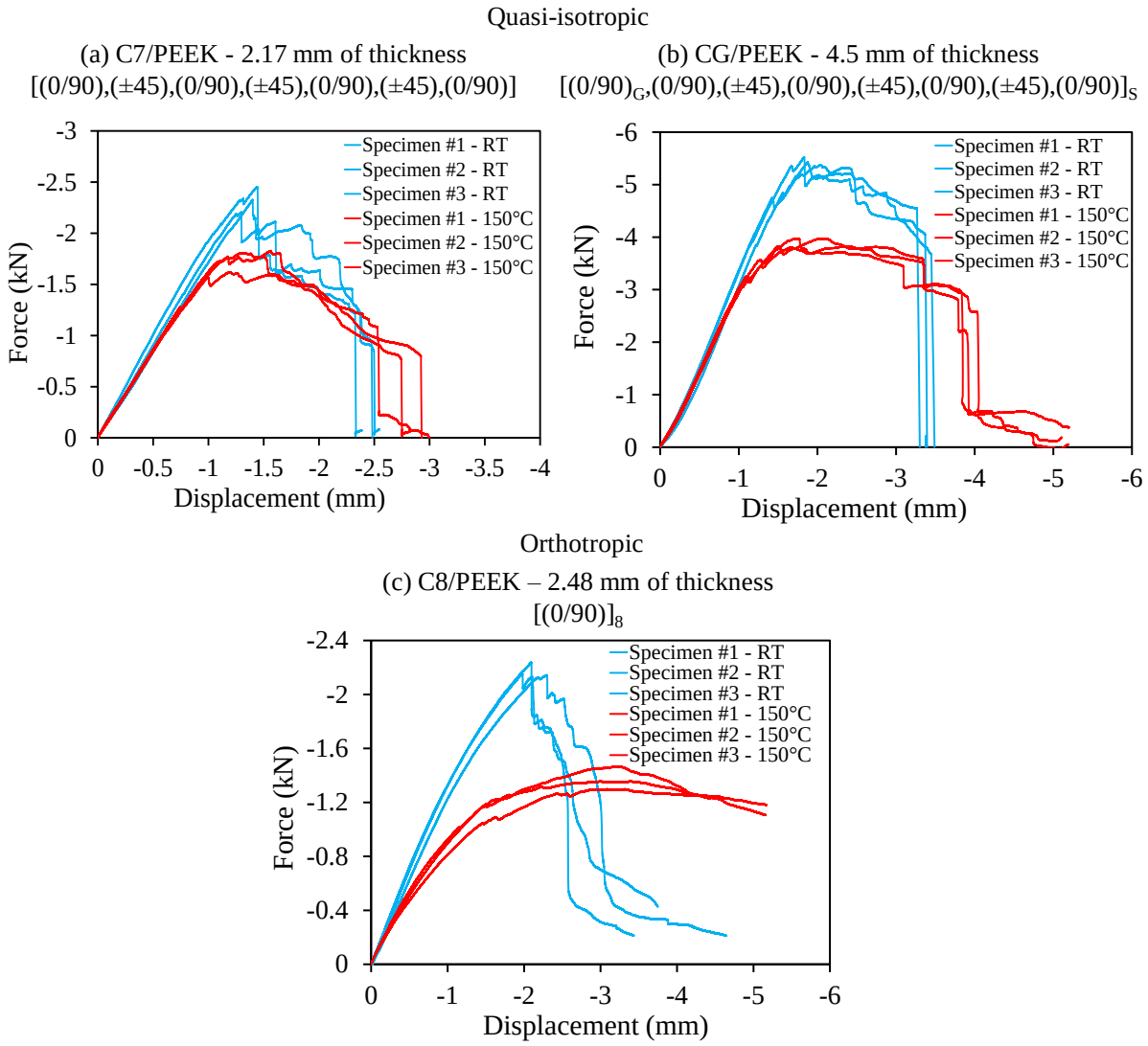

Figure A.3. Force-displacement curves in the case of Compact Compression specimens at RT and at 150°C: (a) and (b) quasi-isotropic laminates. – (b) Orthotropic laminate.

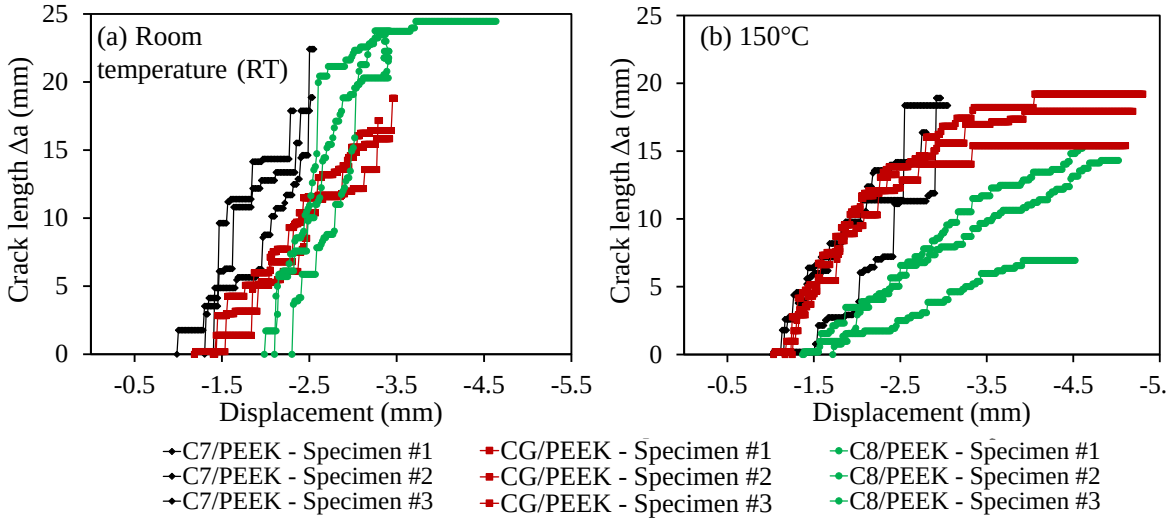

Figure A.4. Crack propagation measurement by means of a Digital Image Correlation (DIC) technique in the case of CC specimens at RT and at 150°C. No secondary crack is shown for better visualization.

List of references

[1] C. Verdeaux. Influence des conditions d'élaboration sur la zone interfaciale des matériaux composites hautes performances à matrice thermoplastique. PhD thesis, Ecole Nationale Supérieur des Mines de Paris, 1988.

[2] C. Cottenot. Comparaison des modes de comportement élémentaires des composites à matrices thermodurcissable et thermoplastique. Thèse de Doctorat de l'Université de Poitiers n°432, 1991.

[3] P. Vautey. Bilan des performances mécaniques des composites carbone/TP pour l'aéronautique. Thèse de Doctorat de l'Université de Technologie de Compiègne, 1993.

[4] F. Touchard. Spécificités du comportement mécanique de composites stratifiés à fibres longues et à matrice thermoplastique. Thèse de Doctorat de l'Université de Poitiers n°502, 1994.

[5] Laffan, M. J., Pinho, S. T., Robinson, P., & McMillan, A. J. (2012). Translaminar fracture toughness testing of composites: A review. Polymer testing, 31(3), 481-489.

[6] M. Torres, B. Plissonneau. Repair of helicopter composite structure: Techniques and Substantiations. Advisory group for aerospace research & development (AGARD) CP402, The Repair of Aircraft Structures Involving Composite Materials, p.6-1-6-21, 1986

[7] W. Albouy. De la contribution de la visco-élasto-plasticité au comportement en fatigue de composites à matrice thermoplastique et thermodurcissable. Thèse de Doctorat de l'INSA Rouen Normandie, 2013.

[8] Bouvet, C., & Vielle, B. (2020). Mécanique de la rupture de fibres dans les composites stratifiés. Editions T.I.

[9] Berthelot, J. M. (2010). Mécanique des matériaux et structures composites. Institut Supérieur des Matériaux et Mécaniques Avancés.

[10] Ogin, S. L. (2000). Textile-reinforced composite materials. Handbook of technical textiles, 12, 264.

[11] Huchette, C., Vandellos, T., & Laurin, F. (2015). Influence of intralaminar damage on the delamination crack evolution. In Damage Growth in Aerospace Composites (pp. 107-140). Springer, Cham.

[12] Irwin, G. R. (1958). Fracture, Hand. Der Physik, Springer, Berlin, vol. VI, p. 551-590.

[13] RICE, J. (1968). A Path Independent Integral and the Approximate Analysis of Strain Concentration by Notches and Cracks. Journal of Applied Mechanics, 35, 379-386.

[14] Pinho, S. T., Robinson, P., & Iannucci, L. (2006). Fracture toughness of the tensile and compressive fibre failure modes in laminated composites. Composites science and technology, 66(13), 2069-2079.

[15] Tada, H., Paris, P. C., & Irwin, G. R. (2000). The stress analysis of cracks. Handbook, Del Research Corporation.

[16] LAFFAN M.J., PINHO S.T., ROBINSON P., IANNUCCI L. – Measurement of the in situ ply fracture toughness associated with mode I fibre tensile failure in FRP. Part II: size and lay-up effects, Composites Science and Technology, 70: 614–621 (2010).

[17] Catalanotti, G., Camanho, P. P., Xavier, J., Dávila, C. G., & Marques, A. T. (2010). Measurement of resistance curves in the longitudinal failure of composites using digital image correlation. Composites Science and Technology, 70(13), 1986-1993.

[18] Teixeira, R. F., Pinho, S. T., & Robinson, P. (2016). Thickness-dependence of the translaminar fracture toughness: experimental study using thin-ply composites. Composites Part A: Applied Science and Manufacturing, 90, 33-44.

[19] Lisle, T., Pastor, M. L., Bouvet, C., & Margueres, P. (2017). Damage of woven composite under translaminar cracking tests using infrared thermography. Composite Structures, 161, 275-286.

[20] Anderson, T. L., & Anderson, T. L. (2005). Fracture Mechanics: Fundamentals and Applications. CRC Press.

[21] Liebowitz, H. (1972). Fracture: an advanced treatise. Volume VII. Fracture of nonmetals and composites.

[22] Krueger, R. (2002). The Virtual Crack Closure Technique: History, Approach and Applications. INSTITUTE FOR COMPUTER APPLICATIONS IN SCIENCE AND ENGINEERING HAMPTON VA.

[23] R. F. Teixeira, S. T. Pinho, P. Robinson. Translaminar fracture toughness on CFRP: from the toughness of individual plies to the toughness of the laminates. ECCM15 -15th European Conference on Composite Materials, Venice, Italy, 24-28 June 2012.

[24] LAFFAN M.J., PINHO S.T., ROBINSON P., IANNUCCI L. – Measurement of the in situ ply fracture toughness associated with mode I fibre tensile failure in FRP. Part I: data reduction, Composites Science and Technology, 70: 606–613 (2010).

[25] Vaidya, R. S., & Sun, C. T. (1997). Fracture criterion for notched thin composite laminates. AIAA journal, 35(2), 311-316.

[26] Poe Jr, C. C. (1983). A unifying strain criterion for fracture of fibrous composite laminates. Engineering Fracture Mechanics, 17(2), 153-171.

[27] Bullegas, G., Benoliel, J., Fenelli, P. L., Pinho, S. T., & Pimenta, S. (2018). Towards quasi isotropic laminates with engineered fracture behaviour for industrial applications. Composites Science and Technology, 165, 290-306.

[28] Bullegas, G., Pinho, S. T., & Pimenta, S. (2016). Engineering the translaminar fracture behaviour of thin-ply composites. Composites Science and Technology, 131, 110-122.

[29] J. Cugnoni, G. Frossard, R. Amacher and J. Botsis. Translaminar fracture of regular and hybrid thin ply composites: experimental characterization and modelling. ECCM18 -18th European Conference on Composite Materials, Athens, Greece, 24-28th June 2018.

[30] Jackson, W. C., & Ratcliffe, J. G. (2004). Measurement of fracture energy for kink-band growth in sandwich specimens. Composites Testing and Model Identification. Bristol, UK, 21-23.

[31] Jones RM. Other analysis and behavior topics. In: Mechanics of composite materials, 2nd ed. London, UK: Taylor & Francis, 1999, p.345.

[32] TAN S.C. – Stress concentration in laminated composites. Lancaster, Pa.: Technomic Pub. Co. (1994).

[33] Ortega, A., Maimí, P., González, E. V., de Aja, J. S., de la Escalera, F. M., & Cruz, P. (2017). Translaminar fracture toughness of interply hybrid laminates under tensile and compressive loads. Composites Science and Technology, 143, 1-12.

[34] Teixeira, R. D. F., Pinho, S. T., & Robinson, P. (2014). Translaminar fracture toughness of CFRP: from the toughness of individual plies to the toughness of the laminate (Doctoral dissertation, Imperial College London).

[35] Jose, S., Kumar, R. R., Jana, M. K., & Rao, G. V. (2001). Intralaminar fracture toughness of a cross-ply laminate and its constituent sub-laminates. Composites Science and Technology, 61(8), 1115-1122.

[36] Mahmoud, M. K. (2003). Fracture Toughness of Single-Edge Notched Fiber Reinforced Composite. Polymer-Plastics Technology and Engineering, 42(4), 659-676.

[37] Laffan, M. J., Pinho, S. T., Robinson, P., Iannucci, L., & McMillan, A. J. (2012). Measurement of the fracture toughness associated with the longitudinal fibre compressive failure mode of laminated composites. Composites Part A: Applied Science and Manufacturing, 43(11), 1930-1938.

[38] Moore, D. R., & Seferis, J. C. (1991). Intrinsic characterization of continuous fibre reinforced thermoplastic composites-I: toughness characterization of carbon fibre/polyether ether ketone (CF/PEEK) laminates. Pure and applied chemistry, 63(11), 1609-1625.

[39] Slepetz, J. M., & Carlson, L. E. O. N. A. R. D. (1975). Fracture of composite compact tension specimens. In Fracture Mechanics of Composites. ASTM International.

[40] Wang, T. W. H., Blum, F. D., & Dharani, L. R. (1999). Effect of interfacial mobility on flexural strength and fracture toughness of glass/epoxy laminates. Journal of materials science, 34(19), 4873-4882.

[41] Rokbi, M., Osmani, H., Benseddiq, N., & Imad, A. (2011). On experimental investigation of failure process of woven-fabric composites. Composites Science and Technology, 71(11), 1375-1384.

[42] Médeau, V., Laurin, F., Rannou, J., Hurmane, A., Quillent, H., & Lachaud, F. (2019). Robust characterization of crack propagation in 3D woven composites and evidences of size dependency. Composite Structures, 111175.

[43] Tretyakov, M. P., & Wildemann, V. E. (2017). Stable crack growth in composite laminates under various stiffness of the loading system. Procedia Structural Integrity, 5, 233-238.

[44] John, R. (1997). Stress intensity factor and compliance solutions for an eccentrically loaded single edge cracked geometry. Engineering fracture mechanics, 58(1-2), 87-96.

[45] Coronado, P., Argüelles, A., Viña, J., Mollón, V., & Viña, I. (2012). Influence of temperature on a carbon–fibre epoxy composite subjected to static and fatigue loading under mode-I delamination. International Journal of Solids and Structures, 49(21), 2934-2940.

[46] Kim, K. Y., Ye, L., & Phoa, K. M. (2004). Interlaminar fracture toughness of CF/PEI and GF/PEI composites at elevated temperatures. Applied Composite Materials, 11(3), 173-190.

[47] Yurchenko, M. E., Huang, J., Robisson, A., McKinley, G. H., & Hammond, P. T. (2010). Synthesis, mechanical properties and chemical/solvent resistance of crosslinked poly (aryl-ether–ether–ketones) at high temperatures. Polymer, 51(9), 1914-1920.

[48] Vieille, B., Chabchoub, M., Bouscarrat, D., & Keller, C. (2016). Prediction of the notched strength of woven-ply PolyPhenylene Sulfide thermoplastic composites at a constant high temperature by a physically-based model. Composite Structures, 153, 529-537.

[49] Vieille, B., Aucher, J., & Taleb, L. (2012). Comparative study on the behavior of woven-ply reinforced thermoplastic or thermosetting laminates under severe environmental conditions. Materials & Design, 35, 707-719.

[50] Vieille, B., Pujols González, J. D. & Bouvet, C. (2019). Fracture mechanics of hybrid composites with ductile matrix and brittle fibers: Influence of temperature and constraint effect. Journal of Composite Materials, Vol. 53 (10), pp. 1361-1376.
[51] Launey, M. E., & Ritchie, R. O. (2009). On the fracture toughness of advanced materials. Advanced Materials, 21(20), 2103-2110.
[52] Standard, A. S. T. M. (2012). E399-12. Standard Test Method for Linear-elastic Plane-strain Fracture Toughness KIc of Metallic Materials, American Society for Testing and Materials, West Conshohocken, PA.
[53] Airbus, S. A. S. (2005). Aircraft characteristics airport and maintenance planning.
[54] Solutions, C. (2009). Vic 2D reference manual. Correlated Solutions, Columbia.
[55] Sutton, M. A., Mingqi, C., Peters, W. H., Chao, Y. J., & McNeill, S. R. (1986). Application of an optimized digital correlation method to planar deformation analysis. Image and Vision Computing, 4(3), 143-150.
[56] Scilab (Version 6.0.1). Available online: http://www.scilab.org/download/6.0.1
[57] A. Ortega, P. Maimí, E.V. González, Ll. Ripoll. Compact tension specimen for orthotropic materials. Composites Part A 2014, 63, 85-93.
[58] Liu, H., Falzon, B. G., Catalanotti, G., & Tan, W. (2018). An experimental method to determine the intralaminar fracture toughness of high-strength carbon-fibre reinforced composite aerostructures. The Aeronautical Journal, 122(1255), 1352-1370.
[59] Blanco, N., Trias, D., Pinho, S. T., & Robinson, P. (2014). Intralaminar fracture toughness characterisation of woven composite laminates. Part I: Design and analysis of a compact tension (CT) specimen. Engineering Fracture Mechanics, 131, 349-360.
[60] Ritchie, R. O. (1999). Mechanisms of fatigue-crack propagation in ductile and brittle solids. International journal of Fracture, 100(1), 55-83.
[61] Hertzberg RW, Vinci RP and Hertzberg JL. Element of fracture mechanics. In: Hertzberg RW (ed.) Deformation and fracture mechanics of engineering materials, 5th ed. Hoboken, USA: Wiley & Sons, 1996.
[62] Tardiff Jr, G. (1973). Fracture mechanics of brittle matrix ductile fiber composites. Engineering Fracture Mechanics, 5(1), 1-10.
[63] Naerheim, Y. (1976). Fracture characteristics of a ductile-matrix/brittle-fiber composite. Metallurgical Transactions A, 7(1), 63-70.
[64] Kim, J., & Mai, Y. W. (1991). Effects of interfacial coating and temperature on the fracture behaviours of unidirectional Kevlar and carbon fibre reinforced epoxy resin composites. Journal of materials science, 26(17), 4702-4720.
[65] Fracasso, R., Rink, M., Pavan, A., & Frassine, R. (2001). The effects of strain-rate and temperature on the interlaminar fracture toughness of interleaved PEEK/CF composites. Composites science and technology, 61(1), 57-63.
[66] Jacob, G. C., Starbuck, J. M., Fellers, J. F., Simunovic, S., & Boeman, R. G. (2005). The effect of loading rate on the fracture toughness of fiber reinforced polymer composites. Journal of applied polymer science, 96(3), 899-904.
[67] Kassapoglou, C. (2015). Modeling the effect of damage in composite structures: Simplified approaches. John Wiley & Sons.
[68] REIFSNIDER, K. L. (1991). Damage and damage mechanics. In Composite Materials Series (Vol. 4, pp. 11-77). Elsevier.

[69] Harris, B. (2003). A historical review of the fatigue behaviour of fibre-reinforced plastics. In Fatigue in composites (pp. 3-35). Woodhead Publishing.

[70] Wells, J. K., & Beaumont, P. W. (1985). Crack-tip energy absorption processes in fibre composites. Journal of materials science, 20(8), 2735-2749.

[71] Vieille, B., Chabchoub, M., Bouscarrat, D., & Gautrelet, C. (2017). A fracture mechanics approach using Acoustic Emission Technique to investigate damage evolution in woven-ply thermoplastic structures at temperatures higher than glass transition temperature. Composites Part B: Engineering, 116, 340-351.

[72] Vieille, B., Chabchoub, M., & Gautrelet, C. (2018). Influence of matrix ductility and toughness on strain energy release rate and failure behavior of woven-ply reinforced thermoplastic structures at high temperature. Composites Part B: Engineering, 132, 125-140.

[73] Beaumont, P. W. R. (2003). Physical modelling of damage development in structural composite materials under stress. Fatigue in composites, 365-410.

[74] Lauke, B., & Pompe, W. (1986). Fracture toughness of short-fibre reinforced thermoplastics. Composites Science and Technology, 26(1), 37-57.

[75] Munro, M., & Lai, C. P. Z. (1988). The elevated-temperature dependence of fracture energy mechanisms of hybrid carbon-glass fibre reinforced composites. Journal of materials science, 23(9), 3129-3136.

[76] Wells, J. K., & Beaumont, P. W. R. (1987). The prediction of R-curves and notched tensile strength for composite laminates. Journal of materials science, 22(4), 1457-1468.

[77] Flore, D., Stampfer, B., & Wegener, K. (2017). Experimental and numerical failure analysis of notched quasi-unidirectional laminates at room temperature and elevated temperature. Composite Structures, 160, 128-141.

[78] Test standard EN 6035, Aerospace series - Fiber-reinforced plastics - Test Method - Determination of notched and unnotched tensile strength. Published by the European Association of Aerospace Industries (AECMA), april 1996.

[79] Test standard EN 2562, Aerospace series – Carbon Fiber-reinforced plastics - Test Method – Unidirectional laminates, flexural test parallel to the fiber direction. Published by the European Association of Aerospace Industries (AECMA), march1997.

[80] SIH, G. (1981). Cracks in Composite Materials. Mechanics of Fracture, 6.

[81] ASTM standard E1820 test method. Standard Test Method for Measurement of Fracture Toughness.

[82] Gross, B., Srawley, J. E., & Brown Jr, W. F. (1964). Stress-intensity factors for a single-edge-notch tension specimen by boundary collocation of a stress function. NATIONAL AERONAUTICS AND SPACE ADMINISTRATION CLEVELAND OH LEWIS RESEARCH CENTER.

[83] Kayamori, Y., Inoue, T., & Hagihara, Y. (2014). Plastic Rotational Factor Calculation for Shallow-Notched SE (B) Specimens. In Materials Science Forum (Vol. 783, pp. 2322-2326). Trans Tech Publications Ltd.

[84] Dubary, N., Taconet, G., Bouvet, C., & Vieille, B. (2017). Influence of temperature on the impact behavior and damage tolerance of hybrid woven-ply thermoplastic laminates for aeronautical applications. Composite Structures, 168, 663-674.

[85] Vieille, B. (2019). Evolution of the strain energy release rate during ductile or brittle failure in woven-ply reinforced thermoplastic laminates under high temperature conditions. Polymer Composites, 40(1), 121-131.

[86] Talreja, R., & Varna, J. (Eds.). (2015). Modeling damage, fatigue and failure of composite materials. Elsevier.

[87] Kim, J. K., Mai, Y. W., & Mai, Y. W. (1998). Interface mechanics and fracture toughness theories. Engineered Interfaces in Fiber Reinforced Composites; Elsevier: Amsterdam, The Netherlands, 239-277.

[88] Chawla, K. K. (1993). Ceramic Matrix Composites. Chapman & Hall, London.

[89] Dávila, C. G., Rose, C. A., & Camanho, P. P. (2009). A procedure for superposing linear cohesive laws to represent multiple damage mechanisms in the fracture of composites. International Journal of Fracture, 158(2), 211-223.

[90] Bergan, A., Dávila, C., Leone, F., Awerbuch, J., & Tan, T. M. (2016). A Mode I cohesive law characterization procedure for through-the-thickness crack propagation in composite laminates. Composites Part B: Engineering, 94, 338-349.

[91] Xu, X., Takeda, S. I., Aoki, Y., Hallett, S. R., & Wisnom, M. R. (2017). Predicting notched tensile strength of full-scale composite structures from small coupons using fracture mechanics. Composite Structures, 180, 386-394.

[92] Zobeiry, N., Forghani, A., McGregor, C., McClennan, S., Vaziri, R., & Poursartip, A. (2017). Effective calibration and validation of a nonlocal continuum damage model for laminated composites. Composite Structures, 173, 188-195.

[93] Xu, X., Wisnom, M. R., & Hallett, S. R. (2019). Deducing the R-curve for trans-laminar fracture from a virtual Over-height Compact Tension (OCT) test. Composites Part A: Applied Science and Manufacturing, 118, 162-170.

[94] Zobeiry, N., Vaziri, R., & Poursartip, A. (2015). Characterization of strain-softening behavior and failure mechanisms of composites under tension and compression. Composites Part A: Applied Science and Manufacturing, 68, 29-41.

[95] Ortega, A., Maimí, P., González, E. V., & Trias, D. (2016). Characterization of the translaminar fracture Cohesive Law. Composites Part A: Applied Science and Manufacturing, 91, 501-509.

[96] Ridha, M., Wang, C. H., Chen, B. Y., & Tay, T. E. (2014). Modelling complex progressive failure in notched composite laminates with varying sizes and stacking sequences. Composites Part A: Applied Science and Manufacturing, 58, 16-23.

[97] Su, Z. C., Tay, T. E., Ridha, M., & Chen, B. Y. (2015). Progressive damage modeling of open-hole composite laminates under compression. Composite Structures, 122, 507-517.

[98] Bouvet, C., Rivallant, S., & Barrau, J. J. (2012). Low velocity impact modeling in composite laminates capturing permanent indentation. Composites Science and Technology, 72(16), 1977-1988.

[99] Iannucci, L., & Willows, M. L. (2006). An energy based damage mechanics approach to modelling impact onto woven composite materials—Part I: Numerical models. Composites Part A: Applied Science and Manufacturing, 37(11), 2041-2056.

[100] Liu, H., Falzon, B. G., Li, S., Tan, W., Liu, J., Chai, H., ... & Dear, J. P. (2019). Compressive failure of woven fabric reinforced thermoplastic composites with an open-hole: an experimental and numerical study. Composite Structures, 213, 108-117.

[101] Jebri, L., Abbassi, F., Demiral, M., Soula, M., & Ahmad, F. (2020). Experimental and numerical analysis of progressive damage and failure behavior of carbon Woven-PPS. Composite Structures, 112234.
[102] Pinho, S. T., Vyas, G. M., & Robinson, P. (2013). Response and damage propagation of polymer-matrix fibre-reinforced composites: Predictions for WWFE-III Part A. Journal of composite materials, 47(20-21), 2595-2612.
[103] Dassault Systemes. (2014). Abaqus User Subroutines Reference Guide, Version 6.14. Dassault Systemes Simulia Corp., Providence, RI, USA.
[104] Dassault Systemes. (2013). Abaqus 6.14–Analysis Users's Guide: Volume V: Prescribed conditions, constraints & interactions. Providence, Rhode Island.
[105] Bažant, Z. P., & Oh, B. H. (1983). Crack band theory for fracture of concrete. Matériaux et construction, 16(3), 155-177.
[106] Toho Tenax – TEIJIN : Product Data Sheet Tenax®-E TPCL PEEK-HTA40
[107] Bassery, J. (2011). Prise en compte du vieillissement et de la fatigue dans le dimensionnement de structures en matériaux composites (Doctoral dissertation).
[108] Ludwik, P. (1909). Fließvorgänge bei einfachen Beanspruchungen. In Elemente der Technologischen Mechanik (pp. 11-35). Springer, Berlin, Heidelberg.
[109] Pinho, S. T., Gutkin, R., Pimenta, S., De Carvalho, N. V., & Robinson, P. (2012). Fibre-dominated compressive failure in polymer matrix composites. In Failure Mechanisms in Polymer Matrix Composites (pp. 183-223). Woodhead Publishing.
[110] De Carvalho, N. V., Pinho, S. T., & Robinson, P. (2011). An experimental study of failure initiation and propagation in 2D woven composites under compression. Composites Science and Technology, 71(10), 1316-1325.
[111] Gutkin, R., & Pinho, S. (2016). Review on failure of laminated composites: Experimental perspective and modelling.

Study of the high temperature translaminar fracture in aeronautical woven-ply thermoplastic laminated composites: experimental characterization and numerical simulation

Abstract

Understanding the fracture behaviour of composite materials is a challenge for the aeronautics industry. The problem is even more complex in a high temperature environment (150°C) within PEEK thermoplastic matrix composites reinforced with woven carbon fibers. Among the most critical failure mechanisms, the translaminar failure associated with fiber breakage requires specific approaches depending on the stress mode (traction, compression, bending). This work has allowed the comparison of different experimental methods, with particular emphasis on optical methods coupled with field measurements making it possible to monitor crack propagation at high temperature. The G-R curves obtained, showing the evolution of the strain energy release rate as a function of the crack length, characterize the translaminar fracture and give essential information on the influence of the thickness of the laminate as well as its draping according to the type of stress. A numerical model implemented in the Abaqus Finite Elements code was used to predict the translaminar fracture behavior. This model, based on an energetic criterion of rupture and a law of plasticity, allows to: (i) simulate the tensile and compressive fracture behaviour – (ii) dissociate the mechanisms responsible for energy dissipation during translaminar fracture. Fracture mechanics and finite elements modelling provide a very efficient framework for better understanding the fracture behavior of woven-ply PEEK-based laminated composites as well as the origin of their damage tolerance. However, the characteristics values of fracture toughness and corresponding G-R curves can be difficult to determine and to interpret. Ultimately, the present work also emphasized the limitations of fracture mechanics concepts applied to laminated composite structures.

Keywords: Thermoplastic matrix, carbon fibers woven ply, translaminar fracture, high temperature, experimental characterization, numerical modelling.

Etude de la rupture translaminaire à haute température dans les stratifiés thermoplastiques à plis tissés pour des applications aéronautiques : caractérisation expérimentale et simulation numérique

Résumé

Appréhender le comportement mécanique à rupture des matériaux composites est un véritable enjeu pour l'industrie aéronautique. La problématique est encore plus complexe dans un environnement haute température (150°C) au sein des composites à matrice thermoplastique PEEK renforcée par des fibres de carbone tissées. Parmi les mécanismes de rupture les plus critiques, la rupture translaminaire associée à la rupture des fibres nécessite des approches spécifiques selon le mode sollicitation (traction, compression, flexion). Ces travaux ont permis de comparer différentes méthodes expérimentales mettant l'accent notamment sur des méthodes optiques couplées à des mesures de champ rendant possible le suivi de la propagation de fissure à haute température. Les courbes G-R obtenues, traduisant l'évolution du taux de restitution d'énergie en fonction de la longueur de fissure, caractérisent la rupture translaminaire et donnent des informations essentielles sur l'influence de l'épaisseur du stratifié ainsi que son drapage selon le type de sollicitation. Un modèle numérique implémenté dans le code Eléments Finis Abaqus a été exploité afin de prédire le comportement en rupture translaminaire. Ce modèle, basé sur un critère énergétique de rupture et une loi de plasticité, permet de : (i) simuler le comportement à rupture en traction et en compression – (ii) dissocier les mécanismes responsables de la dissipation d'énergie lors de la rupture translaminaire. Ainsi, les outils de la mécanique de la rupture et la modélisation par éléments finis sont des approches complémentaires permettant de mieux comprendre le comportement à rupture ainsi que l'origine de la tolérance aux dommages des composites à matrice PEEK et renfort tissé. Cependant, les valeurs caractéristiques de la ténacité à la rupture et les courbes G-R correspondantes peuvent être difficiles à déterminer et à interpréter. Enfin, ces travaux ont également mis en évidence les limites des concepts de mécanique de la rupture appliqués aux structures composites stratifiées.

Mots-clés : Matrice thermoplastique, plis tissés de fibres de carbone, rupture translaminaire, haute température, caractérisation expérimentale, modélisation numérique.